Rheology of Protein Foams

zur Erlangung des akademischen Grades eines
DOKTORS DER INGENIEURWISSENSCHAFTEN (Dr.-Ing.)

der Fakultät für Chemieingenieurwesen und Verfahrenstechnik des
Karlsruher Instituts für Technologie (KIT)

genehmigte
DISSERTATION

von
Dipl.-Ing. (FH) Meike Lexis
aus Speyer

Referent: Prof. Dr. Norbert Willenbacher
Korreferent: Prof. Dr. Antonio Delgado
Tag der mündlichen Prüfung: 15.06.2015

Preface

This dissertation is based on published scientific papers including the main results of my experimental work during August 2010 and September 2014 at the Karlsruhe Institute of Technology, Institute for Mechanical Process Engineering and Mechanics in the group of Applied Mechanics.
The introduction of this thesis will appear in the book Foam Films and Foams[1] as the chapter Foam Rheology. In this part the basics of rheology and rheometry and peculiar challenges of foam rheometry are summarized. Furthermore, recent results in the field of foam rheology are reviewed.
The main part consists of three publications:

1. pH effects on the molecular structure of β-lactoglobulin modified air–water interfaces and its impact on foam rheology

2. Yield stress and elasticity of aqueous foams from protein and surfactant solutions – the role of continuous phase viscosity and interfacial properties

3. Relating foam and interfacial rheological properties of β-lactoglobulin solutions

Closing, an outlook addressing open questions and important issues for future studies is given.

[1] N. Willenbacher, M.Lexis, Rheology of Foams in R. Miller, L. Liggieri (Eds.), Foam Films and Foams: Fundamentals and Applications, Tayler and Francis, in preparation (2015)

Acknowledgements

First of all I would like to thank Prof. Norbert Willenbacher for giving me the opportunity to writing this thesis at the institute for Mechanical Process Engineering and Mechanics in Karlsruhe. He is a great mentor and conversations with him, whether scientific or non-scientific, have always broadened my mind.

Also I would like to thank Prof. Antonio Delgado from the University of Erlangen-Nuremberg, not only for being my second referee but also for the good coordination of the whole cluster project. Among ten different working groups, my dissertation was part of this project. It was a pleasure working together with all of them.

Especially I would like to thank my project partners from the University of Erlangen-Nuremberg, the group of Prof. Peukert, and in particular Kathrin Engelhardt. Not only the excellent collaboration including discussions and exchange of data, but also the opportunity for performing essential measurements at their institute substantially contributed to my work.

I am also grateful to the group of Prof. Hinrichs and Katharina Thienel from the University of Hohenheim for providing the casein and Prof. Kulozik and Jannika Dombrowski from TU Munich for providing β-lactoglobulin.

Thanks to Reinhard Miller and Georgi Gochev from the Max-Planck Institute in Golm who took the time to intensively introduce me into the surface dilational measurement technique at their institute.

A great pleasure to me was working together with the students Mareike Kowalski, Matthias Jaensch, Ceren Yüce, Julia Wagner, Mahdi Behrazm and Patrick Moll who wrote their “Studienarbeit”, bachelor or diploma thesis as part of my project.

I thank my family for always supporting me and especially my partner Hasim Özkan for listening to my scientific problems and helping me practicing my presentations.

Last but not least I thank all my colleagues working with me at the institute for the good time together.

Notations

Latin symbols

a	[-]	numerical pre-factor
A	[m^2]	area
E*	[N/m]	complex surface modulus in dilation
E’	[N/m]	surface elastic modulus in dilation
E’’	[N/m]	surface loss modulus in dilation
f	[Hz]	frequency
f_c	[Hz]	characteristic relaxation frequency
F	[N]	Force
G	[Pa]	elastic modulus
G*	[Pa]	complex shear modulus
G‘	[Pa]	storage modulus
G_0	[Pa]	plateau modulus
G‘‘	[Pa]	loss modulus
h	[m]	vertical gap position
H	[m]	gap width
k	[-]	numerical pre-factor
L	[m]	immersion length of the bob / vane
M	[Nm]	torque
r	[m]	radial position
r_{32}	[m]	mean Sauter radius
R_B	[m]	radius of the inner bob
R_C	[m]	radius of the outer cylinder
R_V	[m]	radius of the vane
t	[s]	time
v	[m/s]	velocity
v_{slip}	[m/s]	slip velocity

Greek symbols

γ	[-]	deformation
γ_c	[-]	critical deformation
$\gamma_{c,foam}$	[-]	critical deformation of the foam
$\gamma_{c,surface}$	[-]	critical deformation of the surface
γ_0	[-]	deformation amplitude
$\dot{\gamma}$	[s^{-1}]	shear rate

$\dot{\gamma}_{app}$	[s^{-1}]	apparent shear rate
δ	[°]	phase shift
ε	[-]	dielectric constant
η_{app}	[Pas]	apparent zero shear viscosity
η_L	[Pas]	liquid phase viscosity
η_W	[Pas]	water viscosity
η_∞	[Pas]	fluid viscosity in the limit of high frequency
κ	[-]	ratio of foam conductivity to continuous phase conductivity at same temperature
κ_{Foam}	[S/m]	foam conductivity
κ_{Liquid}	[S/m]	continuous phase conductivity
σ	[N/m]	surface tension
σ_W	[N/m]	surface tension of water
τ	[Pa]	shear stress
τ_0	[Pa]	shear stress amplitude
$\tau_{c,surface}$	[Pa]	critical shear stress of the surface
τ_y	[Pa]	apparent yield stress
ϕ	[-]	gas volume fraction
ϕ_c	[-]	maximum packing density
$\phi_{c,mono}$	[-]	maximum packing density of a monomodal suspension of spherically shaped particles
ω	[s^{-1}]	angular frequency

Proteins and chemicals

BLG	β-lactoglobulin
$CaCl_2$	calcium chloride
CAPB	cocamidopropyl beataine
CAS	casein
KCl	potassium chloride
LiCl	lithium chloride
LOH	lauryl alcohol
NaCl	sodium chloride
$NdCl_3$	neodymium chloride
NH_4Cl	ammonium chloride
SDS	sodium dodecyl sulfate
SLES	sodium lauryl ether sulfate
TX-100	Triton X-100
WPI	whey protein isolate

Abstract

The focus of this dissertation lies on the rheological characterization of protein foams with gas volume fractions ϕ beyond the maximum packing fraction ϕ_c at which bubbles start to deviate from their spherical shape. For $\phi > \phi_c$ foams possess peculiar rheological properties, a minimum stress called yield stress τ_y is needed to initiate foam flow and below τ_y foams behave as viscoelastic solids with a storage modulus G'≫G'' independent of frequency in a wide range.

It was shown that for β-lactoglobulin (BLG) foams the two rheological quantities yield stress and storage modulus are strongly dependent on solution pH (Fig. 1a,b). In collaboration with the Institute of Particle Technology (LFG) (University of Erlangen-Nuremberg, Germany), the Max-Planck-Institute of Colloids and Interfaces (Potsdam, Germany) and the Institute of Physical Chemistry, Bulgarian Academy of Sciences (Sofia, Bulgaria) it was found for BLG solutions that the interfacial dilational elasticity as well as the thickness of the interfacial layer also vary with solution pH (Fig. 1c,d). At the isoelectric point (IEP) around pH 5 yield stress and storage modulus of the foams as well as dilational elasticity and thickness of the interfacial layer showed maximum values because at this pH BLG molecules carry no net charge and exhibit attractive intermolecular interactions. The latter causes the formation of disordered and presumably agglomerated BLG multilayers resulting in a maximum of the surface coverage of BLG. For increasing alkaline and acidic pH conditions the protein−protein interactions change from attractive to a highly repulsive regime that leads to the formation of BLG monolayers. At pH 3 yield stress and storage modulus of the foams as well as dilational elasticity and thickness of the interfacial layer showed generally lower values than at pH 7 despite the same distance to the IEP. This discrepancy occurs due to differences in protein net charge (pH 3: +20, pH 7: -8) and to changes in the molecular structure. The correlation of the molecular information with the behavior of the macroscopic BLG foam is not trivial because different concentrations have been used for interfacial and foam rheological measurements. Interfacial measurements required low protein concentrations (10-50 µM) guaranteeing the formation of monolayers at the interface, whereas approximately ten times higher concentration was needed to create stable foams ensuring reproducible foam rheological measurements.

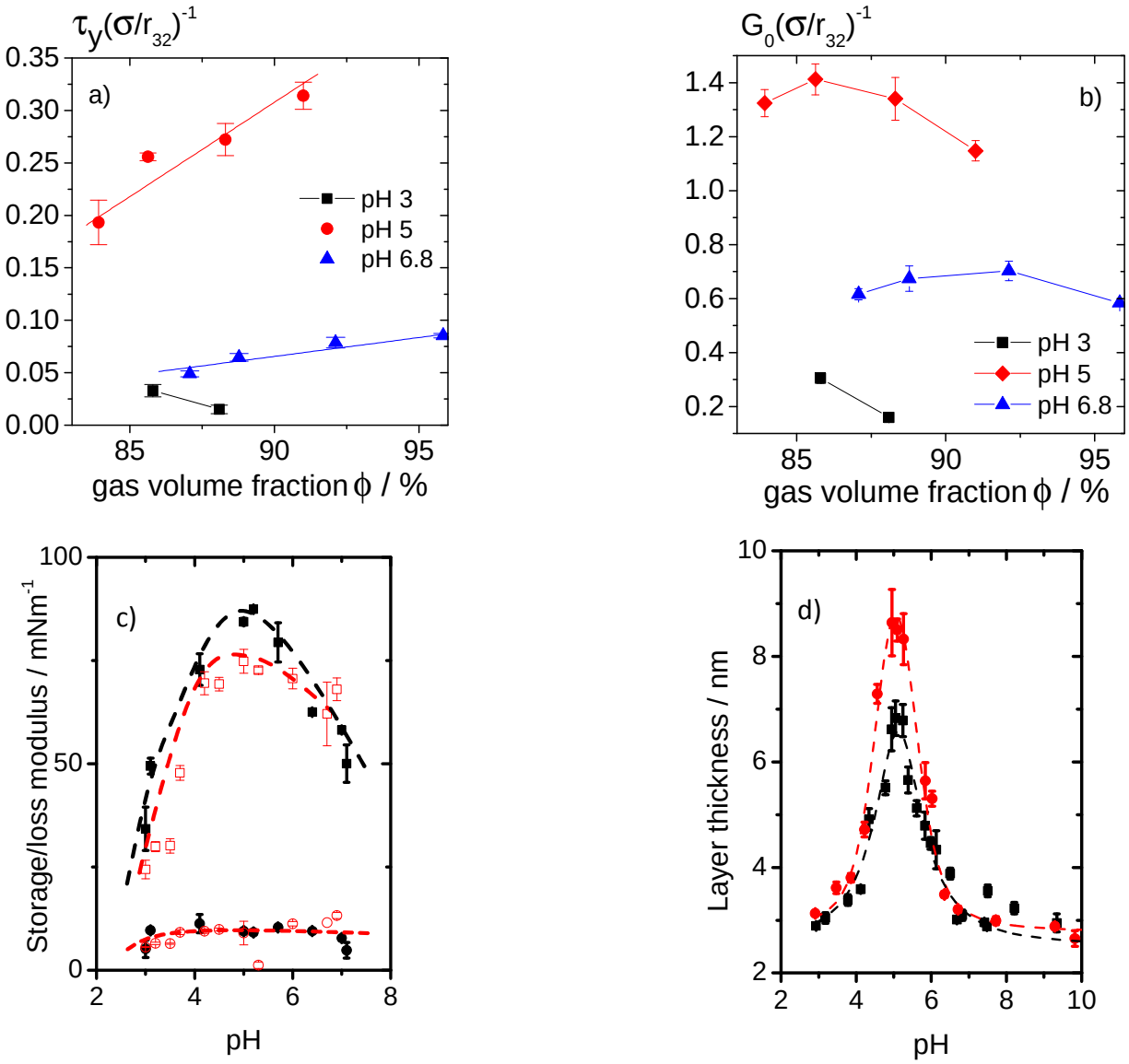

Figure 1: *a) Apparent yield stress τ_y and b) Plateau value of the storage modulus G_0 versus the gas volume fraction ϕ. Both quantities τ_y and G_0 are normalized by Laplace pressure (σ/r_{32}).*

c) Interfacial dilational storage E' (squares) and loss modulus E'' (circles) of BLG solutions. Filled symbols correspond to a BLG concentration of 10 µM, open symbols correspond to 50 µM.

d) Thickness of BLG layers adsorbed to the air-water interface as a function of the electrolyte pH which was determined from ellipsometry. The concentrations of BLG solutions were 15(●) and 54 (▲) µM. The dashed lines are a guide to the eye.

Furthermore, the colloidal physical parameters affecting the rheological quantities yield stress and storage modulus of protein and surfactant foams have been intensively studied. Besides the well-known crucial quantities gas volume fraction, bubble size and surface tension we have investigated the effect of solution viscosity and surface elasticity on the apparent yield stress

and bulk elasticity of foams made from protein (whey protein isolate with different concentrations, micellar casein) and surfactant solutions (mixture of a non-ionic and an ionic surfactant). The bubble size distribution determines the maximum packing fraction ϕ_c of the foam bubbles which has been a fit parameter so far. The critical gas volume fraction ϕ_c was determined from the measured bubble size distribution according to the phenomenological model of Sudduth[1]. Thus, we were able to take into account the bubble size distribution of each individual foam. The bubble sizes were determined from the analysis of foam images taken with an endoscopic CCD camera. The ϕ_C values found for the different foaming systems could be related to foam formation and gas bubble stabilization properties of the employed proteins and surfactants.

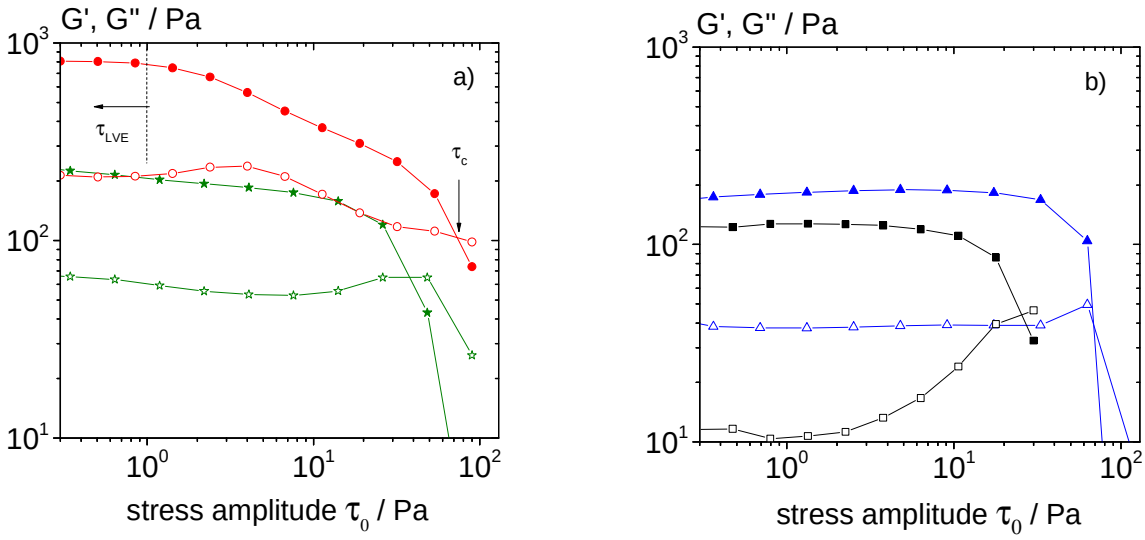

Figure 2: *Oscillatory stress amplitude sweep measurements of G' (closed symbols) and G'' (open symbols) for a) ● 1% WPI foam (ϕ = 0.90, σ/r_{32} = 261 Pa), ★ 0.1% WPI foam (ϕ = 0.92, σ/r_{32} = 369 Pa),*
b) ▲ casein foam (ϕ =0.91, σ/r_{32} = 269 Pa) and ■ surfactant foam (ϕ = 0.89, σ/r_{32} = 241 Pa)

Distinct features of the transition from the linear viscoelastic region (G′>>G″) to the non-linear deformation regime (G″>G′) are observed for the different foam systems and can be attributed to structural features of the foam lamellae (Fig. 2). A sharp transition is found for foams containing the surfactant mixture, micellar casein and low concentrated (0.1%) whey protein isolate (WPI). The higher concentrated (1%) WPI foams show a very short linear viscoelastic regime followed by a gradual transition to the flow regime. This is attributed to the formation of intralamellar structures induced by protein aggregates which occur more frequently at higher

[1] *R. D. Sudduth, Journal of Applied Polymer Science* ***1993****, 48, 37–55.*

protein concentrations. These networks break at $\tau < \tau_y$ and hence, the moduli decrease simultaneously before they cross.

The solution viscosity was varied dissolving the foaming agents in different water/glycerol or water/glucose mixtures. As expected, we found the storage modulus G_0 of foams to be generally independent of solution viscosity. However, for the higher concentrated WPI foams an apparent increase of G_0 with increasing glycerol content was observed which was not attributed to the higher liquid viscosity but rather to modified intramolecular interactions leading to increased protein aggregation and therefore to stronger network formation across the lamellae.

The apparent yield stress τ_y slightly depends on solution viscosity and this relationship is captured by an empirical factor $\left(\eta_L/\eta_W\right)^{0.3}$ valid for all investigated foams irrespective of gas volume fraction and type of foaming agent (Fig. 3), where η_L is the liquid viscosity and η_W the viscosity of water under same conditions. No particular effect of protein aggregation on the yield stress was found since the structure is assumed to be destroyed at $\tau < \tau_y$.

In general, protein-stabilized foams exhibit higher reduced τ_y and G_0 values at given (ϕ - ϕ_c) than the simple surfactant foams investigated here. This is attributed to the surface elasticity of the corresponding solutions which is higher for the protein solutions than for the surfactant solutions investigated here.

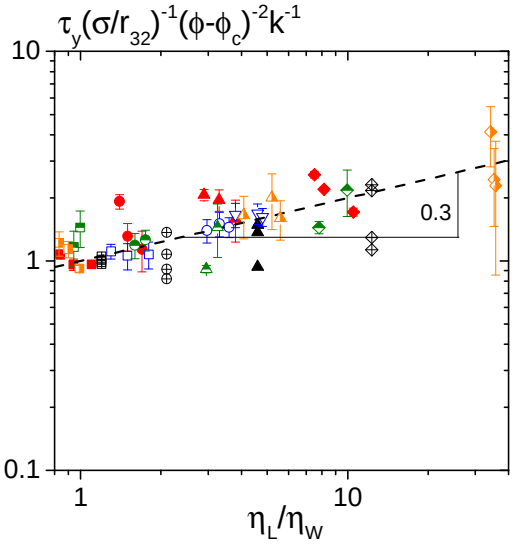

Figure 3: *Apparent yield stress τ_y normalized by Laplace pressure (σ/r_{32}), (ϕ-ϕ_c) and k vs. viscosity ratio (η_L/η_W) for foams made from different protein solutions and a surfactant mixture, the normalization is derived from the equation shown in Fig. 5, perpendicularly halved symbols: 1%WPI dissolved in various water glucose mixtures, closed symbols: 1% WPI, horizontally halved symbols: 0.1% WPI, open symbols: casein and crossed symbols: surfactant mixture dissolved in various water/glycerol mixtures (glycerol or glucose content ■0%,●20%,▼30%, ▲40%, ◆60%).*

In a final step we have investigated the correlation between the rheological behavior of BLG foams and the surface shear and dilational viscoelastic properties of corresponding protein solutions. Solution pH as well as concentration, type and valency of added salt have been varied systematically thus varying foam rheology and surface viscoelasticity in a wide range. Foam rheology was characterized by the storage modulus G_0, the apparent yield stress τ_y, and the critical strain $\gamma_{c,foam}$ defining the cessation of linear viscoelastic response. Surface viscoelasticity was characterized in shear and dilation, corresponding shear and dilational moduli G_i' , E' as well as the critical stress $\tau_{c,surface}$ and strain $\gamma_{c,surface}$ marking the onset of non-linear response in oscillatory surface shear experiments. Surface viscoelastic properties were determined at the same protein concentration as used for foam preparation in contrast to most of the investigations published so far.

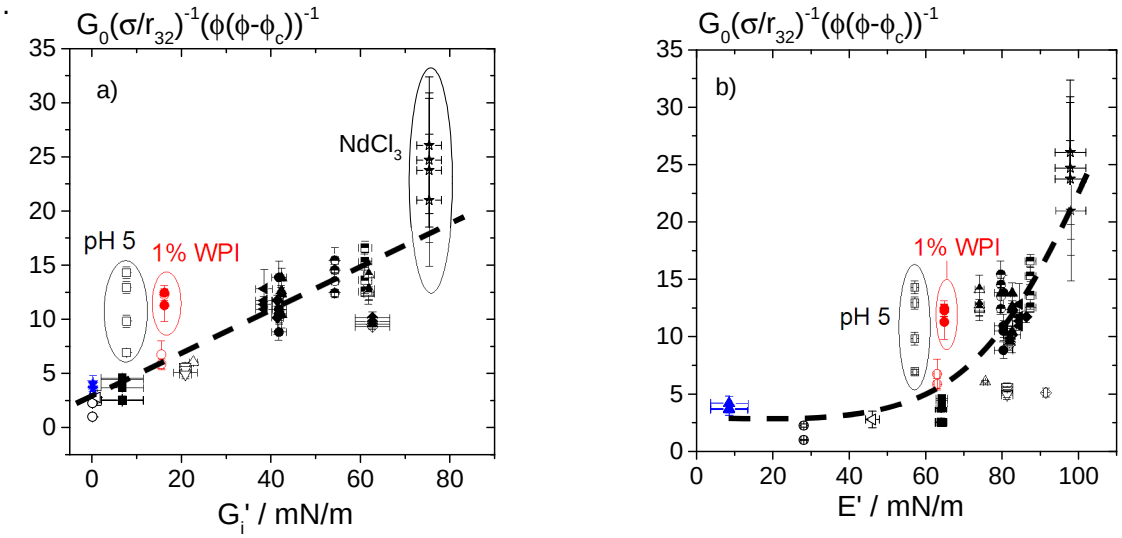

Figure 4: *Storage moduli normalized by Laplace pressure (σ/r_{32}) and $\phi(\phi-\phi_c)$ versus*
a) surface shear elastic modulus G_i'
b) surface dilational eslastic modulus E'
○ *pH 3,* △ *pH 4,* □ *pH 5,* △ *pH 6,* ◇ *pH 8,* ▽ *pH 9,*
pH 6.8 and NaCl: ■ *0 mM,* ◆ *10 mM,* ▲ *50 mM,* ● *80 mM,* ▲ *100 mM,*
50 mM ⬒ *KCl,* △ *NH_4Cl,* ◓ *LiCl,* ◆ *$CaCl_2$,* ★ *$NdCl_3$*
○ *0.1% WPI,* ● *1% WPI,* ▲ *3% casein*

Beyond the widely accepted physical models predicting foam modulus G_0 and yield stress τ_y from the Laplace pressure within the gas bubbles and the gas volume fraction these quantities strongly depend on corresponding interfacial properties. G_0 increases linearly with G_i' and even stronger with E′ (Fig. 4), τ_y varies proportional to $\tau_{c,surface}$ and $\gamma_{c,surface}$, $\gamma_{c,foam}$ scales linearly with $\gamma_{c,surface}$ (Fig. 5). Deviations from these simple scaling laws with significantly higher reduced G_0 and τ_y values are observed only for foams at pH 5 and when trivalent salt was added. Then

also the dependence of these quantities on gas volume fraction ϕ is unusually weak. These findings indicate the formation of an aggregated protein network structure across foam lamellae, which then determines foam properties but does not show up in interfacial viscoelasticity.

Hence, a unique correlation between foam rheological properties and surface viscoelastic parameters was found except in cases where attractive interactions among proteins are dominant and are supposed to be strong enough to form a network structure across foam lamellae

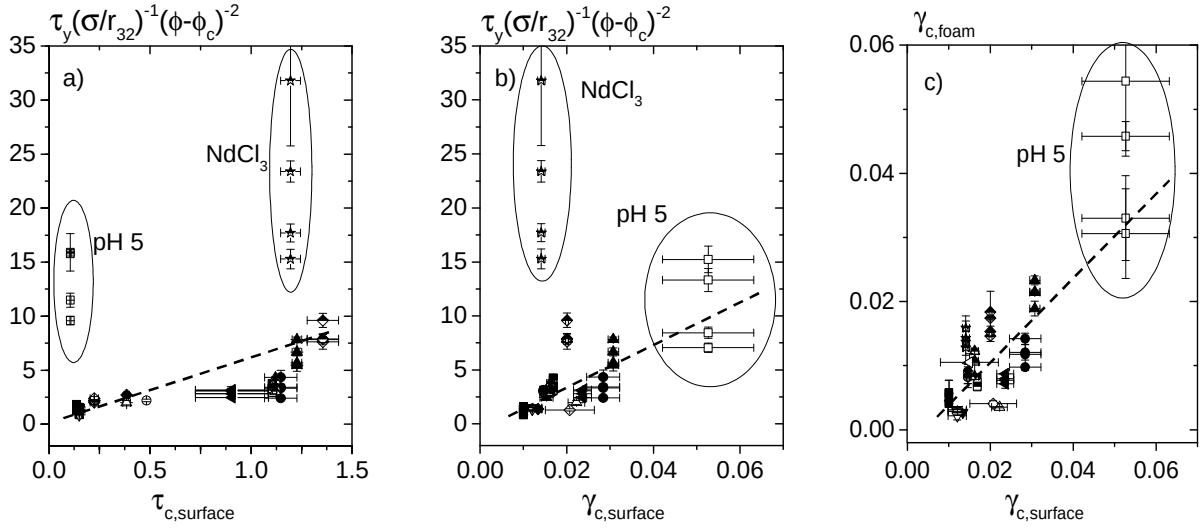

Figure 5: *yield stresses normalized by Laplace pressure and $(\phi-\phi_c)^2$ versus*

a) critical shear stress of the surface $\tau_{c,surface}$,

b) critical shear deformation of the surface $\gamma_{c,surface}$

c) critical deformation of the foams $\gamma_{c,foam}$ versus critical deformation of the surface $\gamma_{c,surface}$

○ pH 3, △ pH 4, □ pH 5, △ pH 6, ◇ pH 8, ▽ pH 9,

pH 6.8 and NaCl: ■ 0 mM, ◆10 mM, ▲ 50 mM, ● 80 mM, ▲ 100 mM,

50 mM ▬ KCl, ▲ NH_4Cl, ◓ LiCl, ◆ $CaCl_2$, ★ $NdCl_3$

Fig. 6 shows the equations for the prediction of the yield stress τ_y and the storage modulus G_0 proposed in the literature[2,3]. As discussed above we were able to extend the knowledge about the parameters having an influence on these rheological quantities. The maximum packing fraction ϕ_c is not a fit parameter anymore and can be calculated from the measured bubble size distribution of the according foam. We have added an empirical factor taking into account

[2] *T. G. Mason, J. Bibette, D. A. Weitz, Physical Review Letters **1995**, 75, 2051–2054.*

[3] *T. G. Mason, J. Bibette, D. A. Weitz, Journal of Colloid and Interface Science **1996**, 179, 439–448.*

the solution viscosity. Our experiments show that the solution viscosity has little influence on the yield stress and no effect for the storage modulus. The fit parameters k and a, which have been treated as numerical pre-factors with values between 0.5 and 1 so far, were found to vary strongly for β-lactoglobulin foams (0.5 < k,a < 30) and correlate with interfacial rheological properties.

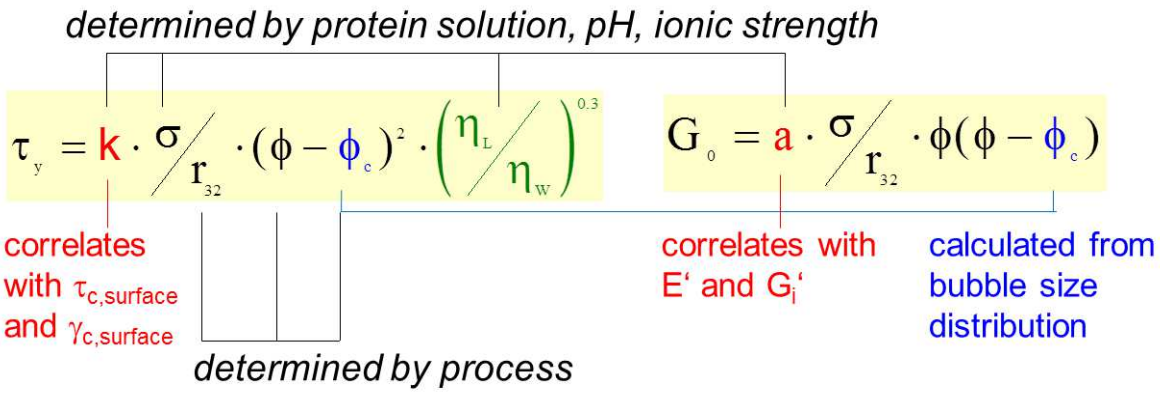

Figure 6: *Equations for predicting yield stress τ_y and storage modulus G_0 initially proposed by Mason et al.[2,3]*

Parameters that can be controlled by the foaming process are the bubble size r_{32}, the gas volume fraction ϕ as well as the maximum packing fraction ϕ_c whereas the surface tension σ, the solution viscosity η_L as well as the parameters k and a depend on physico-chemical properties of the foaming solution.

Zusammenfassung

Der Fokus dieser Dissertation liegt auf der rheologischen Charakterisierung von Proteinschäumen mit Gasvolumenanteilen ϕ höher als die maximale Packungsdichte ϕ_c, ab welcher die kugelförmigen Blasen beginnen, sich zu deformieren. Für $\phi > \phi_c$ besitzen Schäume besondere rheologische Eigenschaften, eine Mindestschubspannung genannt Fließgrenze τ_y ist nötig, um ein Fließen auszulösen und unterhalb τ_y verhalten sich Schäume wie viskoelastische Festkörper mit einem Speichermodul G‘≫G‘‘, welches in einem breiten Bereich frequenzunabhängig ist.

Es wurde gezeigt, dass die beiden rheologischen Größen Fließgrenze und Speichermodul für β-Lactoglobulin(BLG)-Schäume stark vom pH-Wert der Lösung abhängen (Abb. 1a,b). In Zusammenarbeit mit dem Institut für Feststoff- und Grenzflächenverfahrenstechnik (LFG) (Universität Erlangen-Nürnberg, Deutschland), dem Max-Planck-Institut für Kolloid- und Grenzflächenforschung (Potsdam, Deutschland) und dem Institut für physikalische Chemie (Bulgarian Academy of Sciences Sofia, Bulgarien) wurde für BLG-Lösungen gefunden, dass die Grenzflächenelastizität in Dehnung wie auch die Dicke der Grenzflächenschicht ebenso mit dem pH-Wert variieren (Fig. 1c,d). Am isoelektrischen Punkt (IEP) bei ca. pH 5 zeigen die Fließgrenze und der Speichermodul der Schäume wie auch die Dehnelastizität und die Dicke der Grenzflächenschicht maximale Werte, weil an diesem pH die BLG-Moleküle keine Ladung tragen und attraktive intermolekulare Wechselwirkungen aufweisen. Letztere verursachen die Bildung von ungeordneten und wahrscheinlich agglomerierten BLG-Multilagen, was zu einem Maximum in der Oberflächenbelegung von BLG führt. Für steigende alkalische oder saure pH-Werte wechseln die Protein-Protein Wechselwirkungen von attraktiv in einen hochrepulsiven Bereich, was zur Bildung von BLG-Monolagen führt. Bei pH 3 zeigten Fließgrenze und Speichermodul der Schäume wie auch Dehnelastizität und Dicke der Grenzflächenschicht generell niedrigere Werte als bei pH 7 trotz des gleichen Abstandes vom IEP. Diese Diskrepanz tritt wegen Unterschieden in der Proteinladung (pH3: +20, pH7: -8) und wegen Veränderungen der molekularen Struktur auf. Die Korrelation der molekularen Informationen mit dem Verhalten des makroskopischen Schaumes ist nicht trivial, weil unterschiedliche Konzentrationen für die grenzflächen- und schaumrheologischen Messungen verwendet wurden. Die Grenzflächenmessungen erforderten niedrige Proteinkonzentrationen (10-50

µm), welche die Bildung von Monolagen an der Grenzfläche garantierten, wobei ca. zehn Mal höhere Konzentrationen nötig waren, um stabile Schäume zu produzieren, mit denen reproduzierbare rheologische Messungen erzielt werden konnten.

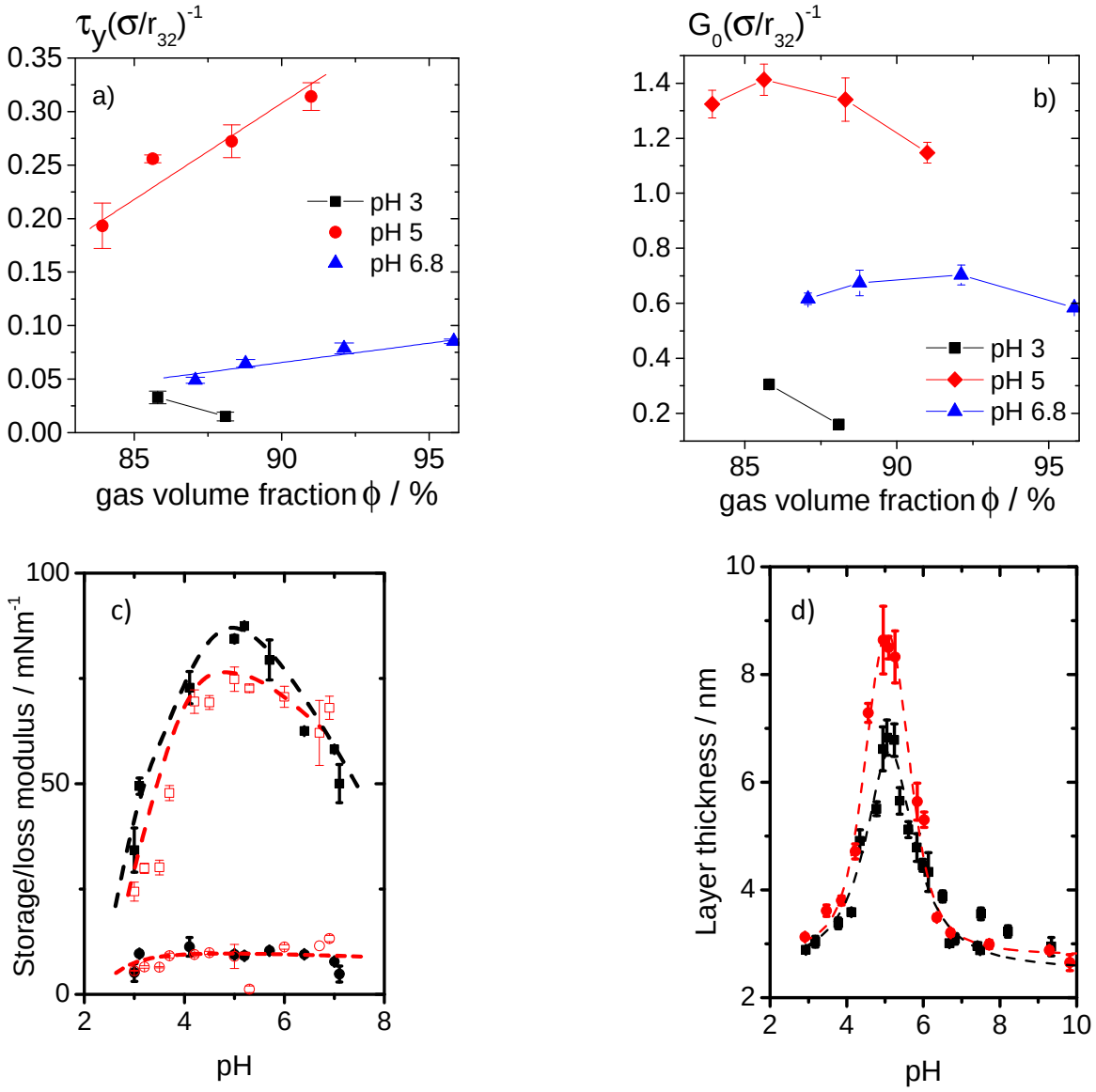

Abbildung 1: *a) Scheinbare Fließgrenze τ_y*

b) Plateauwert des Speichermoduls G_0 über dem Gasvolumenanteil ϕ. Beide Größen τ_y und G_0 sind normiert auf den Laplacedruck (σ/r_{32}).

c) Grenzflächenmoduln in Dehnung: Speicher- E' (Quadrate) und Verlustmodul E'' (Kreise) von BLG-Lösungen. BLG-Konzentration: 10 µM (gefüllte Symbole), 50 µM (offene Symbole).

d) Dicke der BLG-Adsorptionsschichten an der Luft-Wasser Grenzfläche durch Ellipsometrie bestimmt als Funktion des pH-Wertes. BLG Konzentrationen: 15(●) und 54 (▲) µM.

Weiterhin wurden die kolloidal-physikalischen Parameter, welche die rheologischen Eigenschaften Fließgrenze und Speichermodul von Protein- und Tensidschäumen beeinflussen, intensiv untersucht. Neben den bekannten entscheidenden Größen Gasvolumenanteil, Blasengröße und Oberflächenspannung haben wir den Einfluss der Flüssigphasenviskosität und der Oberflächenelastizität auf die scheinbare Fließgrenze und die Elastizität von Schäumen, hergestellt aus Protein- (Molkenproteinisolat in verschiedenen Konzentrationen, mizellares Casein) und Tensidlösungen (Mischung aus einem nichtionischen und einem ionischen Tensid), untersucht. Die Blasengrößenverteilung bestimmt die maximale Packungsdichte ϕ_c der Schaumblasen, welche bislang als Fitparameter behandelt wurde. Der kritische Gasvolumenanteil ϕ_c wurde aus der gemessenen Blasengrößenverteilung gemäß dem phänomenologischen Modell von Sudduth bestimmt. Dadurch war es uns möglich, die Blasengrößenverteilung jedes individuellen Schaums zu berücksichtigen. Die Blasengrößen wurden aus der Analyse von Schaumbildern, welche mit einer endoskopischen CCD-Kamera aufgenommen wurden bestimmt. Die ϕ_c-Werte der verschiedenen Schaumsysteme konnten mit den Schaumbildungs- und den Gasblasenstabilisierungseigenschaften der jeweiligen Proteine und Tenside in Verbindung gebracht werden.

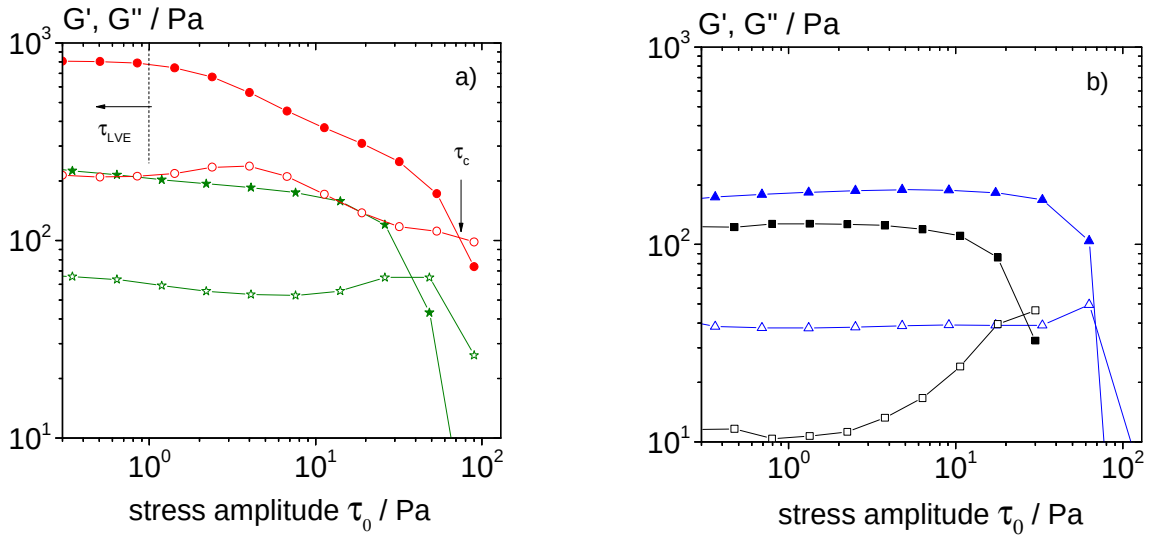

Abbildung 2: *Oszillatorische Schubspannungsamplitudensweeps von G' (geschlossene Symbole) und G'' (offene Symbole) für a) ● 1% WPI-Schaum (ϕ = 0.90, σ/r_{32} = 261 Pa), ★ 0.1% WPI foam (ϕ = 0.92, σ/r_{32} = 369 Pa),*
b) ▲ Casein-Schaum (ϕ =0.91, σ/r_{32} = 269 Pa) und ■ Tensidschaum (ϕ = 0.89, σ/r_{32} = 241 Pa)

Der Übergang vom linear viskoelastischen Bereich (G′>>G″) in den nichtlinearen Deformationsbereich (G″>G′) verlief unterschiedlich für die verschiedenen Schaumsysteme, was

auf strukturelle Eigenschaften der Schaumlamellen zurückgeführt werden kann (Abb. 2). Ein scharfer Übergang wurde für die Schäume gefunden, die aus der Tensidmischung, mit mizellarem Casein und niedrig konzentriertem (0.1%) Molkenproteinisolat (WPI) hergestellt wurden. Die höherkonzentrierten (1%) WPI-Schäume wiesen einen sehr kurzen linear viskoelastischen Bereich auf, welcher graduell in den Fließbereich übergeht. Dies kann auf die Bildung intralamellarer Strukturen zurückgeführt werden, hervorgerufen durch Proteinaggregate, welche bei höheren Proteinkonzentrationen häufiger vorkommen. Diese Netzwerke zerbrechen bei $\tau < \tau_y$ weswegen die Moduln vor ihrem Schnittpunkt gleichzeitig abfallen.

Die Flüssigkeitsviskosität wurde variiert, indem die Schaumbildner in verschiedenen Wasser/Glycerin oder Wasser/Glukose Mischungen gelöst wurden. Wie erwartet verhielt sich der Speichermodul G_0 der Schäume generell unabhängig von der Flüssigkeitsviskosität. Jedoch wurde für die höherkonzentrierten WPI-Schäume ein scheinbarer Anstieg der G_0-Werte mit ansteigendem Glyceringehalt beobachtet, was jedoch nicht auf die höhere Flüssigkeitsviskosität sondern auf veränderte intramolekulare Wechselwirkungen zurückzuführen ist, welche zu einer erhöhten Proteinaggregation und damit zu einer stärkeren Bildung von Netzwerken in der Lamelle führen.

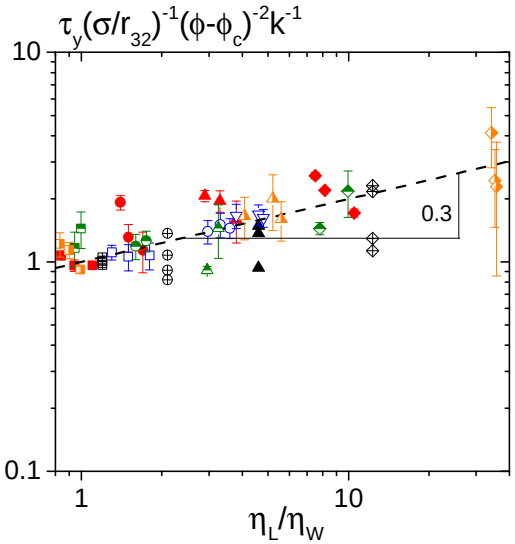

Abbildung 3: *Scheinbare Fließgrenze τ_y normiert auf den Laplacedruck (σ/r_{32}), (ϕ-ϕ_c) und k gegen das Viskositätsverhältnis (η_L/η_W) für Schäume aus verschiedenen Proteinlösungen und einer Tensidmischung, die Normierung ist aus der Gleichung in Abb. 5 abgeleitet, senkrecht halbierte Symbole: 1%WPI gelöst in verschiedenen Wasser/Glukose Mischungen, geschlossene Symbole: 1% WPI, waagerecht halbierte Symbole: 0.1% WPI, offene Symbole: Casein und gekreuzte Symbole: Tensidmischung gelöst in verschiedenen Wasser/Glycerin Mischungen (Glycerin- oder Glukosegehalt ■0%, ● 20%, ▼30%, ▲ 40%, ◆ 60%).*

Die scheinbare Fließgrenze τ_y hängt schwach von der Flüssigkeitsviskosität ab. Diese Beziehung wird mit dem empirischen Faktor $\left(\eta_L/\eta_W\right)^{0.3}$ erfasst, welcher für alle hier untersuchten Schäume gültig ist, unabhängig vom Gasvolumenanteil und Art des Schaumbildners (Abb. 3), wobei η_L die Flüssigkeitsviskosität und η_W die Viskosität von Wasser unter gleichen Bedingungen ist. Auf die Fließgrenze wurde kein besonderer Effekt der Proteinaggregation gefunden, da die Struktur vermutlich bei $\tau < \tau_y$ bereits zerstört wird.

Im Allgemeinen besitzen proteinstabilisierte Schäume höhere reduzierte τ_y und G_0 Werte bei gegebenem $(\phi - \phi_c)$ als die einfachen hier untersuchten Tensidschäume.

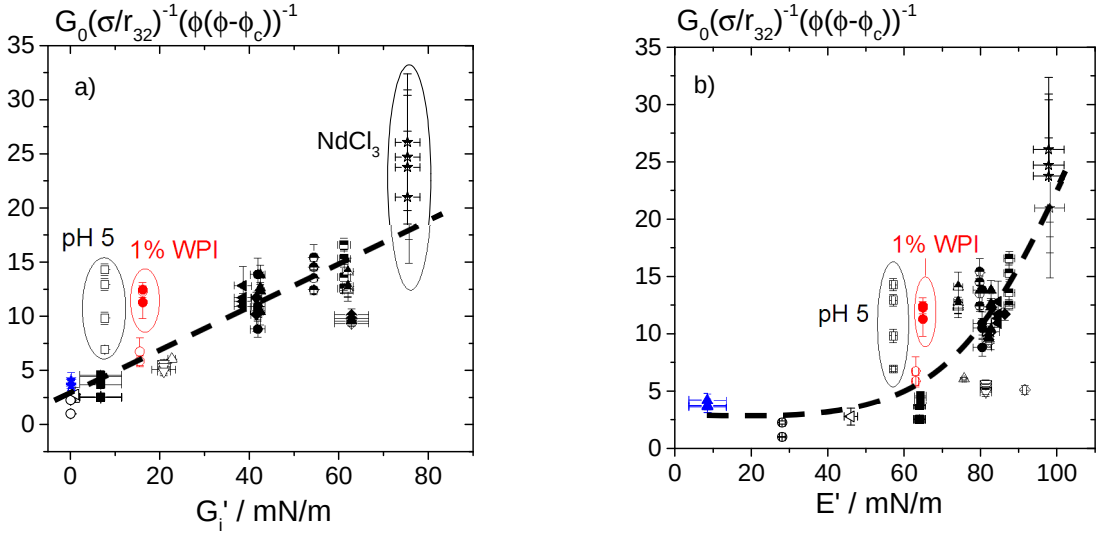

Abbildung 4: *Speichermoduln normiert auf den Laplacedruck (σ/r_{32}) und $\phi(\phi-\phi_c)$ gegen*
a) Speichermodul der Oberfläche in Scherung G_i'
b) Speichermodul der Oberfläche in Dehnung E'
○ pH 3, △ pH 4, □ pH 5, △ pH 6, ◇ pH 8, ▽ pH 9,
pH 6.8 and NaCl: ■ 0 mM, ◆ 10 mM, ▲ 50 mM, ● 80 mM, ▲ 100 mM,
50 mM ⬓ KCl, ▲ NH_4Cl, ◓ LiCl, ◆ $CaCl_2$, ★ $NdCl_3$
○ 0.1% WPI, ● 1% WPI, ▲ 3% casein

Abschließend wurde die Korrelation zwischen dem rheologischen Verhalten von BLG-Schäumen und den viskoelastischen Eigenschaften der Oberfläche in Scherung und Dehnung untersucht. Der pH-Wert der Lösung sowie die Konzentration, Art und Wertigkeit des zugegebenen Salzes wurde systematisch variiert, wodurch gleichzeitig die Schaumrheologie und Oberflächenviskoelastizität in einem großen Bereich variiert wurde. Als charakteristische schaumrheologische Größen wurden der Speichermodul G_0, die scheinbare Fließgrenze τ_y und die kritische Deformation $\gamma_{c,foam}$, welche das Ende des linear viskoelastischen Bereichs

definiert, gewählt. Die Oberflächenviskoelastizität wurde in Scherung und Dehnung charakterisiert. Dazu gehören Scher- und Dehnmoduln G_i‘ und E‘, wie auch die kritische Schubspannung $\tau_{c,surface}$ und Deformation $\gamma_{c,surface}$, welche den Beginn des nichtlinearen Bereichs in oszillatorischen Scherexperimenten kennzeichnen. Im Gegensatz zu den meisten Studien, die bisher veröffentlicht wurden, wurden die viskoelastischen Eigenschaften der Oberfläche bei der gleichen Proteinkonzentration bestimmt wie für die Schaumherstellung verwendet wurde.

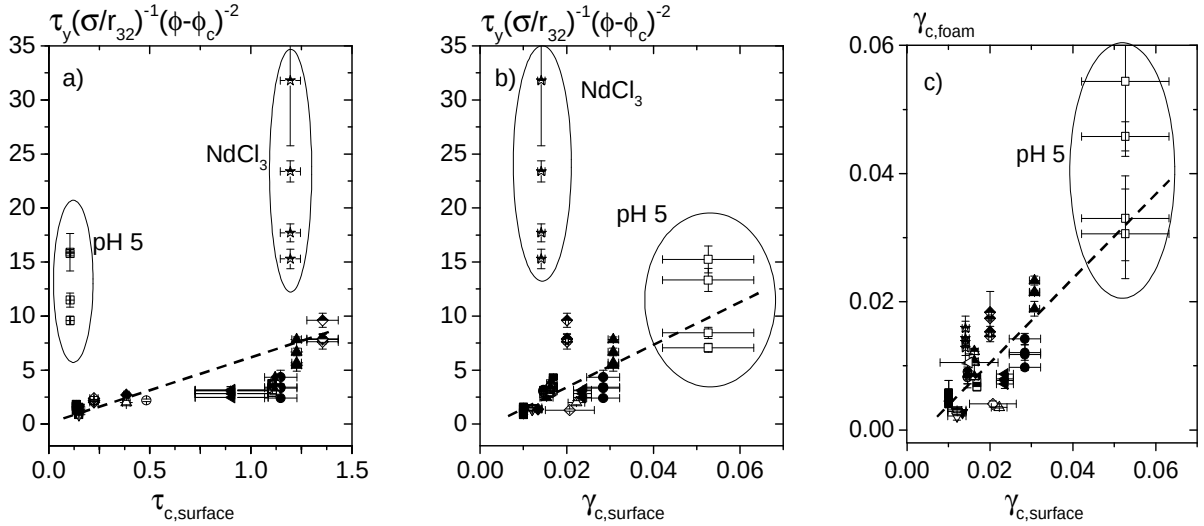

Abbildung 5: *Fließgrenzen normiert auf den Laplacedruck und $(\phi-\phi_c)^2$ gegen*
a) kritische Schubspannung der Oberfläche $\tau_{c,surface}$,
b) kritische Scherdeformation der Oberfläche $\gamma_{c,surface}$
c) kritische Deformation der Schäume $\gamma_{c,foam}$ gegen kritische Deformation der Oberfläche $\gamma_{c,surface}$
○ pH 3, △ pH 4, □ pH 5, △ pH 6, ◇ pH 8, ▽ pH 9,
pH 6.8 und NaCl: ■ 0 mM, ◆10 mM, ▲ 50 mM, ● 80 mM, ▲ 100 mM,
50 mM ▬ KCl, ▲ NH_4Cl, ◓ LiCl, ◆ $CaCl_2$, ★ $NdCl_3$

Über das weithin akzeptierte physikalische Modell hinaus, das den Schaummodul G_0 und die Fließgrenze τ_y aus dem Laplacedruck in den Gasblasen und dem Gasvolumenanteil vorhersagt, hängen diese Größen stark von den jeweiligen Grenzflächeneigenschaften ab. G_0 steigt linear mit G_i’ und sogar stärker mit E′ (Abb. 4), τ_y variiert proportional zu $\tau_{c,surface}$ und $\gamma_{c,surface}$, $\gamma_{c,foam}$ steigt linear mit $\gamma_{c,surface}$ (Abb. 5). Abweichungen von diesen einfachen Abhängigkeiten mit signifikant höheren reduzierten G_0 und τ_y Werten wurden nur für Schäume bei pH 5 und nach Zugabe von trivalentem Salz beobachtet. In diesen Fällen ist auch die Abhängigkeit dieser Größen vom Gasvolumenanteil ϕ ungewöhnlich schwach. Die Befunde deuten auf die Bildung einer aggregierten Proteinnetzwerkstruktur in der Lamelle hin, welche entscheidende

Auswirkungen auf die Schaumeigenschaften hat, an der Grenzfläche jedoch nicht vorzufinden ist.

Es wurde eine eindeutige Korrelation zwischen schaumrheologischen und oberflächenviskoelastischen Eigenschaften gefunden, außer wenn attraktive Wechselwirkungen der Proteine untereinander dominant und wahrscheinlich stark genug sind, um eine Netzwerkstruktur in den Schaumlamellen zu bilden.

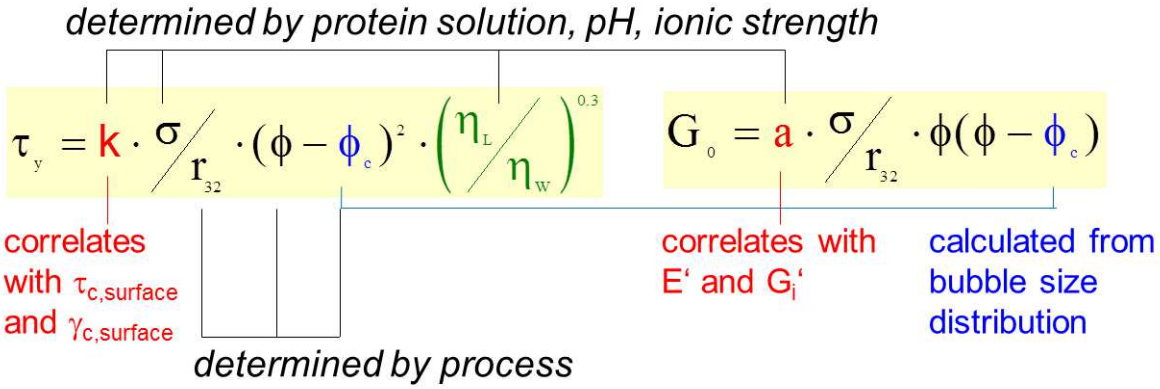

Abbildung 6: *Von Masen et al. ursprünglich vorgeschlagene Gleichungen für die Vorhersage von Fließgrenze τ_y und Speichermodul G_0*

Abb. 6 zeigt die Gleichungen für die Vorhersage von Fließgrenze τ_y und Speichermodul G_0 wie sie in der Literatur vorgeschlagen werden. Wie zuvor erwähnt war es uns möglich, den Wissensstand über die Parameter, die einen Einfluss auf diese rheologischen Größen haben, zu erweitern. Die maximale Packungsdichte ϕ_c wird nicht mehr als Fitparameter behandelt, sondern kann aus der gemessenen Blasengrößenverteilung des zugehörigen Schaums berechnet werden. Ein empirischer Faktor wurde zugefügt, der die Flüssigkeitsviskosität einbezieht, wobei unsere Experimente gezeigt haben, dass diese einen schwachen Einfluss auf die Fließgrenze und keinen Einfluss auf den Speichermodul hat. Die Fitparameter k und a, welche zuvor als numerische Vorfaktoren mit Werten zwischen 0.5 und 1 behandelt wurden, variieren stark für BLG-Schäume ($0.5 < k,a < 30$) und korrelieren mit grenzflächenrheologischen Eigenschaften.

Parameter, die über den Schäumungsprozess gesteuert werden können, sind die Blasengröße r_{32}, der Gasvolumenanteil ϕ sowie die maximale Packungsdichte ϕ_c, währenddessen die Oberflächenspannung σ, die Flüssigkeitsviskosität η_L sowie die Parameter k und a von physikochemischen Eigenschaften der zu schäumenden Lösung abhängen.

Contents

1 Introduction

Liquid foams are concentrated gas dispersions in a liquid with a packing fraction higher than 2/3 where the dispersed gas bubbles are no longer spherical. These jammed systems possess peculiar mechanical properties. The deformation under low stresses is mainly elastic due to capillary effects in the inclined foam films[1]. Above a critical stress, called yield stress, the bubbles are forced to move past each other and the foam flows like a liquid. This special mechanical behavior gives rise to various industrial applications. Foams are used as drilling fluids in oil production or as firefighting agents. They are also used in everyday products, giving a special taste and mouth feel to food products, enhancing the application properties of cosmetics or providing better cleaning properties of detergents. In all these applications rheological properties need to be adapted to meet the according product requirements.
In this chapter we will first give an overview of the basics of rheology and rheometry. We consider peculiarities in foam rheological measurements like wall slip and shear banding. Then we intensively discuss the rheological quantities yield stress and elasticity of foams in terms of their determination as well as the physical parameters determining their rheological properties. Finally, we focus on the correlation between microscopic interfacial phenomena and macroscopic foam behavior.

1.1 Basics of rheology

Rheology describes the flow and deformation behavior of a material exposed to external mechanical stresses. In principal this response can be viscous or elastic. For purely viscous materials, for example water or honey, all of the imposed energy is dissipated. Deformation energy applied to purely elastic materials, for example rubber, is completely stored. Most of the existing materials possess both properties, they behave viscoelastic.
First we will consider the two limiting cases of ideal viscous and ideal elastic behavior. With the help of a parallel plate model (Fig. 1.1) the basic shear rheological parameters can be defined. A homogeneous medium is placed between the two plates with area A and distance *y*. The lower plate is fixed while the upper plate is moved with a constant velocity v. Provided

that the material sticks to the plates it is sheared to the distance *x*. The flow is assumed to be stationary and laminar.

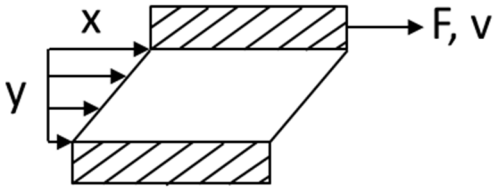

Figure 1.1: *Parallel plate model*

The shear stress σ is defined as the force F acting per area:

$$\tau = \frac{F}{A} \tag{1}$$

The deformation γ_S resulting from the applied shear stress is:

$$\gamma = \frac{x}{y} \tag{2}$$

The slope of the velocity vs. position curve is the velocity gradient $\dot{\gamma}_S$:

$$\dot{\gamma} = \frac{dv}{dy} \tag{3}$$

An imposed stress σ accordingly results in a velocity gradient $\dot{\gamma}$. In the simplest case $\dot{\gamma}$ is constant within the gap and proportional to τ. The proportionality constant η is called shear viscosity.

$$\tau = \eta\dot{\gamma} \tag{4}$$

Materials that exhibit this linear relationship, for example water, honey or glycerol are called Newtonian fluids. For a lot of materials the viscosity is a function of applied shear rate and/or shearing time (Fig. 1.2). They are called non-Newtonian fluids. If the viscosity decreases with increasing shear rate, the material is termed to exhibit shear thinning behavior. If the viscosity increases with shear rate this is named shear thickening or dilatant behavior. The material is called rheopectic or thixotropic if the viscosity reversibly increases or decreases with time, respectively. Another class of materials, called yield stress fluids, esentially behaves like an elastic solid under low stresses and flows like a liquid when a certain critical stress, the yield stress τ_y, is exceeded. Depending on the flow behavior at stresses $\tau > \tau_y$ the material is called Bingham fluid or Herschel-Bulkley fluid if the response is Newtonian or shear thinning, respectively. A wide range of materials like concentrated suspensions, emulsions, foams,

pastes and composites show yield stress behavior. This will be discussed in more detail in chapter 1.4.

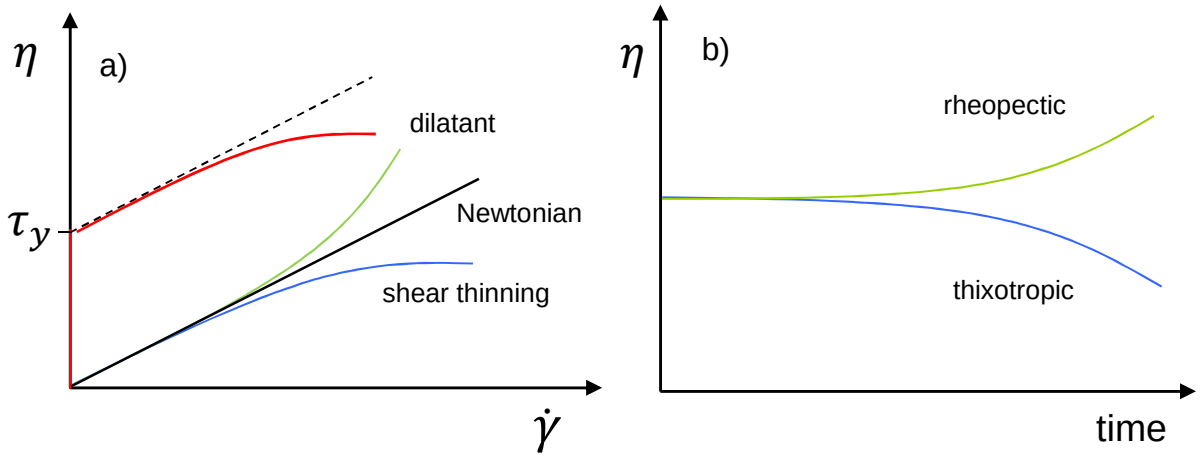

Figure 1.2: *Different flow behavior of materials in dependence of a) shear rate and b) time*

For ideal elastic materials the deformation behavior can be described by Hooke's law:

$$\tau = G\gamma \tag{5}$$

where G is the shear modulus and γ the deformation or strain. After relief of the strain the material relaxes to the initial state without any remaining deformation. This behavior is independent of shear stress and duration of shear load.

Viscoelastic materials possess both, viscous and elastic properties. At constant strain shear stress shows a time dependent decrease and finally relaxes to zero for a viscoelastic fluid or to a finite value for viscoelastic solids. The range in which the resulting stress is proportional to the applied strain is called linear viscoelastic regime (LVE). Strains that exceed this regime lead to a change of the microstructure and to a decrease of the apparent shear modulus. The most commonly used method for characterization of viscoelastic properties are oscillatory shear measurements. A sinusoidal deformation with small amplitude γ_0 and defined angular frequency ω is applied to the material.

$$\gamma = \gamma_0 \cdot \sin(\omega t) \tag{6}$$

The derivative of the deformation with respect to time gives the shear rate:

$$\dot{\gamma} = \omega \cdot \gamma_0 \cdot \cos(\omega t) \tag{7}$$

The response of the shear stress is characterized by the same sinusoidal shape than the input signal with a phase shift δ that is specific to each material:

$$\tau = \tau_0 \cdot \sin(\omega t + \delta) \tag{8}$$

The phase angle δ lies between 0° (ideal elastic solids) and 90° (ideal viscous liquids).
The reduced elastic stress contribution which is in phase with the applied strain is termed storage modulus:

$$G' = \frac{\tau_0}{\gamma_0} \cdot \cos(\delta) \tag{9}$$

whereas

$$G'' = \frac{\tau_0}{\gamma_0} \cdot sin(\delta) \tag{10}$$

characterizes the viscous response which is in phase with the applied strain rate. The storage modulus is a measure of the deformation energy stored in the material, the loss modulus in turn stands for the dissipated energy. Both quantities are used to define the complex shear modulus G*:

$$G^* = G' + iG'' \tag{11}$$

The ratio of loss and storage modulus gives the tangent of the phase angle and is called loss factor:

$$\tan(\delta) = \frac{G''}{G'} \tag{12}$$

Usually the first step in characterizing viscoelastic material properties via oscillatory shear measurements is performing an amplitude sweep, where the deformation amplitude is varied at constant frequency. In this manner the linear viscoelastic regime, where G' and G'' are constant, can be determined (Fig. 1.3).
With the knowledge of the critical deformation γ_c a frequency sweep within the linear viscoelastic regime can be performed at constant deformation amplitude $\gamma_0 < \gamma_c$. This experiment gives information about the time dependent deformation behavior. At low frequencies the microstructure of a material has time to relax the applied stress and the viscous character dominates (G''>G'). At high frequencies materials appear more rigid since stress cannot relax fast enough and hence, the elastic properties dominate (G'>G''). Foams usually exhibit a broad frequency range where elastic response dominates (G'≫G'') and a terminal flow regime with G''>G' is hardly detectable.

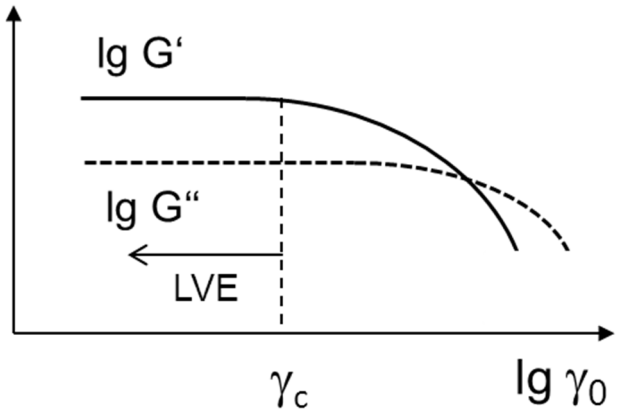

Figure 1.3: *Oscillatory deformation amplitude sweep of G’ and G”*

1.2 Rotational rheometry

Rotational rheometers are widely used for rheological characterization of all kinds of fluids. A manifold of instruments with different specifications is commercially available. These rheometers are either used in a controlled stress or controlled strain / strain rate mode. That means either a torque is applied to the investigated sample and the corresponding angular deflection or speed is measured or vice versa. The torque is related to the stress acting on the fluid via the geometrical specifications of the sample fixture and angular deflection or speed are related to strain and strain rate, respectively. Today most commercial rheometers are stress-controlled devices. Advanced instruments include a sophisticated control loop such that they can be used in a controlled strain mode, too. Basically, rheological measurements are performed in two different modes. The material is either sheared continuously or oscillatory.

Continuous or steady shear measurements are often used to measure the viscosity in dependence of the shear rate, shear strain, shear stress or time. Oscillatory measurements are used to determine the viscoelasticity of materials and the time dependent deformation behavior. There are several fixture geometries used for these measurements briefly described in the next section.

1.2.1 Concentric cylinder / vane geometry

In the concentric cylinder measuring system (Figure 1.4a) a shear gap is generated by placing a bob into a cup, both with the same rotational axis. If the shear gap is small a uniform shear rate can be assumed. Therefore, the ratio between radius of the inner bob R_B and outer cylinder

R_C should be $0.97<R_B/R_C<1$ [2]. There are two possibilities to carry out the measurement. Either the bob rotates (Searle method) or the outer cylinder rotates (Couette method). In both cases the torque acting on the inner bob is measured.

For disperse systems like suspensions, emulsions or foams the required shear gap is given by the particle, droplet or bubble size and hence, the restriction to a narrow shear gap cannot always be met. As a rule of thumb the system can be treated as continuum when the ratio of shear gap to dispersed phase size is at least ten. When adapting the measuring system by increasing the gap width the inaccuracy arising due to varying shear rate across the gap needs to be taken into account.

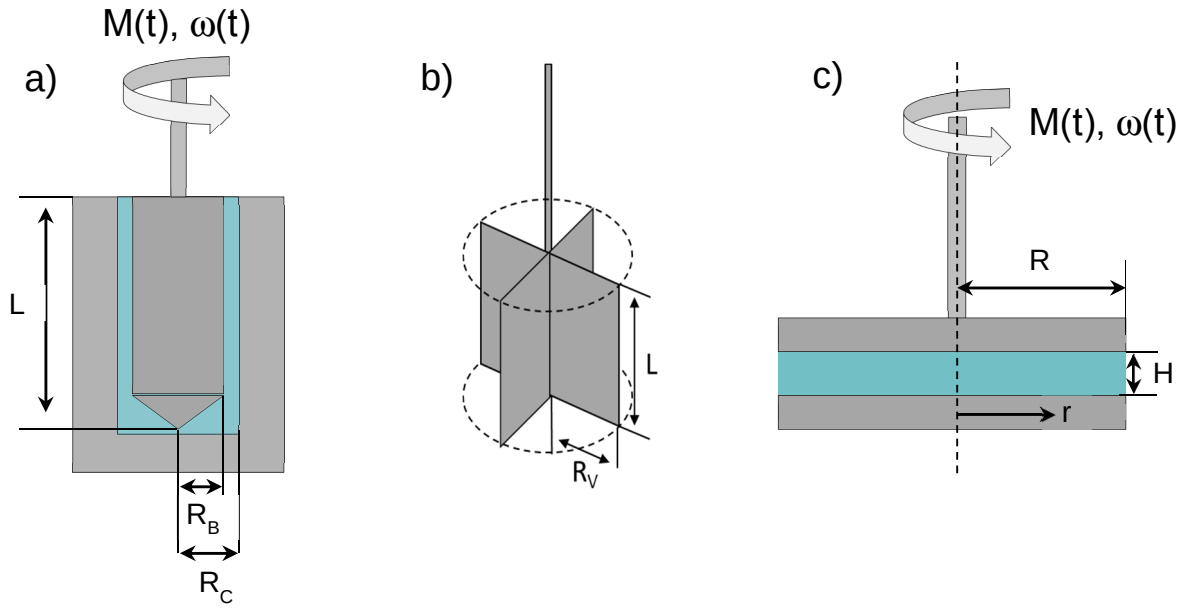

Figure 1.4: *Illustration of (a) concentric cylinder (b) vane measuring system (c) plate/plate*

Consider a sample placed between two concentric cylinders. A rotation of angular frequency ω causes a shear rate $\dot{\gamma}$ at the inner wall that is given by:

$$\dot{\gamma} = 2\omega \frac{R_C^2}{R_C^2 - R_B^2} \tag{13}$$

By measuring the torque M on the bob the shear stress τ can be calculated as follows:

$$\tau = \frac{M}{2\pi R_B^2 L} \tag{14}$$

where L is the immersion length of the bob.

The measured torque has to be corrected for contributions to the fluid deformation at the flat or conically shaped bottom end of the bob. The concentric cylinder system is especially

suitable for low viscosity fluids, as they cannot flow out of the gap and a large area of shear is provided.

Often, the bob is replaced by a vane (Fig. 1.4b) especially for yield stress determination [3-5]. It is tolerant of large particles, droplets or bubbles and most importantly wall slip is avoided. The onset of vane rotation clearly indicates a structural change within the sample. Furthermore, sample damage during loading is reduced due to the thin blade-like profile [6]. The 4-bladed vane is most often used but 2-, 6- or 8-bladed vanes also exist.

For a 4-bladed vane properly filled to the upper edge of the blades the following equation relates the shear stress acting on the fluid at the rim of the vane to the measured torque [5]

$$\tau = M\frac{1}{4\pi R_V^3}\left(\frac{L}{2R_V}+\frac{1}{6}\right)^{-1} \qquad \text{for} \quad {}^{L}/_{R_V} > 4 \tag{15}$$

1.2.2 Parallel plates

In the parallel plate measuring system (Fig. 1.4c) the sample is placed between two plates with a gap width H. One of these plates is moving with angular velocity ω while the other one is fixed. The tangential velocity depends on the radius r and the gap height h:

$$v(r,h) = \omega r\frac{h}{H} \tag{16}$$

The shear rate is given by:

$$\dot{\gamma} = \frac{\omega r}{H} \tag{17}$$

Hence, the shear rate depends on the radial position, it increases from zero in the center to its maximum value at the outer edge.

The shear stress at the rim is related to the torque:

$$\tau = \frac{3M}{2\pi R^3}\left(1+\frac{1}{3}\frac{dln(M)}{dln(\dot{\gamma})}\right) \tag{18}$$

The adjustable gap height makes the parallel plate geometry very useful, especially for the measurement of disperse systems like foams where large bubble radii r_{bubble} require correspondingly large shear gaps ($2r_{bubble} < H/10$) thus permitting evaluation of experimental data within the framework of continuum mechanics.

Another frequently used geometry is the cone and plate system. An advantage of this measuring system is that the shear rate within the gap is constant. However, the cone and plate geometry is not suitable for fluids including large dispersed objects because the continuum approximation is not valid in the vicinity of the gap center.

1.3 Peculiarities in foam rheological measurements

Foams exhibit a complex rheological behavior in various respects very similar to that of highly concentrated emulsions. Accurate determination of the rheological quantities like yield stress or viscosity is often disturbed by phenomena like wall slip, shear localization or shear banding. In general, foams are even less stable than emulsions and foam structure may change during the course of a rheological measurement. Drainage, coalescence and Ostwald ripening are responsible for the thinning and rupture of foam lamellae. Accordingly, average bubble size as well as the gas volume fraction increase with time. Beyond that flow-induced bubble coalescence and structural changes may occur depending on foam stability and have to be considered carefully.

1.3.1 Wall slip

Wall slip occurs due to inhomogeneous fluid properties at a boundary wall that causes a regime with a high shear rate gradient called slipping layer [7]. As a result, the deformation in a rotational rheometer will not be affine anymore and in pipes plug flow will occur [8]. The situation for flow in parallel plates with slip is shown in Fig. 1.5. Wall slip velocities v_{slip} depend on the type of wall material [9] but also on interfacial rheology. Denkov et al. [10] measured the foam wall friction of dry foams (ϕ=0.9) and found different friction laws for foams characterized by different surface elastic moduli.

Wall slip can be detected e.g. by comparing measurements of different geometries or by executing a measurement series using different gap heights. As the width of the slip layer is independent of gap width its relative contribution to the deformation and flow within the gap decreases and the apparent viscosity increases with increasing gap height.

In Fig 1.6 apparent flow curves of a commercial shaving foam measured with different plate materials at different gap heights (3-6 mm) are shown. Sandblasted (almost smooth) plates, a serrated plate and plates covered with sandpaper (grain size around 420 µm) have been used. Obviously, wall slip occurs for the first two measuring systems as the viscosity increases with gap height. When the plate surfaces are covered with sandpaper wall slip can be excluded as the corresponding flow curves do not change with gap height. The yield stress (explained in chapter 1.5) extracted from the data measured with the sandblasted plates is approximately 4-5 times lower than the one measured with sandpaper covered plates clearly showing that large measurement errors can arise when using wrong plate materials.

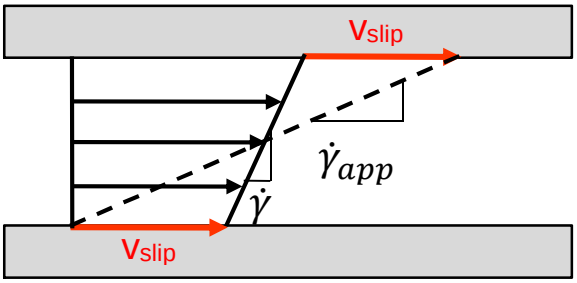

Figure 1.5: *Parallel plate velocity field. The figure shows the velocity field of any particular radius r. The wall slip velocity v_{slip} is the same at each wall. Also shown are the actual shear rate in the fluid $\dot{\gamma}$ determined from the gradient of the linear velocity field and the apparent shear rate $\dot{\gamma}_{app}$ calculated from the relative velocity of the plates without knowledge of the slip layer. Picture redrawn from [11].*

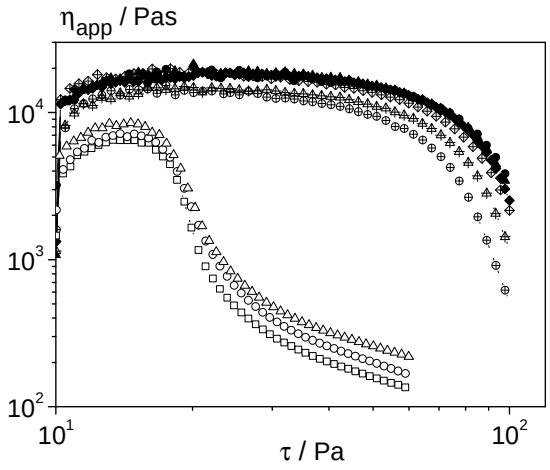

Figure 1.6: *Apparent viscosity of a commercial shaving foam (Balea Men, Mann & Schröder GmbH) versus shear stress measured with a plate/plate set-up using different plate materials and gap heights. Sandblasted plates (open symbols), upper plate serrated/ lower plate sandpaper (crossed symbols), sandpaper attached to both plates (closed symbols). Gap height: ■ 3 mm, ● 4 mm, ▲ 5 mm, ◆ 6 mm*

True shear rates can be calculated with the help of the Mooney-correction, which assumes that the slip velocity v_{slip} only depends on the shear stress at the wall ($v_{slip} \sim \tau$) [12], or the Oldroyd-Jastrzebski method, which assumes that v_{slip} depends not only on the wall stress but also on the pipe diameter ($v_{slip} \sim \tau/H$) [13]. The different methods have been compared to measurements with grooved plate surfaces where wall slip could be excluded for foams made from surfactant mixtures [14]. Fig. 1.7 demonstrates that neither of these correction methods retrieves the true flow curve for this surfactant foam and similar results have been reported

earlier [15,16]. Hence, it is recommended to avoid or minimize wall slip using fixtures with appropriate roughness and selecting a large enough gap width [14,17].

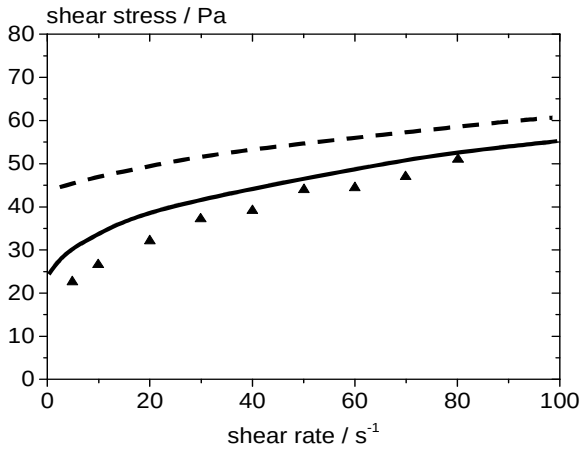

Figure 1.7: *Shear stress versus shear rate for a foam containing 2% of surfactant dissolved in an aqueous solution of 2.5 g/l of Xanthan, 1 g/l of Aquapac regular (anionic cellulose), and 0.5 g/l of NaCl adjusted to pH 9: (▲) experimental data obtained with grooved plate surfaces ($\dot{\gamma}_S$= 5 – 120s^{-1}), (---) data computed with Mooney hypothesis, (–) data computed with Oldroyd–Jastrzebski hypothesis. Data taken from [14].*

1.3.2 Shear banding and shear localization

Shear banding and shear localization often occur in yield stress materials like granular matter, concentrated emulsions, suspensions or foams. In both cases undeformed and sheared regions coexist [18] but these two phenomena differ with respect to the velocity profile in the shear gap.

Shear banding refers to the case where the velocity changes drastically within a narrow region at a critical position inside the gap. The shear rate exhibits a discontinuity at this position. The origin of shear banding is not understood so far. However, shear banding of foams has been reported upon shear start-up [19] and during continuous shear [20] in dry foams. The latter experiments were carried out in a parallel plate rheometer with rough surfaces. The measured velocity profile inside the gap is shown in Fig. 1.8. Clearly, two regimes with different shear rates evolve indicating shear banding behavior.

In the case of shear localization the sheared and unsheared regions evolve due to an inhomogeneous stress distribution across the shear gap like it is found in Couette flows. But the transition from the sheared to the unsheared region is supposed to be continuous and the shear rate decreases gradually to zero. Consider a yield stress material in a wide gap Couette rheometer with the shear stress decreasing as $\tau \sim \frac{1}{r^2}$ where r is the radial coordinate.

At stresses below the yield stress, i.e. at positions at which $\tau < \tau_y$ the material will not flow. With increasing applied stress the material in the vicinity of the rotating bob will start to move because in this region the yield stress is already exceeded, but due to the inhomogeneous stress distribution the applied stress close to the outer cylinder wall is still below the yield stress and the material will not flow there. The sheared region will become larger with increasing applied stress until eventually the yield stress is exceeded in the whole gap [18,21]. Plug flow of pasty materials is a well-known example for shear localization [22].

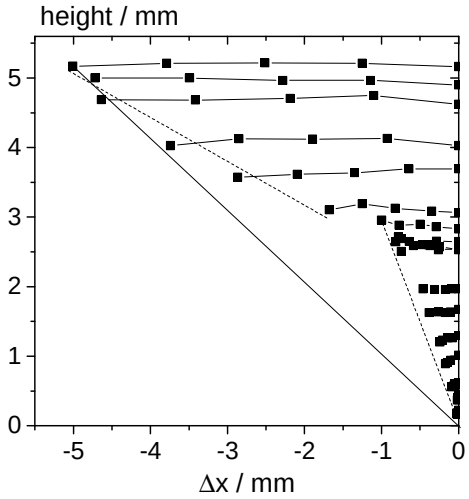

Figure 1.8: *Velocity profile of a surfactant foam in a plate-plate rheometer at a gap height of 5 mm and constant shear rate $\dot{\gamma}$= 0.2 s^{-1} [20].*

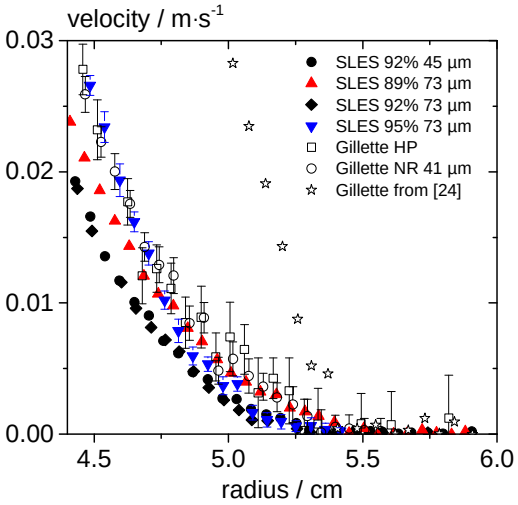

Figure 1.9: *Velocity profiles of foams obtained in a Couette geometry (R_B=4.1 cm, R_C=6 cm and L=11 cm) using magnetic resonance imaging (MRI) [23] and [24]. Two commercial foams (Gilette HP, NR) and four surfactant foams made from a sodium lauryl ether sulfate (SLES) solution but differing in gas volume fraction and bubble size as indicated in the legend.*

Ovarlez et al. [21] observed a continuous decrease of $\dot{\gamma}(r)$ finally approaching zero within the experimental resolution at a distance r = r_{yield} corresponding to the position at which $\tau = \tau_y$ (Fig. 1.9) for surfactant foams with either rigid or mobile interfaces steadily flowing in a wide gap geometry much larger than the bubble size. Obviously, these foams behave as simple yield stress fluids without shear banding behavior. Note that in Fig. 1.9 there are also data plotted from Rodts et al. [22] where shear banding behavior was found for the same commercial shaving foam as used by Ovarlez et al. The authors speculate that the foams used by Rodts et al. contained small impurities like solid particles which can lead to thixotropic effects and induce shear banding. This phenomenon is well-known for densely packed emulsions [25].

1.4 The yield stress

Foams, especially in the dry limit $\phi \rightarrow 1$, are densely packed, jammed systems [26]. They do not flow and deform elastically under stresses below a critical value called yield stress. If this critical value is exceeded, the microstructure, consisting of many interacting bubbles, is forced to rearrange [27] and the foam begins to flow. The yield stress is often defined as the minimum stress that is needed to make a material flow [4,28]. However, the existence of a true yield stress in such soft matter is controversial. Barnes et al. [29,30] for example claim that all fluids that flow under high shear stresses would do so under low stresses. The viscosity would always possess a finite value and it is just a question of measuring technique to determine it in the low stress regime. Other studies [31,32] argue that the yield stress is an “engineering reality” and many fluids exhibit a drastic orders of magnitude drop in viscosity within a narrow range of applied stresses. Even if it may not be a true material constant, it is a useful measurable quantity characterizing processing and application properties also of foam systems [33]. But it should be kept in mind that the absolute value of a measured yield stress not only depends on the material but may be strongly influenced by the type and time scale of sample load and deformation.

In the case of foams the yield stress σ_y is considered as the point where the bubbles start sliding past each other. The bubble rearrangement scheme as proposed in a pioneering work of Princen [34] is shown in Fig. 1.10. Stresses $\tau < \tau_y$ deform the bubbles but do not induce a structure change. When the stability limit is exceeded ($\tau \geq \tau_y$) the bubbles reorient as depicted in Fig. 1.10d.

In real foams bubble rearrangements are additionally induced by destabilization processes like disproportionation, drainage and coarsening.

There are several methods to determine a yield stress value. The most common ones are explained in the following.

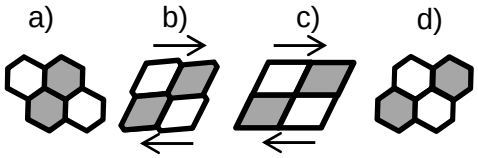

Figure 1.10: *Shear induced bubble rearrangement: a)τ=0, b) $\tau < \tau_y$, bubbles get deformed but no structure change is induced. After release of the stress the bubbles would go back to their initial position, c) $\tau \approx \tau_y$: hexagonal structure turns into a tetragonal structure, stability limit is reached, d) $\tau > \tau_y$: bubbles retain their hexagonal structure and reorient.*

1.4.1 Creep test

In a creep experiment (Fig. 1.11a) a certain stress is applied to the material and the strain response is observed over time. If the strain attains a constant value γ_e, the applied stress is lower than the yield stress. If the strain increases infinitely to eventually reach a constant shear rate $\dot{\gamma}_e$, the yield stress is exceeded. These creep tests can also be applied in series by increasing the stress continuously. The time for this stress ramp has to be selected with respect to the relevant process and material. The resulting strain curve $\gamma(\tau)$ (Fig. 1.11b) can be divided into two regions with different slopes. In the first part the slope is close to one and deformation is only small. In the second part the slope drastically increases indicating the onset of flow. Either the intersection of the tangents of the two regions $\tau_{y,S1}$ or the first point that belongs to the second region $\tau_{y,S2}$ can be selected to characterize the yield stress.

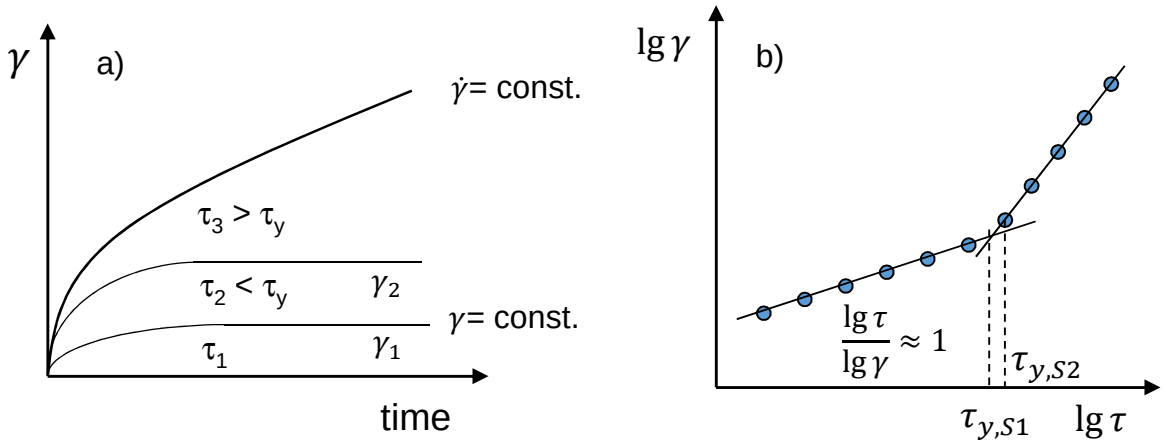

Figure 1.11: *Determination of yield stress by a) creep tests, b) continuously increasing stress*

In real foams the transition between the two regions is not always as sharp as depicted in Fig. 1.11b, instead there is a transition zone in between. Fig. 1.12 shows a deformation versus shear stress curve for a surfactant and a protein foam, respectively. Video recordings have been used to determine the point where the bubbles started sliding past each other. In Fig. 1.12 this stress value has been marked with a circle. For the surfactant foam (Fig. 1.12b) the transition zone is narrow so that $\tau_{y,S1} \approx \tau_{y,S2}$. In contrast, the transition zone for the WPI foam (Fig. 1.12b) spans over a relatively wide range of shear stresses so that $\tau_{y,S1} \approx 2\tau_{y,S2}$. The inserts in Fig. 1.12 showing a magnification of the transition zone indicate that $\tau_{y,S2}$ seems to be closer to the point where bubbles start to slide past each other.

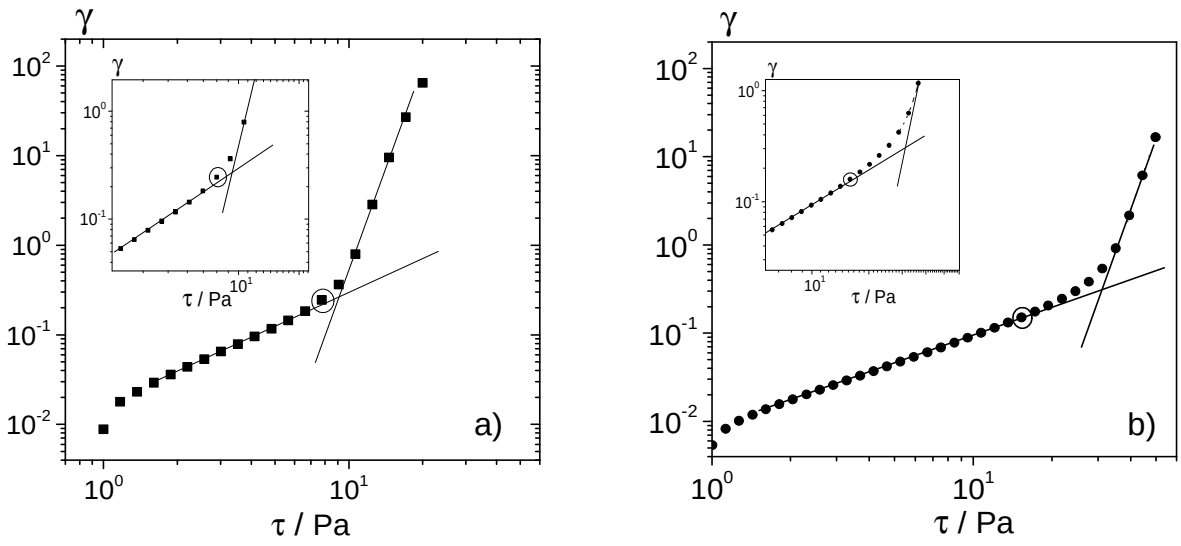

Figure 1.12: *Deformation versus shear stress for a) surfactant foam (2% Triton X-100, 0.2% SDS in water), b) 1% whey protein isolate (WPI) foam. The circles mark the yield point that is visually observable from video recordings of the shear gap and the inserts show a magnification of the transition zone.*

Another protocol for yield stress determination in rotational rheometry is to apply a very slow, constant flow rate and to observe the stress response. The stress increases to a maximum (the yield stress) before it reaches a steady state value [35]. The inclined plane method is another approach to determine the yield stress [36]. Here, a foam is placed on a plane which can be inclined to different angles. From the angle where flow is visually observed, the yield stress can be calculated.

1.4.2 Oscillatory amplitude sweep experiments

An alternative way to access the yield stress can be found in oscillatory amplitude sweep measurements. The stress amplitude is increased while the frequency is kept constant. The end of the LVE is coupled with the onset of flow. The behavior well above and well below the yield stress can be described by power laws corresponding to straight lines in a logarithmic plot as shown schematically in Fig. 1.13. Some authors define the intersection of these lines as yield stress $\tau_{y,i}$ [36-38]. For emulsions and some foams this is a robust and reproducible method. But not all foams show these two well defined deformation regimes (see Fig. 1.14). The crossover of G' and G'' can also be defined as yield stress $\tau_{y,c}$ because this is the point where the viscous properties start to dominate over the elastic ones. For foams it has been reported in several studies that yielding occurs before the crossover point is reached and $\sigma_{y,c}$ does therefore not seem to be an appropriate value [36,38,39].

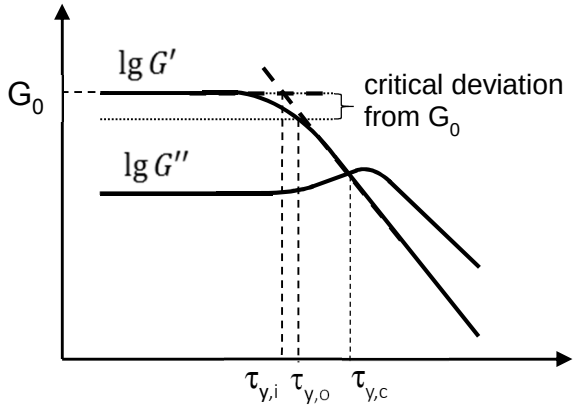

Figure 1.13: *Yield stress determination from oscillatory stress amplitude sweep experiments*

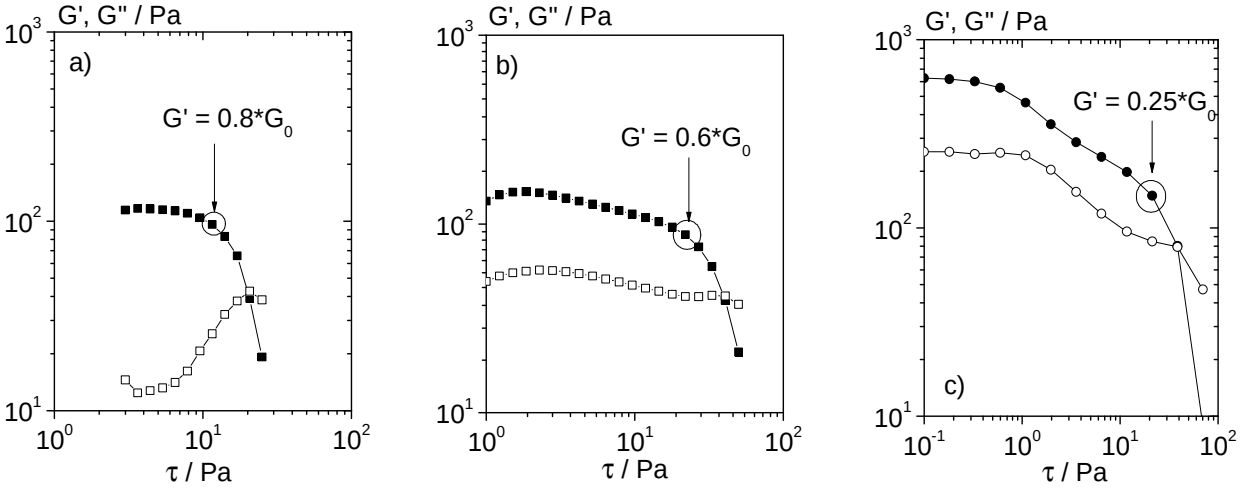

Figure 1.14: *Storage (closed symbols) and loss moduli (open symbols) versus shear stress amplitude at f = 1Hz for a) surfactant foam (2% TX-100, 0.2% SDS), b) 5% casein foam and c) 1% whey protein isolate foam. The circles mark the yield point that is visually observable from video recordings of the shear gap.*

The stress amplitude at which a certain deviation from the plateau value of G' occurs may also be defined as yield stress $\tau_{y,o}$. However, it is not possible to specify a unique deviation criterion that applies for a broad variety of foams. Hence, it is recommended to visualize the bubbles inside the shear gap during the measurement to find an appropriate method for yield stress determination corresponding to the onset of bubbles sliding past each other in a given foam system.

1.4.3 Comparison of yield stresses determined from rotational and oscillatory measurements

Comparison of foam yield stresses determined via different methods is not well discussed in literature since a broad data basis is still lacking. However, Rouyer et al. [36] gathered data from different sources where foam and emulsion yield stresses have been measured by steady (inclined plane method or measurement of the stress response under low shear rate) and oscillatory ($\tau_{y,i}$) shear experiments as shown in Fig. 1.15a. The yield stresses are normalized by G_0 and as both quantities depend on (σ/r_{32}) effects of bubble size and polydispersity can thus be excluded. All data collapse on a master curve with exception of the steady shear experiments of the emulsions carried out by Mason et al. [37]. This deviation was attributed to shear banding phenomena. Shear banding or foam fracture may occur at different shear stresses due to the different kind of deformation that is applied to the foam in oscillatory and steady shear thus leading to different apparent yield stress values. This comparison does not comprise a large variety of foams and therefore it is not yet clear whether the observed agreement is generally valid.

In Fig. 1.15b yield stress values $\sigma_{y,c}$ determined from oscillatory shear measurements are plotted versus $\sigma_{y,S2}$ determined from steady shear measurements for different protein and surfactant foams. The yield stress determined from the crossover of G' and G'' is always approximately 1.5 times higher than $\tau_{y,S2}$. This correlation is useful since this crossover can be determined in a straightforward and highly reproducible manner. But it has to be kept in mind that large deviations are found for β-lactoglobulin foams containing 50 mM of the divalent salt $CaCl_2$, 100 mM NaCl and at pH 5. Under these conditions protein aggregates occur more frequently and substantially different microstructure within the lamellae could lead to differences in the deformation response to oscillatory and steady shear as already mentioned above.

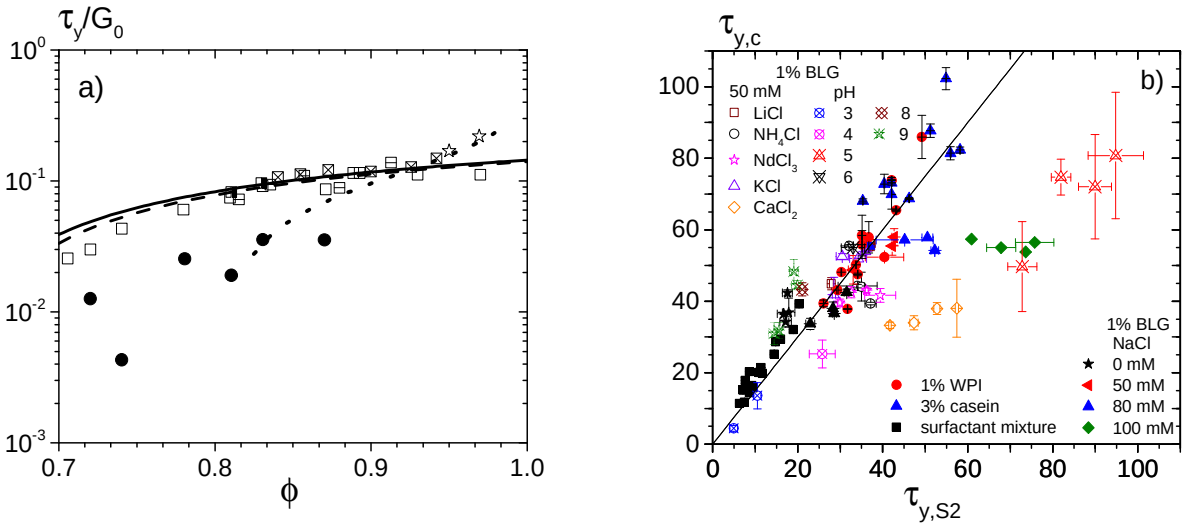

Figure 1.15: *a) Yield stress normalized by elastic shear modulus vs. volume fraction. Comparison of data from Princen and Kiss [17,40] (dotted line), Saint-Jalmes and Durian (oscillatory) [38] (continuous black line), Khan et al. [35] ★, Mason et al. [37]: oscillatory □ and steady shear ● experiments. Rouyer et al. [36]: Gillette foam for oscillatory ⊟ and inclined plane ◨ measurements, TTAB foam (oscillatory) ⊠. The dashed line corresponds to the curve: $\tau_y/G_0 = 0.39(\phi-\phi_c)/\phi$.*

b) Yield stresses determined from oscillatory shear measurements $\sigma_{y,c}$ versus yield stresses determined from rotational shear measurements τ_{S1} 1% BLG foams containing different amounts of NaCl and 50 mM of different kind of salt (more information in ref. [41]), 1% whey protein isolate (WPI) foams, 3% casein foams and foams made from a surfactant mixture containing 2% TX-100 and 0.2% SDS (more information in ref. [29]). The continuous straight line corresponds to $\tau_{y,c} = 1.5\tau_{y,S1}$

1.4.4 Prediction of yield stress

Various studies have confirmed that the yield stress of so-called liquid foams including a low viscosity of the continuous phase depend on the average bubble size, the surface tension the gas volume fraction and the liquid viscosity [29,37,39,40,42] as

$$\tau_y = k \cdot \left(\frac{\sigma}{r_{32}}\right) \cdot \left(\frac{\eta_L}{\eta_W}\right)^{0.3} \cdot (\phi - \phi_c)^2 \qquad (19)$$

where σ is the surface tension, r_{32} the Sauter mean radius, ϕ the gas volume fraction and ϕ_c represents the maximum packing fraction of the bubbles before they start to deform into non-spherical shapes. This is the point where the system becomes jammed so that small stresses result in an elastic deformation and a minimum stress is needed to move the bubbles past each other. Usually, ϕ_c has been an estimated value [38,43] but can also be calculated from the

measured bubble size distribution, as proposed by [29]. They used an empirical model equation established by Sudduth et al. [44]. The equation is based on a large number of experimental data for suspensions of non-Brownian particles. This restriction to undeformable spheres is not as serious constraint here since even the gas bubbles in foams at such low gas volume fractions are essentially spherical. The maximum packing fraction ϕ_c is calculated from the size distribution of the suspended particles. Assuming a n-modal discrete distribution results in Eq. 20, where $\phi_{c,mono}$ is the maximum packing fraction of a monodisperse suspension ($\phi_{c,mono}$ = *0.63)* and r_x is the x-th moment of the particle size distribution.

$$\phi_c = \phi_n - \left(\phi_n - \phi_{c,mono}\right) exp\left(0.271 - \left(1 - \frac{r_5}{r_1}\right)\right) \tag{20}$$

with $\phi_n = 1 - \left(1 - \phi_{c,mono}\right)^n$ and $r_x = \frac{\sum_{i=1}^{n} N_i r_i^x}{\sum_{i=1}^{n} N_i r_i^{x-1}}$

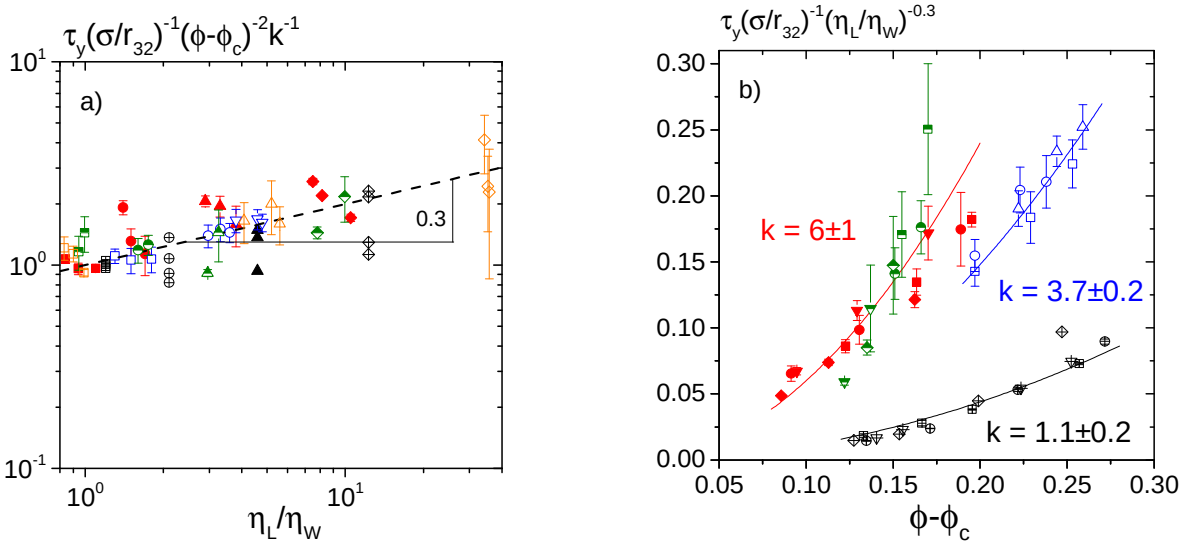

Figure 1.16: *a) Apparent yield stress τ_y normalized by Laplace pressure (σ/r_{32}), (ϕ-ϕ_c) and k vs. viscosity ratio (η_L/η_W)*

b) apparent yield stress τ_y normalized by Laplace pressure (σ/r_{32}) and solution viscosity ratio (η_L/η_W) vs. ϕ-ϕ_c for foams made from different proteins and a surfactant mixture, vertically halved symbols: 1%WPI dissolved in various water glucose mixtures, closed symbols: 1% WPI, semi-closed symbols: 0.1% WPI, open symbols: casein and crossed symbols: surfactant mixture dissolved in various water/glycerol mixtures (glycerol or glucose content ■0%,●20%,▼30%, ▲40%, ◆60%).

The prediction of the yield stress also includes an empirically determined factor for the (weak) contribution of the liquid viscosity, where η_L is the continuous phase viscosity and η_w the water viscosity at same conditions. This phenomenological extension of the model equation proposed by Lexis et al. [29,42] has been derived from measurements on foams made from casein, whey protein isolate and a mixture of synthetic surfactants (Fig 1.16a). The solvent viscosity was varied using different water / glycerol mixtures and sugar solutions.
Furthermore, the equation includes a numerical pre-factor *k* that varies depending on the kind of adsorbed amphiphile molecule at the interface (Fig. 1.16b) In the literature k-values between 0.5 and 30 are found [29,37,41,45]. In [41] it was shown that these k-values are directly correlated with interfacial viscoelastic properties what will be discussed in chapter 1.7 in more detail.

1.5 Flow behavior of foams under steady shear

In Fig 1.17a flow curves of surfactant foams are shown. All curves possess an almost constant apparent viscosity η_{app} at low stresses $\tau < \tau_y$ followed by a drastic decrease of η_{app} in a narrow range of shear stresses around $\tau \approx \tau_y$. For $\tau > \tau_y$ the foams behave as shear thinning liquids. The apparent viscosity below the yield stress is a result of bubble coalescence and rearrangement resulting in a motion of the upper plate [46,47]. For a given foam system this quantity also depends on measuring parameters like initial and final stress of the measurement or the measurement time per data point. In Fig. 1.17b it can be seen that at stresses far below the yield stress ($\tau \ll \tau_y$) of η_{app} increases over time. The reason therefor is that the coalescence rate decreases with time due to decreasing number of separating lamellae [29]. For stresses close to but still below the yield stress ($\tau > \tau_y$) the foam starts to flow after a certain time period, for the example shown in Fig. 1.17b after 160 s. This happens because the absolute value of the yield stress ($\tau_y \sim \frac{1}{r_{32}}$) of a foam decreases with foam age because the average bubble size increases and the distribution broadens with time. For $\tau > \tau_y$ the apparent viscosity decreases over time due to (shear induced) coalescence of the bubbles.

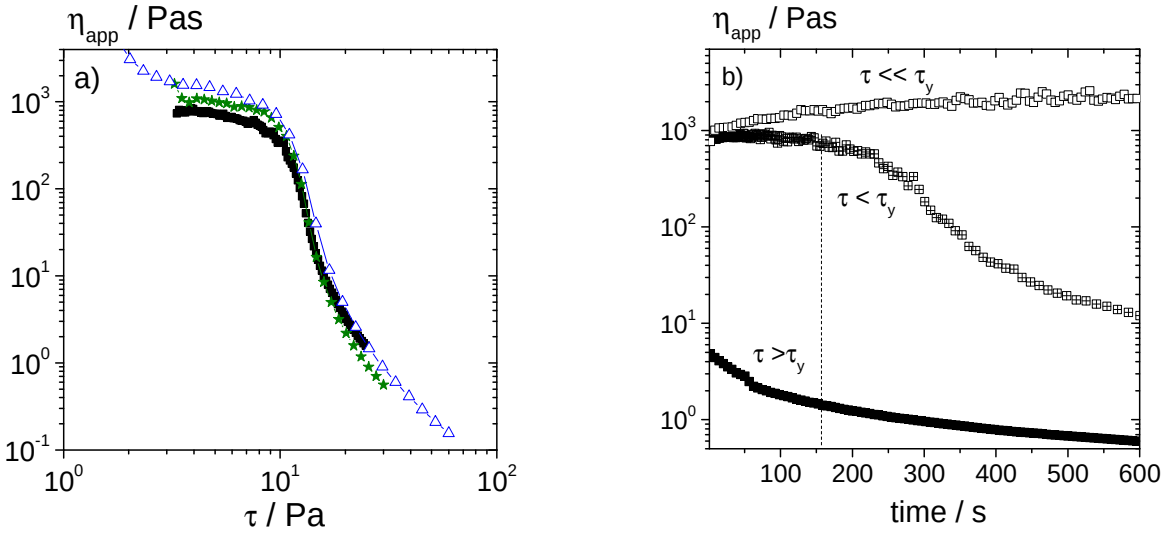

***Figure 1.17**: a) apparent viscosity versus shear stress for a foam made from a surfactant mixture (2% TX 100, 0.2% SDS) dissolved in water under different measurement conditions at a constant measurement time of 60 s: ■ shear stress continuously increasing from 3-25 Pa, ★stepwise increase of shear stress from 3-30 Pa (2 s per data point), △ stepwise increase of shear stress from 1-60 Pa (2 s per data point),*

b) creep tests for the same surfactant foam with $\sigma \ll \sigma_y$ at 1 Pa (open symbols), $\tau < \tau_y$ at 8 Pa (crossed symbols) and $\tau > \tau_y$ at 20 Pa (closed symbols), b) Data taken from [94]. All measurements were carried out with a plate/plate rheometer.

Beyond the yield stress foams flow as shear thinning fluids well described by a phenomenological Herschel-Bulkley law:

$$\tau = \tau_y + \tau_v(\dot{\gamma}) = \tau_y + k_v\dot{\gamma}^n \qquad (21)$$

Where τ_y is the yield stress, k_v the foam consistency and n a power law index. The term $\tau_v(\dot{\gamma})$ is the rate dependent fraction of the total stress which is estimated as $\tau(\dot{\gamma}) - \tau_y$ and scales as σ/r_{32} [1,10,17]. The index $n < 1$ is a characteristic of the shear-thinning behavior of foams and depends on the specific mechanism of viscous dissipation during flow. Denkov et al. [1,10,48] found the exponent n to depend on surface mobility and viscoelasticity. For different surfactant foams ($0.88 \leq \phi \leq 0.95$) they found $n \approx$ ½ in the case of mobile interfaces (low surface modulus E^* of a few mN/m) and $n \approx$ ¼ in the case of rigid interfaces ($E^* > 60$ mN/m) as depicted in Fig. 1.18.

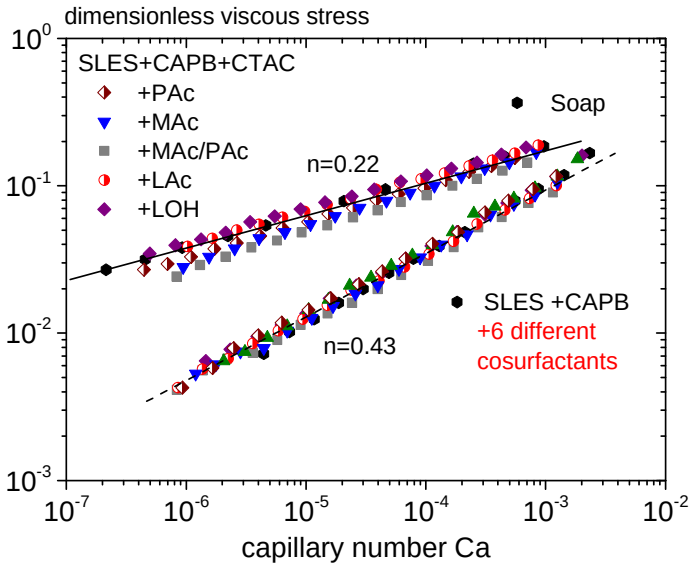

Figure 1.18: *Dimensionless viscous stress $\tau_v(\dot{\gamma})/(\sigma/r_{32})$ vs. capillary number $Ca = \eta\dot{\gamma}r_{32}\sigma$ for foams stabilized by SLES + CAPB mixture (0.33 + 0.17 wt%), without and with different cosurfactants added (0.02 wt%), which differ in their headgroups and for foams made from soap solution (mixture of potassium salts of fatty acids, pH = 10.2). The lines represent power law behavior with indices n as given in the figure. Data taken from [1].*

1.6 Storage and loss modulus

1.6.1 Plateau modulus

When small stresses below the yield stress are applied to foams the response is linear viscoelastic and the storage modulus G' which represents the elastic behavior is usually found to be much higher than the viscous modulus G''. The elasticity arises from the interfacial energy density ($\approx \sigma/r_{32}$) [49].

At low frequencies between 0.1 and 10 Hz the storage modulus is usually frequency independent, it is therefore often denoted as plateau modulus G_0 and can be predicted as

$$G_0 = a \cdot \left(\frac{\sigma}{r_{32}}\right) \cdot \phi(\phi - \phi_c) \qquad (22)$$

where r_{32} is the average Sauter radius, γ the surface tension, ϕ the gas volume fraction and ϕ_c the critical gas volume fraction (see chapter 1.4.4). The pre-factor *a* varies for different foaming systems (Fig. 1.19). Values between 0.5 and 30 have been reported, depending on interfacial rheological properties [29,41,43,45]. This will be discussed in more detail in chapter 1.7.

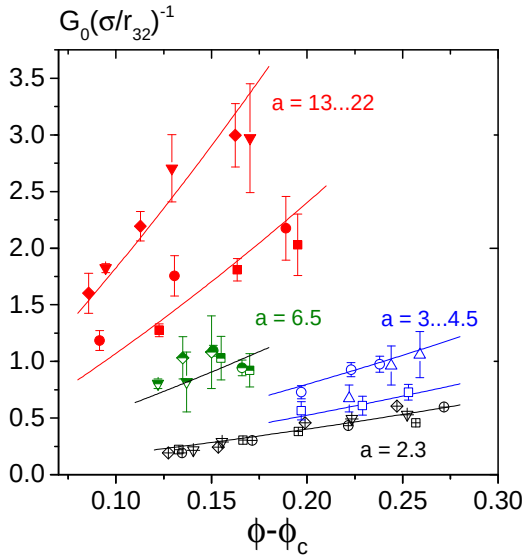

Figure 1.19: *Plateau moduli normalized by Laplace pressure vs. ϕ-ϕ_c for foams made from 1% WPI (closed symbols), 0.1% WPI (semi-closed symbols), casein (open symbols) and surfactant mixture (crossed symbols) dissolved in various water/glycerol mixtures (glycerol content ■0%, ●20%, ▼30%, ▲40%, ◆60%)*

1.6.2 Variation of frequency

The frequency dependence of the complex modulus *G** for jammed systems is described by the following scaling law:

$$G^*(f) = G_0\left(1 + \sqrt{\frac{if}{f_c}}\right) + 2i\pi\eta_\infty f \qquad (23)$$

where G_0 is the plateau modulus (Eq. 22), f_c the characteristic relaxation frequency and η_∞ the fluid viscosity in the limit of high frequency. This prediction has been confirmed experimentally in various investigations on foam systems [49-51]. The characteristic relaxation frequency is assumed to be proportional to the ratio of the dilational modulus E' and an effective interfacial viscosity including the surface viscosity E''/f_c, the solution viscosity and the lamellar thickness as well as the bubble diameter [50]. Different scaling laws relating f_c to the foam modulus G_0 are predicted for rigid and mobile interfaces. This was confirmed experimentally for two different types of surfactant foams with E'= 67 mN/m and E' ≤20 mN/m as shown in Fig. 1.20.

For foams with even higher interfacial rigidity (E^* ≥100 mN/m) it was shown that G* cannot be described by Eq. (23) in the whole frequency range and for each bubble size anymore, above 10 Hz $G'' \sim f^{\Delta}$ with $\Delta < ½$ was found. This deviation becomes more pronounced with increasing interfacial rigidity and increasing bubble size [49].

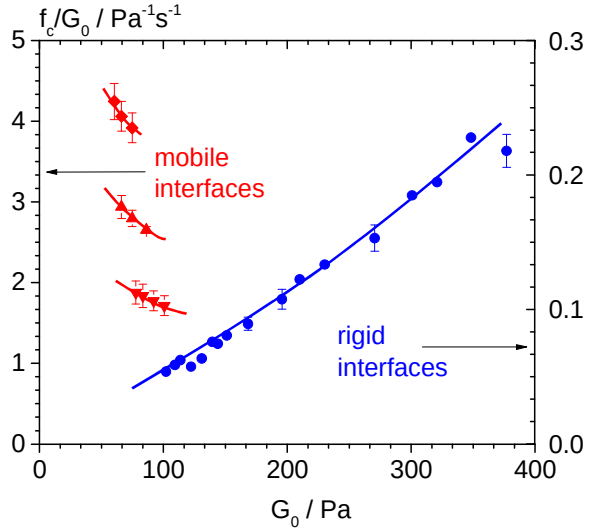

Figure 1.20: *Scaled characteristic frequency f_c/G_0 of the collective bubble relaxation mode versus the elastic modulus G_0: ● Gilette shaving foam, ◆ SLES (sodium lauryl ether sulfate) 40% glycerol, ▲SLES 50% glycerol and ▼ SLES 60% glycerol foams. Data taken from [50].*

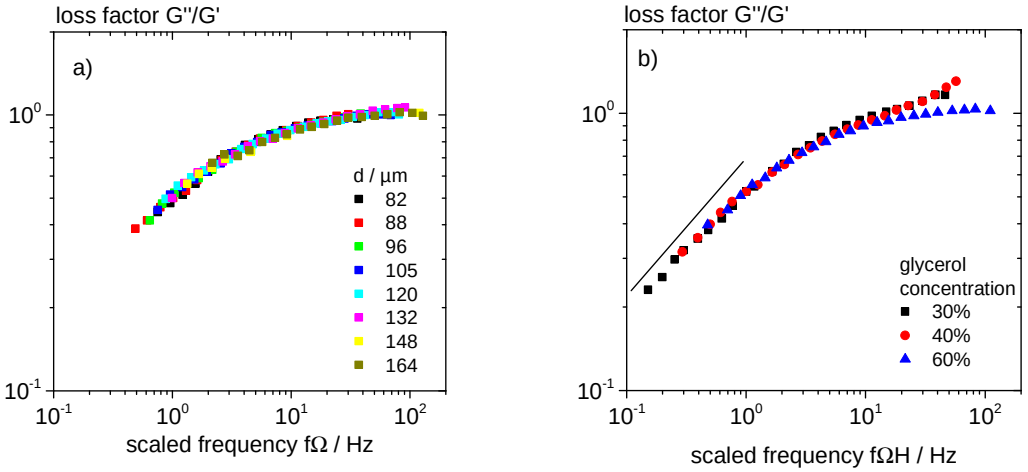

Figure 1.21: *Loss factor of SLS-CAPB-LOH (sodium lauryl-dioxyethylene sulfate - cocoamidopropyl betaine – lauryl alcohol) foams versus scaled frequency a) for different bubble sizes (d_{ref}=132 µm, E^*= 132 mN/m, η=10.5 mPas). The continuous line represents Eq. (24) with the best fitted parameters f_c=0.2 s^{-1}, η_∞= 0, b) for different continuous phase viscosities (η = 2.5-10.5 mPas, E^*= 88-132 mN/m, d_{ref}= 133 µm and η_{ref}= 10.5 mPas). d varies between 80 and 160 µm. The straight line has a slope = ½ and is a guide to the eye. Data taken from [49]*

More insight into relaxation mechanisms and how they are affected by bubble size and continuous phase viscosity is gained from the loss factor G''/G'. The curves for foams with

moderate interfacial rigidity ($100 < E^* < 130$ mN/m) were found to collapse on a master curve when the frequency is rescaled by a factor $\widetilde{\Omega}(d,\eta)$ (Fig. 1.21a,b).

$$\widetilde{\Omega}(d,\eta) = \Omega(d)H(\eta) = \left(\frac{d}{d_{ref}}\right)^2 \frac{\eta}{\eta_{ref}} \quad (24)$$

For foams with $E^* > 130$ mN/m there is more than one characteristic frequency of viscoelastic response and no master curve could be found so far.

1.6.3 Variation of shear stress amplitude

Depending on the type of adsorbed molecule at the interface, G' and G'' can show different behavior in dependence of applied shear stress amplitude as shown in Fig. 1.14 exemplary for different aqueous foaming systems containing either 1% whey protein isolate (WPI), 3% casein or a surfactant mixture (0.2% SDS, 2% Triton X-100). More details about these foams can be found in [29]. All systems show a linear regime with G'>G'' at low stress amplitudes and a flow regime with G''>G' at high stress amplitudes. For the casein system there is a sharp transition between both regimes but for the WPI and the surfactant foams a third regime can be distinguished between linear viscoelastic and flow regime. For the former the moduli decrease simultaneously and for the latter G' decreases while G'' increases before crossing. The 1% WPI foams exhibit high storage modulus values at very low stress amplitudes. In [29] it was concluded that the whey proteins build a network across the lamella that causes such high moduli. Intermediate stress amplitudes probably destroy this network without moving the bubbles past each other and hence, G' decreases but is still higher than G''. The increase in G'' for the surfactant foams can be explained as follows. As the stress amplitude is applied some of the foam films get stretched while others are being compressed leading to regions with lower and regions with higher surfactant concentrations. In order to equilibrate this imbalance, a Marangoni flow from the compressed regions to the stretched ones is induced [52]. This is a dissipative process that becomes stronger with higher stress amplitudes and therefore leads to an increase in G''.

1.7 Relating interfacial and foam elasticity

Foam rheological properties are affected by interfacial rheology since shearing a foam induces stretching and compression of the lamellae and hence, the surfactant layer at the air liquid interface. In chapter 1.4.4 and 1.6 it was already shown that viscosity and moduli of foams with rigid and mobile interfaces exhibit distinctly different behavior. Here, we focus on direct correlations between interfacial and bulk foam rheological properties. Besson et al. [53]

investigated the dynamic response to sinusoidal variation of the distance between the bubble centers of two adjacent bubbles connected by a single lamella (Fig. 1.22a). In the linear viscoelastic regime the dimensionless complex angular modulus $A^*(\omega) = A' + iA''$can be deduced. The quantity A*(Ω) is further assumed to scale with the ratio of dilational surface modulus to surface tension ($A^* \sim E^*/\gamma$) and based on the model of Princen [34] a relationship between the complex foam modulus G*(ω) and the complex angular modulus A*(ω) measured for a single lamella is proposed:

$$\frac{G^*}{G_0} = \frac{i\omega\lambda}{1 + i\omega\lambda}(1 + \alpha A^*) \tag{25}$$

where λ is a characteristic time that is needed to equilibrate surface tension gradients between adjacent interfaces via coupled surface and bulk diffusive transport and α is a geometrical constant equal to $\sqrt{3}$ for a 2D hexagonal dry film network.

In Fig. 1.22c G'/G_0 and G''/G_0 data for a surfactant foam are compared to values plotted together with the data predicted by Eq. (28) based on the two-bubble response experiments. The good agreement between the data demonstrates that the fast relaxation processes observed in foams are determined by surfactant transport within the liquid films.

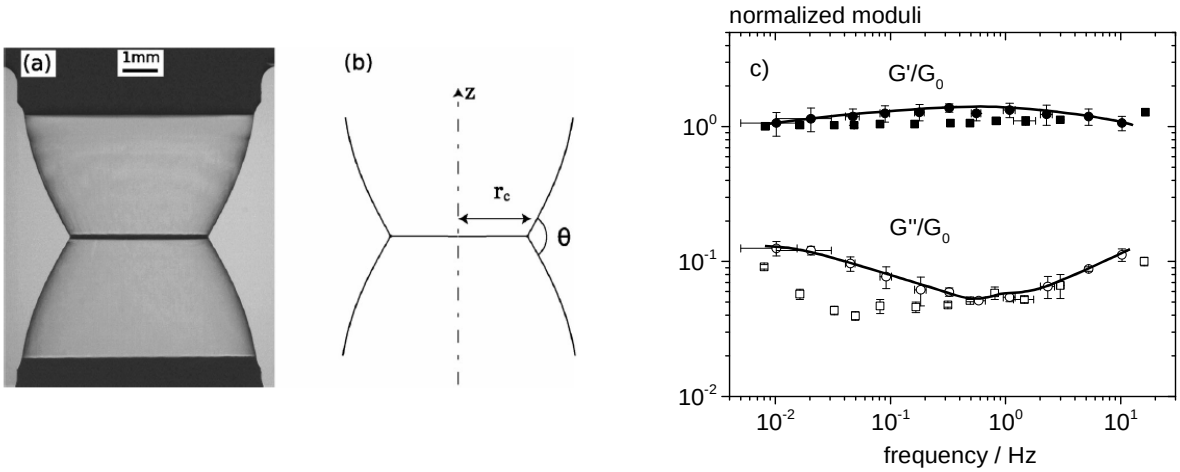

Figure 1.22: *a) Image of two contacting bubbles,*
b) adhesion profile obtained after fitting the shape of the bubbles using the Young-Laplace equation. The contact radius r_c and the contact angle Θ are determined from the intersection of the reconstructed profiles,
c) measured (● G', ○ G'') and predicted by Eq. (26) (■ G', □ G'') normalized elastic and loss moduli versus frequency with G_0 = 206 Pa, κ = 246 s and α = 0.12 is based on experimental angular moduli. The lines are guides to the eye. Data taken from [53].

A direct empirical correlation between the yield stress and the interfacial dilational modulus E' of whey protein foams made at different pH, concentration and valency of added salt has been

proposed by Davis et al. [54]. However, they do not take into account the effect of bubble size (distribution) and gas volume fraction on σ_y, although pH and ionic strength are known to affect the absolute value of this quantity substantially. A systematic investigation of the influence of interfacial layer properties on the yield stress and the plateau modulus of different protein foams (mainly β-lactoglobulin) was done by Lexis et al. [29,41] who found that foam rheology is tightly related to surface rheological properties of the corresponding protein solutions. The interfacial rheology was varied by adding different amounts and kind of salt or changing the pH. Interfacial elastic moduli in shear and dilation were found to directly correlate with the normalized bulk foam plateau modulus G_0 (equal to pre-factor *a* according to Eq. (22)) as depicted in Fig. 1.23. Exceptions were found for foams where protein aggregation and structure or network formation across foam lamellae are supposed to be decisive for the bulk foam elastic modulus, e.g. around the isoelectric point, at high ionic strength or for foams made from 1% whey protein isolate solutions.

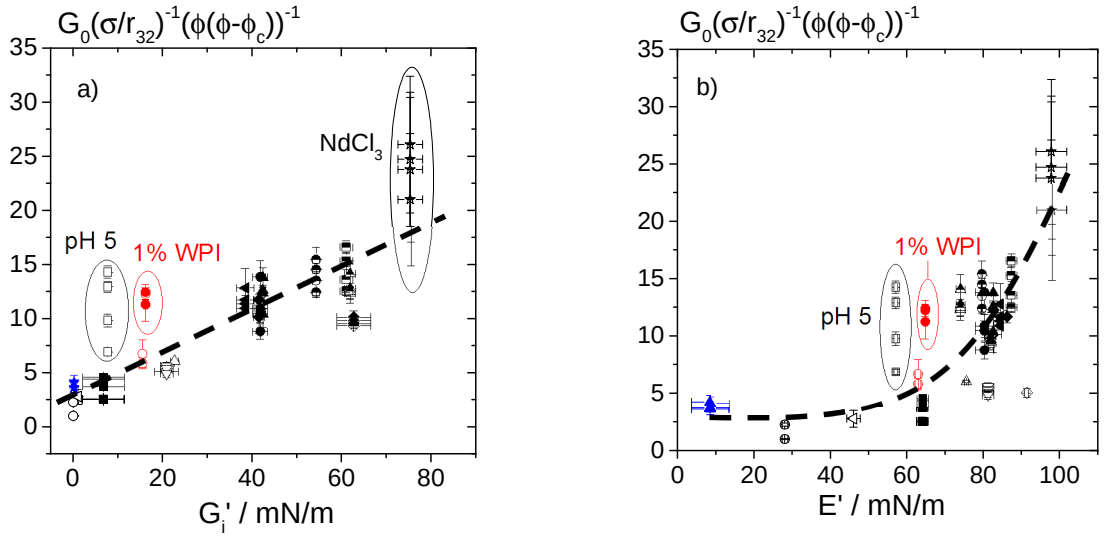

Figure 1.23: *Storage moduli normalized by Laplace pressure (σ/r_{32}) and $\phi(\phi-\phi_c)$ versus a)* surface shear elastic modulus G_i'

b) surface dilational eslastic modulus E' *[41]*

○ *pH 3,* △ *pH 4,* □ *pH 5,* △ *pH 6,* ◇ *pH 8,* ▽ *pH 9,*

pH 6.8 and NaCl: ■ *0 mM,* ◆ *10 mM,* ▲ *50 mM,* ● *80 mM,* ▲ *100 mM,*

50 mM ▬ *KCl,* ▲ *NH_4Cl,* ◓ *LiCl,* ◆ *$CaCl_2$,* ★ *$NdCl_3$*

○ *0.1% WPI,* ● *1% WPI,* ▲ *3% casein*

Reduced yield stresses (equal to pre-factor *k* in Eq. (19)) of the same BLG foams as in Fig. 1.23 are plotted in Fig. 1.24 a and b versus the critical stress $\tau_{c,surface}$ or the critical deformation $\gamma_{c,surface}$. These latter two quantities were determined from interfacial shear rheology and characterize the onset of non-linear response of the corresponding protein solution. The clear

correlations between the parameter *k* and $\tau_{c,surface}$ or $\gamma_{c,surface}$ show that *k* is determined by surface rheological features as well. Exceptions are again found for the foams made at pH 5 and those made from the BLG solutions including 50 mM $NdCl_3$. For these foams structure or network formation across foam lamellae are supposed to dominate foam yielding as discussed above. Also, a clear correlation between the critical deformation $\gamma_{c,foam}$ characterizing the onset of non-linear response during oscillatory shear of the foams and the critical deformation $\gamma_{c,surface}$ obtained in oscillatory surface shear experiments was found (Fig. 1.24c) except for the foams at pH 5. Hence, as long as no structure or network formation inside the foam lamellae occurs, bulk foam and interfacial rheological properties are directly correlated.

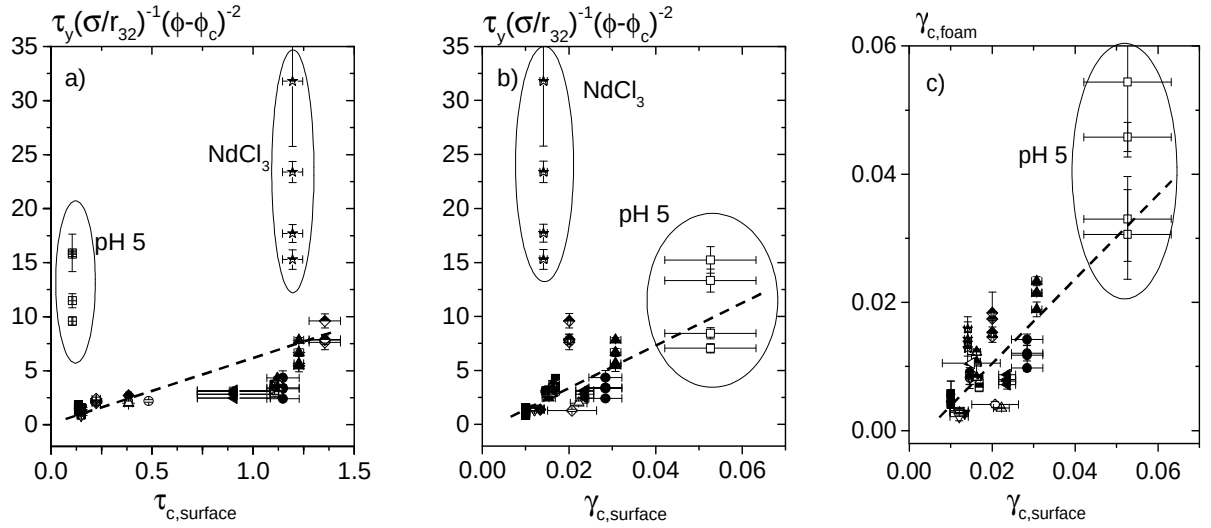

Figure 1.24: *Yield stresses normalized by Laplace pressure and $(\phi-\phi_c)^2$ versus*
a) critical shear deformation of the surface $\tau_{c,surface}$,
b) critical shear deformation of the surface $\gamma_{c,surface}$,
c) critical deformation of the foams $\gamma_{c,foam}$ versus critical deformation of the surface $\gamma_{c,surface}$ [41]
○ pH 3, △ pH 4, □ pH 5, △ pH 6, ◇ pH 8, ▽ pH 9,
pH 6.8 and NaCl: ■ 0 mM, ◆ 10 mM, ▲ 50 mM, ● 80 mM, ▲ 100 mM,
50 mM ⬒ KCl, ▲ NH_4Cl, ◓ LiCl, ◆ $CaCl_2$, ★ $NdCl_3$

References

[1] N. D. Denkov, S. Tcholakova, K. Golemanov, K. P. Ananthpadmanabhan, A. Lips, Soft Matter **2009**, 5, 3389-3408.

[2] H. A. Barnes, J. F. Hutton, K. Walters, An introduction to rheology, Rheology series vol. 3, Elsevier Science B.V. Amsterdam and New York **1989.**

[3] Q. D. Nguyen, D. V. Boger, Journal of Rheology **1983**, 27, 321-349.

[4] Q. D. Nguyen, D. V. Boger, Annu. Rev. Fluid Mech. **1992**, 47–88.

[5] N. J. Alderman, G. H. Meeten, J. D. Sherwood, Journal of Non-Newtonian Fluid Mechanics **1991**, 39, 291–310.

[6] S. Carozza, Rheological characterisation of gels and foams for food, Nr. 101, VDI-Verl, Düsseldorf **2001**.

[7] A. Yoshimura, Journal of Rheology **1988**, 32, 53.

[8] B. Herzhaft, S. Kakadjian, M. Moan, Colloids and Surfaces A: Physicochemical and Engineering Aspects **2005**, 263, 153-164

[9] B. Herzhaft, Oil & Gas Science and Technology - Rev. IFP **1999**, 54, 587–596.

[10] N. D. Denkov, V. Subramanian, D. Gurovich, A. Lips, Colloids and Surfaces A: Physicochemical and Engineering Aspects **2005**, 263, 129–145.

[11] A. Yoshimura, Journal of Rheology **1988**, 32, 53.

[12] M. Mooney, Journal of Rheology **1931**, 2, 210–222.

[13] Z. D. Jastrzebski, Ind. Eng. Chem. Fundam. **1967**, 6, 445–453.

[14] B. Herzhaft, Journal of Colloid and Interface Science **2002**, 247, 412–423.

[15] J. P. Heller, M. S. Kuntamukkula, Ind. Eng. Chem. Res. **1987**, 318–325.

[16] C. Enzendorfer, Journal of Rheology **1995**, 39, 345.

[17] H. M. Princen, A. D. Kiss, Journal of Colloid and Interface Science **1989**, 128, 176–187.

[18] P. Coussot, J. Raynaud, F. Bertrand, P. Moucheront, J. Guilbaud, H. Huynh, S. Jarny, D. Lesueur, Physical Review Letters **2002**, 88, 218301.

[19] F. Rouyer, S. Cohen-Addad, M. Vignes-Adler, R. Höhler, Physical Review E **2003**, 67, 21405.

[20] M. Lexis, N. Willenbacher, Colloids and Surfaces A: Physicochemical and Engineering Aspects **2014**, 459, 177–185.

[21] G. Ovarlez, S. Rodts, X. Chateau, P. Coussot, Rheologica Acta **2009**, 48, 831-844.

[22] R. B. Bird, D. Gance, B. J. Yarusso, Rev Chem Eng **1982**, 1, 1-70.

[23] G. Ovarlez, K. Krishan, S. Cohen-Addad, Europhysics Letters **2010**, 91, 68005.

[24] S. Rodts, J. C. Baudez, P. Coussot, Europhysics Letters **2005**, 69, 636-642.

[25] A. Ragouilliaux, G. Ovarlez, N. Shahidzadeh-Bonn, B. Herzhaft, T. Palermo, P. Coussot, Phys. Rev. E **2007**, 76, 51408.

[26] A. J. Liu, S. R. Nagel, Nature **1998**, 396, 21–22.

[27] R. Höhler, S. Cohen-Addad, Journal of Physics: Condensed Matter **2005**, 17, R1041-R1069.

[28] P. C. F. Møller, J. Mewis, D. Bonn, Soft Matter **2006**, 2, 274-283.

[29] Barnes, H. A.; Walters, K., Rheologica Acta **1985**, 24, 323-326.

[30] H. A. Barnes, J. Non-Newtonian Fluid Mech **1999**, 133–178.

[31] J. P. Hartnett, Journal of Rheology **1989**, 33, 671.

[32] J. Schurz, Rheologica Acta **1990**, 170–171.

[33] D. C.-H. Cheng, Rheologica Acta **1986**, 542–554.

[34] H. M. Princen, Journal of Colloid and Interface Science **1983**, 91, 160-175.

[35] S. A. Khan, J. Rheol. **1988**, 32, 69-92.

[36] F. Rouyer, S. Cohen-Addad, R. Höhler, Colloids and Surfaces A: Physicochemical and Engineering Aspects **2005**, 263, 111–116.

[37] T. G. Mason, J. Bibette, D. A. Weitz, Journal of Colloid and Interface Science **1996**, 179, 439–448.

[38] A. Saint-Jalmes, D. J. Durian, Journal of Rheology **1999**, 43, 1411–1422.

[39] S. Marze, R. M. Guillermic, A. Saint-Jalmes, Soft Matter **2009**, 5, 1937-1946.
[40] H. M. Princen, Journal of Colloid and Interface Science **1986**, 112, 427–437.
[41] M. Lexis, N. Willenbacher, Soft Matter **2014**, 10, 9626–9636
[42] M. Lexis, N. Willenbacher, Chemie Ingenieur Technik **2013**, 85, 1317–1323.
[43] T. G. Mason, J. Bibette, D. A. Weitz, Physical Review Letters **1995**, 75, 2051–2054.
[44] R. D. Sudduth, Journal of Applied Polymer Science **1993**, 48, 37–55.
[45] S. Marze, A. Saint-Jalmes, D. Langevin, Colloids and Surfaces A: Physicochemical and Engineering Aspects **2005**, 263, 121–128.
[46] S. Cohen-Addad, R. Höhler, Y. Khidas, Physical Review Letters **2004**, 93, 28302.
[47] S. Vincent-Bonnieu, R. Höhler, S. Cohen-Addad, Europhysics Letters **2006**, 74, 533–539.
[48] N. Denkov, S. Tcholakova, K. Golemanov, K. Ananthapadmanabhan, A. Lips, Physical Review Letters **2008**, 100, 138301.
[49] S. Costa, R. Höhler, S. Cohen-Addad, Soft Matter **2012**, 9, 1100-1112.
[50] K. Krishan, A. Helal, R. Höhler, S. Cohen-Addad, Physical Review E **2010**, 82, 11405.
[51] S. Cohen-Addad, H. Hoballah, R. Höhler, Phys. Rev. E **1998**, 57, 6897–6901.
[52] D. M. A Buzza,., C.-Y. D. Lu, M. E. Cates, J. Phys II France **1995**, 5, 37–52.
[53] S. Besson, G. Debrégeas, S. Cohen-Addad, R. Höhler, Phys. Rev. Lett. **2008**, 101, 214504.
[54] J. P. Davis, E. A. Foegeding, F. K. Hansen, Colloids and Surfaces B: Biointerfaces **2004**, 34, 13–23.

2 pH effects on the molecular structure of β-lactoglobulin modified air–water interfaces and its impact on foam rheology

Langmuir

Article

pubs.acs.org/Langmuir

pH Effects on the Molecular Structure of β-Lactoglobulin Modified Air−Water Interfaces and Its Impact on Foam Rheology

Kathrin Engelhardt,[†] Meike Lexis,[‡] Georgi Gochev,[§,∥] Christoph Konnerth,[†] Reinhard Miller,[§] Norbert Willenbacher,[‡] Wolfgang Peukert,[†] and Björn Braunschweig[†,*]

[†]Institute of Particle Technology (LFG), University of Erlangen-Nuremberg, Cauerstrasse 4, 91058 Erlangen, Germany

[‡]Institute of Mechanical Engineering, Karlsruhe Institute of Technology (KIT), Gotthard-Franz-Strasse 3, 76131 Karlsruhe, Germany

[§]Max-Planck-Institute of Colloids and Interfaces, Am Mühlenberg 1, 14476 Potsdam, Germany

[∥]Institute of Physical Chemistry, Bulgarian Academy of Sciences, 1113 Sofia, Bulgaria

ABSTRACT: Macroscopic properties of aqueous β-lactoglobulin (BLG) foams and the molecular properties of BLG modified air−water interfaces as their major structural element were investigated with a unique combination of foam rheology measurements and interfacial sensitive methods such as sum-frequency generation and interfacial dilatational rheology. The molecular structure and protein−protein interactions at the air−water interface can be changed substantially with the solution pH and result in major changes in interfacial dilational and foam rheology. At a pH near the interfacial isoelectric point BLG molecules carry zero net charge and disordered multilayers with the highest interfacial dilatational elasticity are formed at the air−water interface. Increasing or decreasing the pH with respect to the isoelectric point leads to the formation of a BLG monolayer with repulsive electrostatic interactions among the adsorbed molecules which decrease the interfacial dilational elasticity. The latter molecular information does explain the behavior of BLG foams in our rheological studies, where in fact the highest apparent yield stresses and storage moduli are established with foams from electrolyte solutions with a pH close to the isoelectric point of BLG. At this pH the gas bubbles of the foam are stabilized by BLG multilayers with attractive intermolecular interactions at the ubiquitous air−water interfaces, while BLG layers with repulsive interactions decrease the apparent yield stress and storage moduli as stabilization of gas bubbles with a monolayer of BLG is less effective.

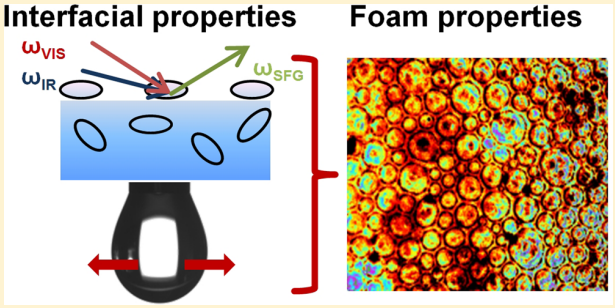

1. INTRODUCTION

Foams as dispersions of gases in liquids show unique rheological properties: Under the application of comparatively small stresses they behave like a viscoelastic solid, while at higher stresses they become shear thinning and flow like a liquid. This mechanical behavior of foams in combination with a remarkably high surface area and low density leads to a variety of demanding applications.[1,2] Among the latter, protein foams that are present in dairy products[3−5] are in particular interesting since the physical and chemical properties of the inherent air−water interfaces largely determine the macroscopic properties of the foam.[6] As air−water interfaces are a basic structure element of aqueous foams, they can control foam rheology and other macroscopic properties such as foam stability.[7,8] For that reason it is of great importance to increase our level of understanding of protein adsorption and stabilization mechanisms at the interface of a foam lamella. The latter information would help to control and to tune foam properties such as foamability, foam stability, or mechanical properties of the macroscopic foam. In general, in situ molecular level studies of protein adsorption are needed to address changes in the composition and molecular structure of protein adsorption layers at the air−water interface directly.

In the past, protein interfaces were studied with techniques such as ellipsometry,[9] neutron reflection,[10,11] X-ray reflectivity,[12] Brewster angle microscopy,[13] and with surface tension measurements.[14,15] However, in recent years vibrational sum-frequency generation (SFG) has become a powerful tool for surface science studies of biointerfaces.[6,16−23]

In this article we report the use of a combination of established analytical techniques such as bubble profile analysis tensiometry, surface dilational rheology, ellipsometry, and foam rheology measurements with vibrational SFG spectroscopy. This unique approach allows us to address not only single properties of foams or interfaces but also provides information on several length scales. As we will demonstrate the latter approach has enabled us to reveal composition, structure, and mechanical properties of β-lactoglobulin (BLG) interfacial

Received: July 18, 2013
Revised: August 19, 2013
Published: August 20, 2013

layers and foams and thus to bridge the gap between the molecular level and the macroscopic aqueous foam.

2. EXPERIMENTAL DETAILS

2.1. Sample Preparation. BLG was isolated as described previously[24] and kindly provided by the group of Ulrich Kulozik (Technische Universität München, Germany). BLG solutions were prepared by dissolving the dry protein in ultrapure water (18.2 MΩ·cm; total oxidizable carbon <5 ppb). The pH was adjusted by adding either HCl or NaOH (Merck; Suprapur grade or Carl Roth 1 N standard solution K021) and, subsequently, measured with a pH electrode. In order to remove possible organic contaminations, the necessary glassware for spectroscopic studies was soaked in a mixture of concentrated sulfuric acid (98%; analytical grade) and NOCHROMIX for at least 24 h and was subsequently thoroughly rinsed with ultrapure water. All measurements were performed at room temperature. The foams were produced by purging nitrogen (60 mL/min) through a porous glass filter (pore size 9−16 μm) that was fused to a glass pipe of 60 mm diameter and 53 mm height, while the sample solution was placed on top of this filter. The protein solutions were previously heated to 50 °C in order to obtain foams that are stable enough for reproducible rheological measurements. This temperature treatment only increases the adsorption kinetics but also is still low enough to exclude denaturation of BLG. In fact, BLG is being denatured between 70 and 85 °C.[25]

2.2. Zeta Potential Measurements. Zeta potentials were measured with a Zetasizer Nano ZS from Malvern Instruments. With the Zetasizer Nano ZS reproducible zeta potentials of BLG could only be recorded for concentrations >546 μM. Therefore, higher BLG concentrations had to be chosen for measurements of the bulk zeta potential compared to the measurements at the air−water interface. Before the solution was transferred into the cuvettes for zeta potential measurements, BLG dilutions are filtered with a 0.2 μm cellulose acetate filter (VWR 514-0060) and a thoroughly acid cleaned glass syringe. For each pH value at least five measurements with different cuvettes were performed.

2.3. Bubble Shape Analysis. Surface tensions σ of protein modified air−water interfaces were determined with drop/bubble profile analysis[26] using a PAT-1 tensiometer (SINTERFACE Technologies, Germany). The variation of the Laplacian shape of an emerging bubble with a constant volume of 12 μL in the protein solution was measured as a function of adsorption time and was used to determine the dynamic surface tension. The establishment of equilibrium surface tension of protein solutions is a continuous process, which has been analyzed by a quasi-equilibrium state approach.[27,28] In this study we chose a reference adsorption time of 30 min, during which a sufficiently high surface saturation was ensured for the two BLG concentrations measured. In order to monitor the surface dilational rheological properties of the adsorbed layer, sinusoidal oscillations with 10% amplitude with respect to the bubble area and a frequency of 0.1 Hz were applied, and the response in surface tension was recorded. The experimental data were processed for the surface dilational viscoelastic modulus $E = E' + E''$, whereby E' the storage and E'' the loss moduli account respectively for the dilational elasticity and dilational viscosity of an adsorption layer.[29]

2.4. Ellipsometry. The thickness of adsorbed protein layers was determined with a phase modulated ellipsometer (Beaglehole Instruments, Picometer ellipsometer) that was operated with a wavelength of 632.8 nm. For each experiment 15 μM BLG sample solution was poured into a Petri dish with a diameter of 10 cm and was allowed to equilibrate for about 30 min. Angle scans between 51° and 55° vs the surface normal were performed with a step width of 0.5°. In order to ensure reproducibility, at least six measurements were recorded and averaged for every pH value. Angle-resolved data from ellipsometry were fitted using a three-layer model with refractive indices of 1.33, 1.40, and 1.00 for the electrolyte subphase, the protein layer, and air, respectively. In general two parameters are unknown in this three-layer system: the layer thickness of the adsorbed protein layer and the corresponding refractive index. Because of the fact that these parameters cannot be determined independently, one of them—in our case the refractive index—has to be chosen as a fixed input parameter for all model calculations. The assumption of $n = 1.40$ for the protein layer is in accordance with reported layer thicknesses of around 3−4 nm for a BLG layer at pH 6−7,[11,30] which is comparable to the diameter of a BLG monomer of around 3.6 nm.[31,32] Since the refractive index of BLG at an interface is a priori unknown, the assumption of a fixed value for the refractive index causes a systematic error of the layer thickness that depends on the deviation of the assumed refractive index from its actual value. However, since we compare only relative changes of the layer thickness as a function of the solution pH, our interpretations are not impaired in this respect.

2.5. Vibrational Sum-Frequency Generation (SFG). SFG is a second-order nonlinear optical process[33] and is inherently interfacial specific for materials with inversion symmetry such as liquids and gases in the time average. For SFG spectroscopy two laser beams, one with a fixed wavelength (vis) and another with tunable infrared (IR) wavelength, are combined at the interface of interest, where the sum frequency of the two impinging laser fields is generated. The intensity of sum-frequency output I_{SF} depends on the intensities of the impinging laser beams as well as on the nonresonant $\chi^{(2)}_{NR}$ and resonant parts of the second-order nonlinear susceptibility $\chi^{(2)}$:

$$I_{SF}(\omega_{SF}) \propto \left| {\chi_{NR}}^2 + \sum_k \frac{A_k \exp(i\varphi_k)}{\omega_k - \omega + i\Gamma_k} \right|^2 I_{VIS} I_{IR} \quad (1)$$

The resonant contribution is a function of the oscillator strength $A_k = N\langle \alpha_k \mu_k \rangle$, the relative phase φ_k, the resonance frequency ω_k, and of the bandwidth Γ_k of the vibrational mode k. Furthermore, A_κ depends on the number density N of the molecular species which gives rise to the vibrational mode k, and due to the coherent process of sum-frequency generation, A_κ is an orientational average of the Raman polarizability α_k and the dynamic dipole moment μ_k. This orientational average can have a dramatic effect on the SFG intensity because only a perfectly ordered adsorption layer results in the highest possible SFG intensity, while a layer with identical coverage, but randomly oriented interfacial molecules, has a negligible SFG intensity. Consequently, SFG is sensitive not only to changes in the adsorbate composition and coverage at the interface but also to the inherent molecular order of the adsorbate layer.

Our SFG measurements were performed with a home build broadband SFG spectrometer that is described elsewhere.[34] The spectrometer is equipped with a tunable femtosecond IR laser (fwhm bandwidth >200 cm^{-1}) and an etalon filtered pulse at 800 nm wavelength (fwhm bandwidth <6 cm^{-1}). All spectra were recorded with s-polarized sum frequency, s-polarized visible, and p-polarized IR beams (ssp). The presented spectra were normalized to a reference spectrum of an oxygen plasma cleaned polycrystalline Au sample. SFG spectra were collected from 15 μM BLG solution in a Petri dish. Each spectrum was measured by scanning the broadband IR beam with a step width of 130 cm^{-1} and a total acquisition time of 8 min for the frequency range 2800−3800 cm^{-1}.

2.6. Properties of the Protein Solutions and Foams Used for Foam Rheological Measurements. The continuous phase viscosity of foams is supposed to have an influence on their rheology.[35] Therefore, the viscosities of the BLG solutions were measured with the Ares rheometer from TA Instruments using concentric cylinder geometry with double gap (32/34 mm). Shear rates between 10 and 250 s^{-1} were imposed, and the solutions showed Newtonian behavior as expected. The variation of the viscosities was negligibly low with $\eta = 0.93$−1.1 mPa·s.

The equilibrium values of the surface tension σ for the normalization of apparent foam yield stress τ_y and storage modulus G_0 were measured at 21 °C after 20 min adsorption time using the pendant drop method (Dataphysics SCA 20) (Table 1). The surface tension shows a temperature dependence that is attributable to the change of the surface tension of pure water.[36] It also shows a time dependence rising from the time-dependent adsorption of the proteins. Since the foams possess different temperatures and ages, an error arises in our calculations by using the equilibrium surface

Table 1. Equilibrium Surface Tension and Mean Bubble Radius at Initial and Final ϕ Used for Normalization of τ_y and G_0

pH	σ/mN m^{-1}	r_{32}/μm (initial ϕ)	r_{32}/μm (final ϕ)
3	47.6 ± 0.2	208 ± 12	219 ± 4
5	45.5 ± 0.4	187 ± 6	289 ± 1
6.8	51.5 ± 0.1	219 ± 3	307 ± 2

tension at 21 °C. This error can be estimated to be less than 5% which does not impair the interpretation of our results.

The gas volume fraction was determined as a function of foam age with a conductivity electrode (WTW, Cond 340i) including a temperature sensor.

The gas volume fraction ϕ can be calculated from the ratio of foam and solution conductivity κ according to the method described by Feitosa et al.:[37]

$$\phi = 1 - \frac{3\kappa(1 + 11\kappa)}{1 + 25\kappa + 10\kappa^2}$$

with $\kappa = \kappa_{foam}/\kappa_{liquid}$. The foam cools down during aging which leads to a change in the liquid conductivity κ_{liquid} with decreasing temperature. This temperature dependence was determined separately and taken into account when calculating ϕ.

Another important parameter for the rheology of disperse systems is the size distribution of the gas bubbles. Therefore, images of the bubbles were taken with the help of an endoscopic CCD camera (Lumenera LU 160; resolution 1392 × 1040 pixels) that was placed inside the foam. The image analysis was carried out with the software iPS (Visiometrics, Germany), and the Sauter mean radius r_{32}—the ratio between the third and the second moment of the size distribution—was extracted (Table 1).

Foam Rheology: A Rheoscope 1 (Thermofisher, Germany) equipped with a plate−plate system with a diameter of 60 mm was used for the rheological measurements of BLG foams. The surfaces of the plates were covered with sandpaper, and the gap between the plates was set to 6 mm. Preliminary experiments confirmed that wall slip effects can be neglected with this setup. The acquisition time for all foam rheological measurements was set to 60 s in order to limit the effect of aging processes during the measurements.

Apparent foam yield stress τ_y was determined by steady shear experiments. The foams were exposed to increasing shear stresses from initial values τ_i = 0.1−1 Pa to final stresses τ_f = 30−150 Pa depending on foam composition. Furthermore, we have confirmed that on the time scale of our measurements the apparent yield stress is independent of the initial and final stress values as well as on the number of data points selected for a stress ramp experiment.

Amplitude sweep experiments allow for the measurement of the storage and loss modulus (G' and G'') of the foam and were performed by varying the stress amplitude at a fixed frequency f = 1 Hz. In the frequency range of 0.01−10 Hz the plateau value of G' at low stresses was shown to be virtually frequency independent and is henceforth named G_0.

3. RESULTS AND DISCUSSION

The surface charge of proteins and the resulting electric double layer is determined in bulk solutions by the solution pH. At mild pH (3 < pH < 9) stable suspensions composed of proteins in their inherent folded structure can be formed,[38] whereas at extreme pH protein unfolding and denaturation has to be considered.[39,40] As a positive or negative net charge on the protein surface gives rise to strong repulsive intermolecular interactions, protein aggregation can be prevented. At pH values around the bulk isoelectric point (IEP) where proteins carry no net charge, they tend to aggregate and are less soluble.[39] These examples demonstrate that charge has a tremendous effect on the physicochemical behavior of proteins. In order to understand the more complex behavior of proteins at aqueous interfaces, we have first determined the charging of BLG proteins with zeta potential measurements, and as we will show later, these results are extremely helpful for the understanding of molecular level properties of protein layers and macroscopic properties of protein foams.

3.1. The Zeta Potential of β-Lactoglobulin. In Figure 1 the zeta potential of BLG dilutions is presented as a function of

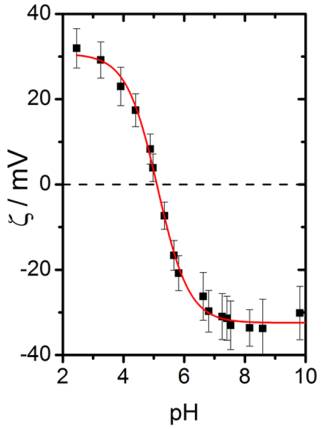

Figure 1. Zeta potential of BLG as a function of solution pH. The red line is a guide to the eye.

the solution pH. At pH ∼ 5.1 we observe a zeta potential of 0 mV which is indicative for zero net charge and consequently for the IEP of BLG. Solution pH higher or lower compared to the IEP leads to a substantial increase in zeta potential to a maximum absolute value of 32 mV, respectively. In order to reveal the effects of protein charging on the physicochemical properties of BLG modified air−water interfaces, it is particularly interesting to compare the observed changes in zeta potential with the structure, composition, and rheological properties of the latter. Such a comparison is of great importance for the molecular level understanding of protein interfaces because interfacial properties can be significantly different from the properties of proteins in the bulk electrolyte.[41] The latter is caused by local ion concentrations and pH conditions that can differ significantly from the bulk at the interface.[42]

3.2. Surface Tension and Interfacial Dilatational Rheology of β-Lactoglobulin Layers. In a first step we have measured the surface tension and its dependence on the solution pH. In Figure 2 we compare the results for 10 and 50 μM protein concentrations. For both concentrations a pronounced minimum in surface tension is observed at a pH of ∼5. The minimum in surface tension at 47−50 mN/m can be attributed to an excess of BLG because the presence of proteins decreases the surface tension of the air−water interface compared to the unperturbed interface.[43] For both concentrations the pH at which the minimum in surface tension occurs is close to the pH of the IEP in bulk solutions. Obviously, the tendency for protein adsorption increases for pH values which are close to the IEP. Furthermore, the rate of adsorption is highest at the IEP leading to the lowest final surface tension values.[44] Consequently, the overall changes in surface tension with pH can be directly related to protein net charge effects. The highest surface activity is due to the lack of protein net charge at the IEP (Figure 1) which leads to much weaker

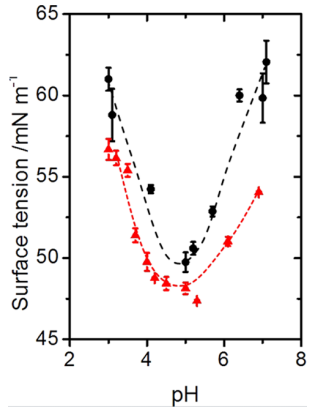

Figure 2. Surface tension for 10 (●) and 50 μM (red triangle) BLG aqueous solutions as a function of pH. Each data point corresponds to a measured value after 30 min. The dashed lines guide the eye.

repulsive interactions between the protein molecules and presumably to an increase of protein hydrophobicity.

Further insights into the intermolecular interactions of the interfacial layer can be gained by measurements of the interfacial dilational rheology of BLG adsorption layers. In Figure 3 we present the interfacial dilational elasticity E' and

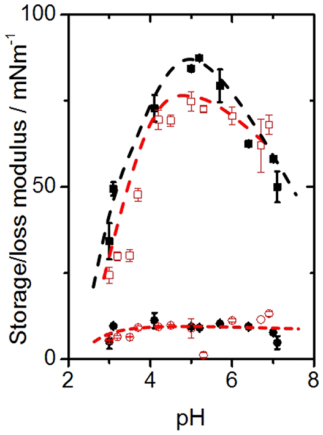

Figure 3. Interfacial dilational elasticity E' (squares) and viscosity E'' (circles) of BLG. Filled symbols correspond to a BLG concentration of 10 μM while open symbols correspond to 50 μM. The dashed lines guide the eye.

the interfacial dilational viscosity E'' as a function of the bulk pH at the same BLG concentrations as in Figure 2. A strong pH dependence of E' is observed whereby E' reaches a maximum at a pH near the bulk IEP (pH ~5), while E'' is an order of magnitude smaller than E' and shows virtually no pH dependence. The absence of a strong $E'' = |E| \sin \delta$, $|E|$ being the complex viscoelastic modulus,[29] indicates that the phase lag δ between the stress applied to the surface adsorbed protein layer and strain yield is negligible. Thus, dynamic deformations of BLG adsorption layers at the air–water interface are predominantly elastic rather than viscous.[28,29]

The presented results in Figures 2 and 3 show that the interfacial dilational elasticity changes in accordance with the variation of the surface tension, as discussed in ref 28, exhibiting a maximum which corresponds to a minimum in the surface tension, both extremes being localized around pH 5. This behavior is attributed to negligible electrostatic repulsive interaction which favors stronger attractive intermolecular interactions, e.g., hydrophobic interactions at the IEP. As the surface concentration is pH dependent, the formation of multilayer structures was further analyzed by ellipsometry measurements of the layer thickness and the composition and molecular order of adsorbed BLG layers with sum-frequency generation.

3.3. Composition and Structure of Surface-Adsorbed β-Lactoglobulin Layers. In Figure 4 the thickness of BLG

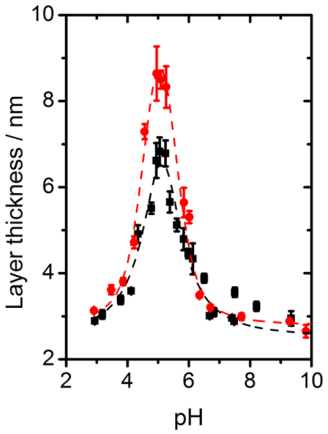

Figure 4. Thickness of BLG layers adsorbed to the air–water interface as a function of the solution pH which was determined from ellipsometry. The concentrations of BLG solutions were 15 (■) and 54 μM (red circle). The dashed lines are a guide to the eye.

layers is shown as a function of solution pH for 15 and 54 μM bulk concentrations. Similar behavior is observed for both concentrations: at acidic conditions layers with a thickness of ~3 nm are established, while the thickness increases with increasing pH, reaches a pronounced maximum around the bulk IEP, and decreases subsequently for higher pH values. In particular, pH values >7 result into layers with thicknesses comparable to those at acidic electrolytes with pH < 4. Here, variations of the pH had little effect on the layer thickness. Therefore, we attribute the minimum thickness which has been observed with ellipsometry to the formation of a monolayer with BLG molecules at the air–water interface. This hypothesis is corroborated by previous X-ray and neutron reflectometry studies[11,45] of BLG at the air–water interface which have observed a thickness of ~3.6 nm for BLG layers. This value is close to the shortest axis of the monomer.[31,45] On the other hand, the hydrodynamic radius of BLG molecules in solution was reported to be 2.75 ± 0.2 nm,[46] which is in a good agreement with our measured monolayer thickness of ~3 nm. Two possible explanations can be given for the increase in layer thickness at the bulk IEP. As we have previously discussed, the protein net charge is dramatically decreased near the IEP (Figure 1), which can lead to an accumulation of additional proteins in the adsorbed layer (Figure 2) and, consequently, to a more densely packed layer. At pH around the IEP the formation of oligomer (octamer) structures was reported.[40,47,48] Additional multilayers could form on top of the already existing first layer, which results into a more compact protein film compared to pH conditions where only a highly charged monolayer exists at the interface. In fact, the formation of multilayers is confirmed by the thickness of proteins films at

the IEP (Figure 4) that indicates the presence of 2−3 layers of BLG at a pH of ∼5. Further support comes from the observed increase in storage modulus E' (Figure 3) and the decreased surface tension (Figure 2) near the IEP.

Vibrational SFG spectra of BLG proteins adsorbed to the air−water interface were recorded at different pH and provide information on the interfacial molecular structure (Figure 5a).

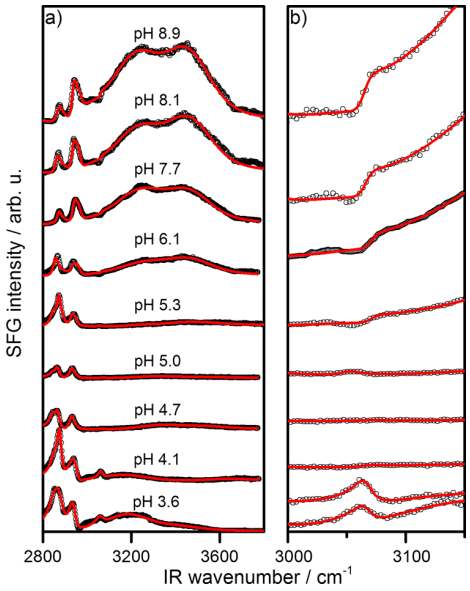

Figure 5. (a) Vibrational SFG spectra in the region of CH (2800−3100 cm^{-1}) and OH stretching vibrations (3000−3800 cm^{-1}) for BLG adsorbed to the air−water interface. Spectra were recorded at different pH as indicated in the figure. (b) Magnification of the spectra in (a) showing changes in the polarity of aromatic CH stretching band at 3050 cm^{-1} in more detail. Solid lines are fits to the experimental data according to eq 1.

In the frequency region of 2800−3100 cm^{-1} SFG spectra show strong vibrational bands centered at 2877 and 2936 cm^{-1} and a much weaker band at 3050 cm^{-1}. These bands are attributable to symmetric CH_3 stretching vibrations, the CH_3 Fermi resonance, and aromatic CH stretching vibrations of BLG proteins at the air−water interface.[6,18,49−51] Broad vibrational bands are observed at 3200 and 3450 cm^{-1} and are due to symmetric OH stretching vibrations of tetrahedrally coordinated interfacial water molecules and molecules with lower coordination, respectively.[52,53] The intensity of both CH and OH vibrational bands shows substantial changes when the solution pH is changed. In particular, near the bulk IEP (pH ∼5) the intensity of OH stretching bands is close to zero while they dominate the SFG spectra at alkaline and acidic pH.

It is now interesting to discuss the origin of the observed changes in SFG intensities with variation in solution pH. We recall that the SFG amplitude $A_k \propto N\langle\alpha_k\mu_k\rangle$ is a function of both the number density and the orientational average of dynamic dipole moment and Raman polarizabilities. As we have shown before, the thickness of protein layers does increase at a pH where we observe only weak SFG contributions of all interfacial molecules. However, the number density of proteins as far as it can be deduced from the layer thickness (Figure 4) does not decrease at this point but actually increases, while the number density of interfacial water necessarily has to be similar for all pH values. For that reason the net orientation of interfacial proteins and H_2O does dominate the SFG signals. As interfacial layers of charged proteins can create a strong unidirectional electric field E_{dc} perpendicular to the interface, interfacial dipoles such as H_2O or to some extend BLG are ordered in the electric field E_{dc} (Figure 6). This electric field induced polar ordering provides a direct dependence of the oscillator strength $A_k \propto \langle\alpha_k\mu_k\rangle$ on the local field E_{dc}.[6,52,53]

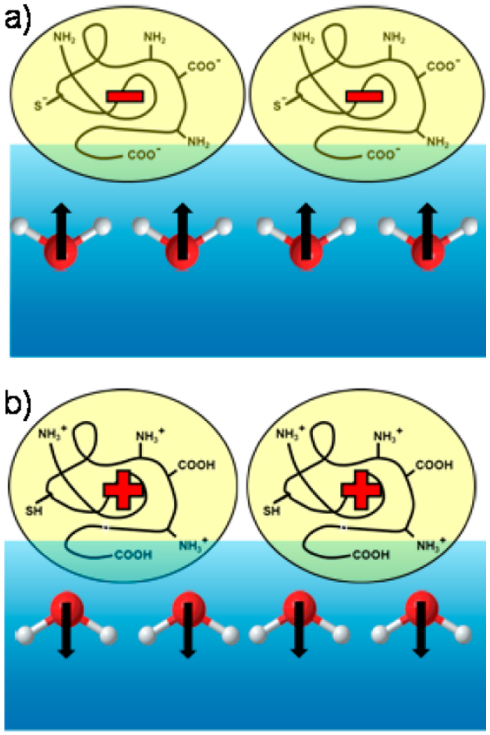

Figure 6. Simplified schematic representation of the adsorbed protein layer and the water subphase for (a) negatively charged proteins at pH below the point of zero charge and (b) positively charged proteins for a pH above the point of zero charge.

In order to analyze changes of the OH bands in more detail, we have fitted our spectra according to eq 1 where we have

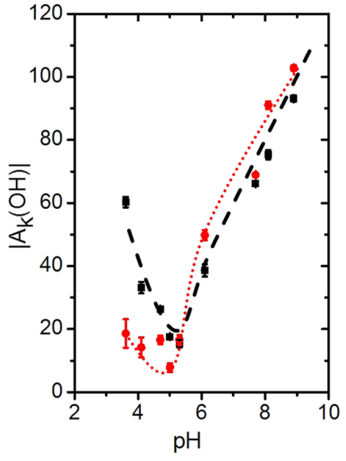

Figure 7. pH dependence of the amplitudes of the OH stretching vibration at 3200 (■) and 3450 cm^{-1} (red circle). The dotted lines guide the eye.

dx.doi.org/10.1021/la402729g | Langmuir 2013, 29, 11646−11655

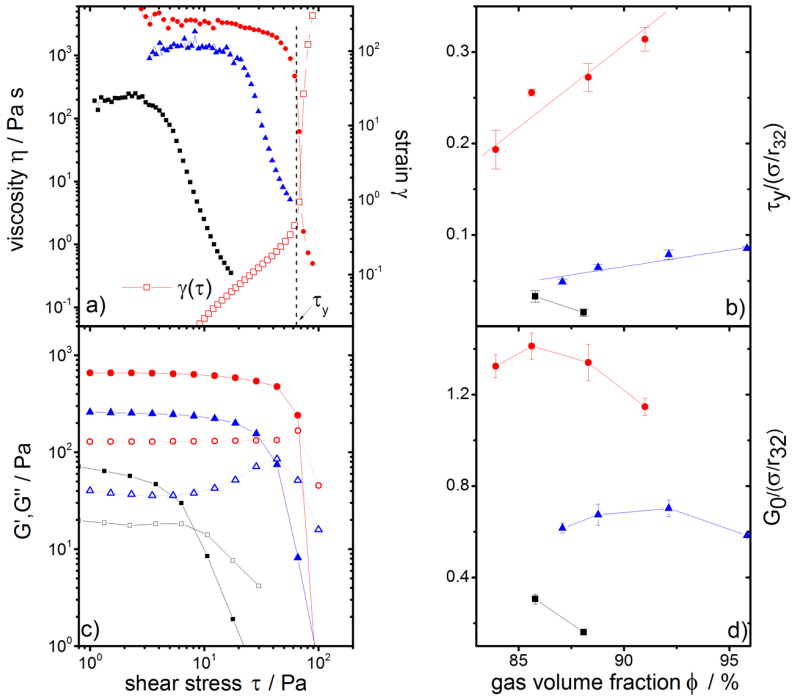

Figure 8. Steady and oscillatory shear (f = 1 Hz) measurements for BLG foams at different pH: ■, pH 3; red circle, pH 5; blue triangle, pH 6.8. (a) The viscosity η and (c) the moduli $G'$and G'' plotted as a function of applied stress τ at similar gas volume fractions ($\phi \approx 0.85$).The vertical dashed line in (a) shows the position of the yield stress that is derived from the strain versus stress graph $\gamma(\tau)$ as plotted exemplary for pH 5 (open red square). (c) Apparent yield stress τ_y and (d) plateau value of the storage modulus G_0 in dependence of the gas volume fraction. Both quantities τ_y and G_0 are normalized by Laplace pressure (σ/r_{32}).

considered additional inhomogeneous broadening of the OH line shapes by convoluting the homogeneous (Lorentzian) lines by Gaussians. Figure 7 presents the oscillator strength A_k of OH bands as a function of pH. A pronounced decrease in the amplitude for pH ∼5 with a subsequent increase is observed.

As the OH amplitudes are highly sensitive to the electric field induced by the charge of BLG, a minimum in the amplitudes around the IEP can be attributed to a minimum in protein charge and, consequently, to the interfacial point of zero net charge. For more acidic and alkaline pH, BLG carries a positive and negative net charge, respectively, which leads to a high orientation of the water dipoles. Crossing the point of zero net charge at the interface causes a change in the sign of E_{dc} and, hence, a change in net orientation of interfacial H_2O by 180° (Figure 6). The latter can be confirmed by the changes in polarity of the vibrational band around 3050 cm^{-1} which appears as positive going feature for pH <5 and as a negative going feature for pH >5 (Figure 5b). However, the origin of this apparent phase reversal lies not within net orientation of the BLG layer and its CH groups, but in the orientation of the interfacial H_2O, which can be easily orientated and polarized. In fact, changes in net orientation of interfacial H_2O lead pH <5 to constructive interference conditions of the 3050 cm^{-1} band with the broad OH stretching band, while destructive interference at pH >5 is observed. Obviously the net orientation of CH groups from the BLG layers does not change when the interfacial isoelectric point is crossed at pH 5; otherwise, the relative phase would not change and as consequence the appearance of the 3050 cm^{-1} band would be unchanged.

Obviously, the bulk isoelectric point at pH ∼5.1 (Figure 1), the minimum in surface tension (Figure 2), the maximum in storage modulus E' (Figure 3), and layer thickness (Figure 4) correspond to a minimum in the SFG amplitudes of the interfacial water molecules (Figure 7) that is indicative for zero net charge at the interface.

3.4. Rheology of Foams from β-Lactoglobulin Solutions. As the interfacial properties of the BLG layers can influence foam properties substantially,[54] measurements of the rheology of BLG foams were performed. The apparent yield stresses and the elastic moduli of the foams are presented in Figure 8. In Figure 8a, the flow curves of the BLG foams at similar gas volume fractions are shown. All curves exhibit the same characteristic features. At low stresses a very high constant apparent viscosity is measured before a sharp decrease appears that is coupled with the onset of foam flow. The point of yielding can be obtained by plotting the strain γ against the applied shear stress τ. The strain curve $\gamma(\tau)$ can be divided in two regions with different slopes: in the first region the slope is close to 1, and consequently, only very small deformations of the foam occur. In the second region the slope increases drastically, indicating flowing of the foam. Hence, the point of change in slope is determined as apparent yield stress. As can be seen in Figure 8b, the apparent yield stress is maximal for pH 5 followed by pH 6.8 and pH 3. The storage modulus G' (Figure 8c) stays constant at low stress amplitudes which is indicative for the linear viscoelastic regime. Videos show that in this range the bubble network can withstand the applied stress and the bubbles stay at their original positions. The end of the linear viscoelastic regime, where G' starts to decrease, is coupled with the yielding of the foam (see Figure 8a). Here, the gas bubbles of the foam start to move past each other. The pH dependence of the storage modulus is similar as for the yield

dx.doi.org/10.1021/la402729g | Langmuir 2013, 29, 11646−11655

stress, giving the highest values at pH 5, followed by pH 6.8 and the lowest values for pH 3.

Figures 8b and 8d show that the described behavior of the foam is consistent over the whole range of measured gas volume fractions. In these graphs the yield stress and storage modulus are normalized by the Laplace pressure to account for the bubble sizes. Foams at pH 3 with $\phi > 88\%$ could not be generated due to a very high coalescence rate. For pH 6.8 and 5, $\tau_y/(\sigma/r_{32})$ increases linearly with the gas volume fraction. For $G_0/(\sigma/r_{32})$ there is no obvious ϕ dependence identifiable. In both cases this behavior of the BLG foams is different compared to the behavior of surfactant and casein foams where several studies[55,56] report a quadratic increase of $\tau_y/(\sigma/r_{32})$ and G_0 with gas volume fraction.

To summarize the results of our foam rheology studies, the highest apparent yield stress and storage moduli can be found in foams from solutions with a pH close to the IEP of BLG. Obviously, the rheology of macrocopic foams is closely related to the properties of BLG modified air−water interfaces, e.g., the already discussed pH-dependent behavior of E' (Figure 3). Higher surface dilational moduli E' lead to higher foam stabilities, yield stresses, and storage moduli, which is in accordance with reported results.[57]

4. GENERAL DISCUSSION

In order to understand the macroscopic behavior of foams from a microscopic picture of the ubiquitous air−water interface, we will now combine the above-discussed information on BLG interfacial layers with the rheological properties of macroscopic BLG foams.

Using interface analysis, we find that the solution pH can be used to tune the interaction potential of proteins at the air−water interface from a repulsive to an attractive regime. We have identified three pH regions where BLG carries either positive, negative, or zero net charge which results to substantial changes in the molecular structure of BLG adsorption layers.

At a pH near the IEP, the absence of net charge minimizes the electrostatic repulsion of proteins to a point where the protein−protein interaction becomes attractive. The latter allows the formation of multilayers with a dense BLG network with high interfacial dilational elasticity while protein charging leads to a decrease of interfacial dilational elasticity of the BLG layers as the elastic behavior of such layers is affected by the protein−protein interactions. The change from repulsive interaction for highly charged proteins to attractive interactions and the increased number density of BLG at the IEP account for the observed maximum in the interfacial dilational elasticity E'. Higher E' at the IEP hinder the foam from destabilization, drainage, and disproportionation as the increased E' decreases the rate of these destabilization mechanisms.[58] The network of BLG multilayers formed around the gas bubbles of the foam at the interfacial IEP increases therefore the foam stability. This network is beneficial to prevent foam drainage and coarsening[6] and increases the resistance of the foam toward mechanical stress as was shown by our foam rheological measurements. The electrostatic repulsions among charged BLG molecules within the layers at pH <4 and pH >7 prevent the formation of multiple layers, and only a monolayer of BLG can exist at the interface. Consequently, the interfacial dilational elasticity together with the resistance to shear is decreasing with increasing repulsion between the BLG molecules.

Although the overall interfacial and macroscopic behaviors are very similar for pH values below and above the interfacial IEP, mechanical properties such as E', G', and τ_y are at pH 3 systematically smaller compared to pH 6.8 on the one hand. However, surface tension (Figure 2) and ellipsometry (Figure 4) show no differences between very acidic and basic pH with similar absolute values of the zeta potentials (Figure 1). It is now interesting to analyze the pH dependence of the SFG amplitude from OH stretching vibrations which is very sensitive to the local electric field. At a pH more acidic than the interfacial IEP, the 3200 cm^{-1} band is much more pronounced compared to more alkaline pH, which becomes even more obvious when the oscillator strength of the OH stretching bands in Figure 7 is analyzed. At pH 3.6 the oscillator strength of the band centered at 3200 cm^{-1} is ∼60 arbitrary units while the amplitude of the 3450 cm^{-1} band is ∼18 arbitrary units only. At pH of 7 the oscillator strengths of both bands are on a similar level of ∼67 arbitrary units. Previously, the 3200 cm^{-1} band was attributed to a more ordered tetrahedrally coordinated network of hydrogen-bonded water molecules, while the 3450 cm^{-1} band was assigned to a more disordered network.[53] As the SFG intensity of OH stretching bands can be related to the local electric field that is generated by the adsorbed proteins at the interface, the observed intensity differences in the discussed pH regions can be related to different charging conditions. In fact, at pH 3 and 7 an overall charge of +20 e and −8 e, respectively, was calculated from the amino acid sequence and determined by titration, respectively.[57,59] Consequently, the significantly higher charging of the interface at pH 3 compared to pH 7 leads to strong polar ordering of interfacial water molecules and much weaker contributions from disordered water molecules to the SFG intensity. Therefore, the SFG intensity of the 3200 cm^{-1} band due to tetrahedrally coordinated H_2O is much higher than the intensity of the 3450 cm^{-1} band due disordered interfacial water molecules. The situation at pH 7 changes as the local electric field is weaker and results in an increase of the SFG contributions from less ordered water molecules. Regarding the charge effects, it is interesting to note that our zeta potential measurements of the bulk BLG do not resolve differences in the protein net charge between pH 3 and pH 7, which seemingly contradicts our conclusions from SFG spectra. However, the zeta potential is determined from electrophoretic mobility measurements where the electric potential at the slipping plane is probed. Here, ions that migrate with the protein are separated from ions not migrating with the protein in the electric field. What seems to be more important is the charge (distribution) directly at the protein surface. The difference between SFG data and zeta potential at acidic pH and the comparison with the estimated charge of BLG indicate that SFG probes the field in the compact double layer close to the protein surface and that the zeta potential is obviously modified by charge screening within the compact double layer (see also below).

For pH values where only a monolayer of BLG is established at the air−water interface, changes in surface charging do not lead to noticeable changes in the coverage of BLG at the air−water interface but rather influence the intermolecular interactions and thus the interfacial elasticity. As the higher local electric field at pH 3 leads to stronger electrostatic repulsions within BLG layers, systematically lower values in E', G', and τ_y are not surprising but are consistent with the change in interaction potential of interfacial proteins which determines

these rheological properties. Our results from foam rheology measurements show a clear difference in foam stability at pH 3 and pH 6.8, which might not only affected by the discussed electrostatic effects directly at the protein surface: As already mentioned, our measurements of the surface tension (Figure 2) do not show a difference between acidic and basic pH at comparatively low BLG concentrations. Since the pH is adjusted by adding diluted HCl or NaOH to the BLG solutions, the ionic strength of the resulting electrolyte is pH dependent. At a pH of 3 the ionic strength is necessarily higher compared to a pH near 7. As a consequence, the higher surface charge at pH 3 and thus the electrostatic repulsion will be partially screened by additional ions in the electric double layer, which also shrinks in its size as the Debye length decreases with increasing ionic strength. This charge screening is higher for pH 3 compared to pH 7 and presumably results into very similar intermolecular interactions at these pH values outside the compact double layer. In fact, this conclusion is corroborated by our observation of an identical absolute value of the zeta potential (Figure 1)—the potential at the shear plane—and similar surface tensions (Figure 2) as well as layer thicknesses (Figure 4).

By increasing the BLG concentration for our foam rheology measurements, this effect is even intensified as more HCl needs to be added in order to adjust the pH to a value of 3. As shown in Table 1, the surface tension is then smaller at pH 3 compared to pH 6.8. The rheology of BLG layers at the air−water interface and macroscopic BLG foams is, however, also dependent on the composition of the entire interfacial layer that includes BLG proteins, solvating water molecules, and ions which stabilize the charged layer at interface. Crossing the isoelectric point will necessarily lead to substantial changes in the electric double layer around the proteins, which is also influenced by the ionic strength (see above). For that reason, differences in foam rheology and surface dilational rheology are not surprising for pH values of 3 and 7.

In addition to the discussed pH-dependent properties of the interfacial layer, it is interesting to discuss also possible structural changes of the BLG molecule that might occur at different pH. In fact, in their NMR study Molinari et al. report that at acidic pH the conformation of BLG is likely to consist of a stable core together with disordered regions.[60] Furthermore, a buried hydrophobic cluster was identified, and it was suggested that this cluster leads to high structural stability of BLG at acidic pH[61] which is consistent with thermodynamic studies.[62] In addition to these observations, Shimizu et al.[63] found a clear increase in hydrophobicity from pH 7 to 3 that is accompanied by decreased foam stability.[57] Taking the latter observations into account, an increase in hydrophobicity might result into a protein layer with the molecules protruding farther into the air phase which then will lead necessarily to weaker screening of the BLG surface charges as less water molecules and ions can be involved into the stabilization of the charged layer. Hence, repulsive interaction within the BLG layer increases.

5. SUMMARY AND CONCLUSION

In this study we have addressed macroscopic properties of aqueous β-lactoglobulin (BLG) foams and the molecular properties of BLG modified air−water interfaces which are inherently connected to the macroscopic foam as they constitute its major structural element. For that purpose we have applied a unique combination of foam rheology measurements and interfacial sensitive methods such as sum-frequency generation, ellipsometry, bubble profile analysis tensiometry, and surface dilational rheology.

We identify three regions of different pH, where both macroscopic and microscopic properties change quite dramatically and are interconnected. At pH conditions around 5—which we identify as the isoelectric point of the interface—interfacial layers of BLG carry no net charge and exhibit attractive intermolecular interactions. The latter causes the formation of disordered and presumably agglomerated BLG multilayers, resulting in a maximum in the surface coverage of BLG. For increasingly alkaline and acidic pH conditions the protein−protein interactions change from attractive to a highly repulsive regime that leads to a formation of BLG monolayers and to highly polar ordered water molecules. Changes in layer thickness and protein−protein interaction (attractive or repulsive) are shown to dramatically change the interfacial dilational elasticity E' which exhibits a maximum around pH 5 where multilayers with zero net charge exists at the air−water surface. This molecular information was correlated with the behavior of the macroscopic BLG foam. Thick and disordered adsorption layers lead to highest foam stability and maximum yield stress as the gas bubbles are protected by the proteins arranged around them. Thin and more ordered layers with strong electrostatic repulsions show a significantly decreased resistance to mechanical stress that is strongly influenced by the actual net charge on the protein surface.

AUTHOR INFORMATION

Corresponding Author

*E-mail: Bjoern.Braunschweig@lfg.fau.de.

Notes

The authors declare no competing financial interest.

ACKNOWLEDGMENTS

The authors thank the group of Ulrich Kulozik (Technische Universität München, Germany) for the supply of high quality β-lactoglobulin.

K.E., C.K., B.B., and W.P. gratefully acknowledge the funding by the German National Science Foundation (DFG) through the Leibniz program and the DFG-AiF cluster project on "Protein Foams" project PE427/21-1. G.G. and R.M. as well as M.L. and N.W. acknowledge also the funding by the DFG-AiF cluster project on "Protein Foams" Mi418/20-1 and Wi 3138/10-1.

REFERENCES

(1) Lefebvre, L.-P.; Banhart, J.; Dunand, D. C. Porous metals and metallic foams: current status and recent developments. *Adv. Eng. Mater* **2008**, *10*, 775−787.

(2) Fameau, A.-L.; Saint-Jalmes, A.; Cousin, F.; Houinsou Houssou, B.; Novales, B.; Navailles, L.; Nallet, F.; Gaillard, C.; Boué, F.; Douliez, J.-P. Smart foams: switching reversibly between ultrastable and unstable foams. *Angew. Chem.* **2011**, *123*, 8414−8419.

(3) Prud'homme, R. K.; Khan, S. A. *Foams: Theory, Measurements, and Applications*; Marcel Dekker, Inc.: New York,1996.

(4) Mezzenga, R.; Schurtenberger, P.; Burbidge, A.; Michel, M. Understanding foods as soft materials. *Nat. Mater.* **2005**, *4*, 729−740.

(5) Foegeding, E. A.; Luck, P. J.; Davis, J. P. Factors determining the physical properties of protein foams. *Food Hydrocolloids* **2006**, *20*, 284−292.

(6) Engelhardt, K.; Rumpel, A.; Walter, J.; Dombrowski, J.; Kulozik, U.; Braunschweig, B.; Peukert, W. Protein adsorption at the electrified air−water interface: implications on foam stability. *Langmuir* **2012**, *28*, 7780−7787.

(7) Dickinson, E.; Ettelaie, R.; Murray, B. S.; Du, Z. Kinetics of disproportionation of air bubbles beneath a planar air-water interface stabilized by food proteins. *J. Colloid Interface Sc.* **2002**, *252*, 202−213.
(8) Davis, J. P.; Foegeding, E. A. Foaming and interfacial properties of polymerized whey protein isolate. *J. Food Sci.* **2004**, *69*, C404.
(9) McClellan, S. J.; Franses, E. I. Effect of concentration and denaturation on adsorption and surface tension of bovine serum albumin. *Colloids Surf., B* **2003**, *28*, 63−75.
(10) Lu, J. R.; Su, T. J.; Penfold, J. Adsorption of serum albumins at the air/water interface. *Langmuir* **1999**, *15*, 6975−6983.
(11) Atkinson, P. J.; Dickinson, E.; Horne, D. S.; Richardson, R. M. Neutron reflectivity of adsorbed β-casein and β-lactoglobulin at the air/water interface. *J. Chem. Soc., Faraday Trans.* **1995**, *91*, 2847−2854.
(12) Richter, A. G.; Kuzmenko, I. Using in situ X-ray reflectivity to study protein adsorption on hydrophilic and hydrophobic surfaces: benefits and limitations. *Langmuir* **2013**, *29*, 5167−5180.
(13) Stocco, A.; Drenckhan, W.; Rio, E.; Langevin, D.; Binks, B. P. Particle-stabilised foams: an interfacial study. *Soft Matter* **2009**, *5*, 2215−2222.
(14) Miller, R.; Fainerman, V. B.; Wüstneck, R.; Krägel, J.; Trukhin, D. V. Characterisation of the initial period of protein adsorption by dynamic surface tension measurements using different drop techniques. *Colloids Surf., A* **1998**, *131*, 225−230.
(15) Bouyer, E.; Mekhloufi, G.; Huang, N.; Rosilio, V.; Agnely, F. β-Lactoglobulin, gum arabic, and xanthan gum for emulsifying sweet almond oil: formulation and stabilization mechanisms of pharmaceutical emulsions. *Colloids Surf., A* **2013**, *433*, 77−87.
(16) Zhang, C.; Myers, J. N.; Chen, Z. Elucidation of molecular structures at buried polymer interfaces and biological interfaces using sum frequency generation vibrational spectroscopy. *Soft Matter* **2013**, *9*, 4738−4761.
(17) Roke, S. Nonlinear optical spectroscopy of soft matter interfaces. *ChemPhysChem* **2009**, *10*, 1380−1388.
(18) Wang, J.; Buck, S. M.; Chen, Z. Sum frequency generation vibrational spectroscopy studies on protein adsorption. *J. Phys. Chem. B* **2002**, *106*, 11666−11672.
(19) Kim, G.; Gurau, M.; Kim, J.; Cremer, P. S. Investigations of lysozyme adsorption at the air/water and quartz/water interfaces by vibrational sum frequency spectroscopy. *Langmuir* **2002**, *18*, 2807−2811.
(20) Fu, L.; Ma, G.; Yan, E. C. Y. In situ misfolding of human islet amyloid polypeptide at interfaces probed by vibrational sum frequency generation. *J. Am. Chem. Soc.* **2010**, *132*, 5405−5412.
(21) Liu, Y.; Jasensky, J.; Chen, Z. Molecular interactions of proteins and peptides at interfaces studied by sum frequency generation vibrational spectroscopy. *Langmuir* **2012**, *28*, 2113−2121.
(22) Ding, B.; Soblosky, L.; Nguyen, K.; Geng, J.; Yu, X.; Ramamoorthy, A.; Chen, Z. Physiologically-relevant modes of membrane interactions by the human antimicrobial peptide, LL-37, revealed by SFG experiments. *Sci. Rep.* **2013**, *3*, 1854.
(23) Thennarasu, S.; Huang, R.; Lee, D.-K.; Yang, P.; Maloy, L.; Chen, Z.; Ramamoorthy, A. Limiting an antimicrobial peptide to the lipid-water interface enhances its bacterial membrane selectivity: a case study of MSI-367. *Biochemistry* **2010**, *49*, 10595−10605.
(24) Toro-Sierra, J.; Tolkach, A.; Kulozik, U. Fractionation of α-Lactalbumin and β-Lactoglobulin from whey protein isolate ssing selective thermal aggregation, an optimized membrane separation procedure and resolubilization techniques at pilot plant scale. *Food Bioprocess. Technol.* **2013**, *6*, 1032−1043.
(25) Wit, J. N. de Thermal behaviour of bovine β-lactoglobulin at temperatures up to 1500°C. a review. *Trends Food Sci. Technol.* **2009**, *20*, 27−34.
(26) Loglio, G.; Pandolfini, P.; Miller, R.; Makievski, A.; Ravera, F.; Ferrari, M.; Liggieri, L. Drop and bubble shape analysis as tool for dilational rheology studies of interfacial layers. In *Novel Methods to Study Interfacial Layers*, 1st ed.; Möbius, D., Miller, R., Eds.; Elsevier: Amsterdam, 2001.
(27) Wüstneck, R.; Fainerman, V. B.; Aksenenko, E. V.; Kotsmar, C.; Pradines, V.; Krägel, J.; Miller, R. Surface dilatational behavior of β-casein at the solution/air interface at different pH values. *Colloids Surf., A* **2012**, *404*, 17−24.
(28) Gochev, G.; Retzlaff, I.; Aksenenko, E. V.; Fainerman, V. B.; Miller, R. Adsorption isotherm and equation of state for β-Lactoglobulin layers at the air/water surface. *Colloids Surf., A* **2013**, *422*, 33−38.
(29) Benjamins, J.; Lucassen-Reynder, E. H. Interfacial rheology of adsorbed protein layers. In *Interfacial Rheology*; Liggieri, L., Miller, R., Krotov, V. V., Eds.; Brill: Leiden, 2009.
(30) Holt, S. A.; White, J. W. The molecular structure of the surface of commercial cow's milk. *Phys. Chem. Chem. Phys.* **1999**, *1*, 5139−5145.
(31) Marsh, R. J.; Jones, R. A. L.; Sferrazza, M.; Penfold, J. Neutron reflectivity study of the adsorption of β-Lactoglobulin at a hydrophilic solid/liquid interface. *J. Colloid Interface Sci.* **1999**, *218*, 347−349.
(32) Verheul, M.; Pedersen, J. S.; Roefs, S. P. F. M.; Kruif, K. G. de Association behavior of native β-lactoglobulin. *Biopolymers* **1999**, *49*, 11−20.
(33) Shen, Y. R. *The Principles of Nonlinear Optics*: John Wiley & Sons: New York,1984.
(34) Rumpel, A.; Novak, M.; Walter, J.; Braunschweig, B.; Halik, M.; Peukert, W. Tuning the molecular order of C60 functionalized phosphonic acid monolayers. *Langmuir* **2011**, *27*, 15016−15023.
(35) Wierenga, P. A.; Gruppen, H. New views on foams from protein solutions. *Curr. Opin. Colloid Interface Sci.* **2010**, *15*, 365−373.
(36) Nino, M. R.; Sanchez, C. C.; Fernandez, M. C.; Patino, J. M. Protein and lipid films at equilibrium at air-water interface. *J. Am. Oil. Chem. Soc.* **2001**, *78*, 873−879.
(37) Feitosa, K.; Marze, S.; Saint-Jalmes, A. Durian, D. Electrical conductivity of dispersions: from dry foams to dilute suspensions. *J. Phys.: Conden. Matter* **2005**, *17*, 6301.
(38) Chi, E. Y.; Krishnan, S.; Randolph, T. W.; Carpenter, J. F. Physical stability of proteins in aqueous solution: mechanism and driving forces in nonnative protein aggregation. *Pharm. Res.* **2003**, *20*, 1325−1336.
(39) Fennema, O. R. *Food Chemistry*, 3rd ed.; Marcel Dekker: New York, 1996.
(40) Wong, D. W. S.; Camirand, W. M.; Pavlath, A. E.; Parris, N.; Friedman, M. Structures and functionalities of milk proteins. *Crit. Rev. Food Sci. Nutr.* **1996**, *36*, 807−844.
(41) Bhandari, B., Roos, Y. H., Eds.; *Food Materials Science and Engineering*; Wiley-Blackwell: Ames, IA, 2012.
(42) Mucha, M.; Frigato, T.; Levering, L. M.; Allen, H. C.; Tobias, D. J.; Dang, L. X.; Jungwirth, P. Unified molecular picture of the surfaces of aqueous acid, base, and salt solutions. *J. Phys. Chem. B* **2005**, *109*, 7617−7623.
(43) Dickinson, E. Proteins at interfaces and in emulsions stability, rheology and interactions. *J. Chem. Soc., Faraday Trans* **1998**, *94*, 1657−1669.
(44) Wüstneck, R.; Krägel, J.; Miller, R.; Fainerman, V. B.; Wilde, P. J.; Sarker, D. K.; Clark, D. C. Dynamic surface tension and adsorption properties of β-casein and β-lactoglobulin. *Food Hydrocolloids* **1996**, *10*, 395−405.
(45) Perriman, A. W.; Henderson, M. J.; Holt, S. A.; White, J. W. Effect of the air−water interface on the stability of β-Lactoglobulin. *J. Phys. Chem. B* **2007**, *111*, 13527−13537.
(46) Beretta, S.; Chirico, G.; Baldini, G. Short-range interactions of globular proteins at high ionic strengths. *Macromolecules* **2000**, *33*, 8663−8670.
(47) Majhi, P. R.; Ganta, R. R.; Vanam, R. P.; Seyrek, E.; Giger, K.; Dubin, P. L. Electrostatically driven protein aggregation: β-Lactoglobulin at low ionic strength. *Langmuir* **2006**, *22*, 9150−9159.
(48) Gottschalk, M.; Nilsson, H.; Roos, H.; Halle, B. Protein self-association in solution: the bovine β -lactoglobulin dimer and octamer. *Protein Sci.* **2003**, *12*, 2404−2411.
(49) Wang, J.; Buck, S. M.; Chen, Z. The effect of surface coverage on conformation changes of bovine serum albumin molecules at the air-solution interface detected by sum frequency generation vibrational spectroscopy. *Analyst* **2003**, *128*, 773−778.

(50) Chen, X.; Flores, S. C.; Lim, S.-M.; Zhang, Y.; Yang, T.; Kherb, J.; Cremer, P. S. Specific anion effects on water structure adjacent to protein monolayers. *Langmuir* **2010**, *26*, 16447−16454.
(51) Chen, X.; Yang, T.; Kataoka, S.; Cremer, P. S. Specific ion effects on interfacial water structure near macromolecules. *J. Am. Chem. Soc.* **2007**, *129*, 12272−12279.
(52) Richmond, G. L. Molecular bonding and interactions at aqueous surfaces as probed by vibrational sum frequency spectroscopy. *Chem. Rev.* **2002**, *102*, 2693−2724.
(53) Shen, Y. R.; Ostroverkhov, V. Sum-frequency vibrational spectroscopy on water interfaces: polar orientation of water molecules at interfaces. *Chem. Rev.* **2006**, *106*, 1140−1154.
(54) Georgieva, D.; Cagna, A.; Langevin, D. Link between surface elasticity and foam stability. *Soft Matter* **2009**, *5*, 2063−2071.
(55) Marze, S.; Guillermic, R. M.; Saint-Jalmes, A. Oscillatory rheology of aqueous foams: surfactant, liquid fraction, experimental protocol and aging effects. *Soft Matter* **2009**, *5*, 1937−1946.
(56) Mason, T. G.; Bibette, J.; Weitz, D. A. Elasticity of compressed emulsions. *Phys. Rev. Lett.* **1995**, *75*, 2051−2054.
(57) Davis, J. P.; Foegeding, E. A.; Hansen, F. K. Electrostatic effects on the yield stress of whey protein isolate foams. *Colloids Surf., B* **2004**, *34*, 13−23.
(58) van Prins, A. B. M.; Boerboom, F.; Kalsbeek, H. Relation between surface rheology and foaming behavior of aqueous protein solutions. In *Proteins at liquid interfaces*; Miller, R., Möbius, D., Eds.; Elsevier: Amsterdam, 1998.
(59) Nozaki, Y.; Bunville, L. G.; Tanford, C. Hydrogen ion titration curves of β-lactoglobulin. *J. Am. Chem. Soc.* **1959**, *81*, 5523−5529.
(60) Molinari, H.; Ragona, L.; Varani, L.; Musco, G.; Consonni, R.; Zetta, L.; Monaco, H. L. Partially folded structure of monomeric bovine β-lactoglobulin. *FEBS Lett.* **1996**, *381*, 237−243.
(61) Ragona, L.; Pusterla, F.; Zetta, L.; Monaco, H. L.; Molinari, H. Identification of a conserved hydrophobic cluster in partially folded bovine β-lactoglobulin at pH 2. *Folding Des.* **1997**, *2*, 281−290.
(62) Kella, N. K.; Kinsella, J. E. Enhanced thermodynamic stability of beta-lactoglobulin at low pH. A possible mechanism. *Biochem. J.* **1988**, *255*, 113−118.
(63) Shimizu, M.; Saito, M.; Yamauchi, K. Emulsifying and structural properties of beta-lactoglobulin at different pHs. *Agric. Biol. Chem.* **1985**, *49*, 189−194.

3 Yield stress and elasticity of aqueous foams from protein and surfactant solutions – the role of continuous phase viscosity and interfacial properties

Colloids and Surfaces A: Physicochem. Eng. Aspects 459 (2014) 177–185

Contents lists available at ScienceDirect

Colloids and Surfaces A: Physicochemical and Engineering Aspects

journal homepage: www.elsevier.com/locate/colsurfa

Yield stress and elasticity of aqueous foams from protein and surfactant solutions – The role of continuous phase viscosity and interfacial properties

M. Lexis*, N. Willenbacher

Department of Chemical Engineering, Karlsruhe Institute of Technology, 76131 Karlsruhe, Germany

HIGHLIGHTS

- We discuss the influence of liquid phase viscosity on yield stress and storage modulus of aqueous foams.
- We investigate the correlation between foam rheology and interfacial rheology.
- Higher interfacial elasticity increases yield stress and storage modulus of the foams.
- Aggregation of proteins lowers interfacial but increases foam elastic modulus.

GRAPHICAL ABSTRACT

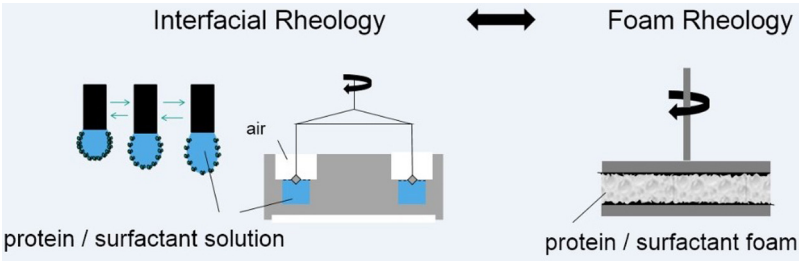

ARTICLE INFO

Article history:
Received 16 April 2014
Received in revised form 29 May 2014
Accepted 16 June 2014
Available online 5 July 2014

Keywords:
Rheology
Foams
Proteins
Surfactants
Interfaces

ABSTRACT

We discuss the effect of solvent viscosity η_L and interfacial elasticity (E', G') on apparent yield stress τ_y and storage modulus G_0 of protein and surfactant foams made from solutions of these amphiphiles in various water/glycerol mixtures. The critical volume fraction at which τ_y and G_0 occur is calculated from the bubble size distribution and is related to the adsorption kinetics of the corresponding amphiphile. Dependence of τ_y on η_L is weak ($\tau_y \sim \eta_L^{0.3}$). Generally, higher interfacial moduli correspond to higher τ_y and G_0, but the relationship is non-trivial when protein interaction and structure formation get relevant. Increasing glycerol fraction reduces electrostatic interaction range and solvent quality for the proteins. This leads to an increase in E' as well as G_0 for casein. For whey protein isolate (WPI) at 1% concentration, this results in an increase in G_0, a decrease in E', and a broad transition region between linear and non-linear stress response. These findings are consistently attributed to protein aggregation finally resulting in network formation across lamellae. This network does not form at 0.1% WPI concentration and accordingly G_0 increases with WPI concentration. In contrast, τ_y remains constant suggesting that this network is destroyed at this stress level.

1. Introduction

Aqueous foams are dispersions of gas in a liquid. Here, we restrict ourselves to dispersions with gas volume fractions beyond the maximum packing fraction ϕ_c at which gas bubbles start to deviate from their spherical shape. The bubbles need to be stabilized, e.g. by amphiphilic molecules like surfactants or proteins. Foams can be found in numerous industrial applications and especially in the food sector the creation of foamed products is a rapidly growing process [1]. From a rheological point of view foams are complex systems that exhibit viscoelastic behavior and an apparent yield stress. Below a critical shear stress the jammed foam bubbles

* Corresponding author. Tel.: +49 72160842805.
E-mail address: meike.lexis@kit.edu (M. Lexis).

http://dx.doi.org/10.1016/j.colsurfa.2014.06.030
0927-7757/

do not move past each other. In this regime foams behave as viscoelastic solids with $G' \gg G''$ and initially start flowing above this critical stress, called apparent yield stress.

Investigation of the parameters having an impact on the yield stress of foams as well as the elastic properties at low stresses has been subject to many studies [2–9]. Most of the studies were performed on surfactant foams or emulsions (as model system for foams) and some additionally on protein foams. They all agree in the point that the crucial parameters determining foam rheology are gas volume fraction, surface tension, as well as bubble size distribution. Generally, the yield stress and the storage modulus were found to be proportional to $(\sigma/r_{32})^*\phi^2$ where σ is the surface tension, r_{32} the Sauter mean radius and ϕ the gas volume fraction. Some authors additionally mention the continuous phase viscosity and the interfacial viscoelasticity of the adsorbed layer to be important for the stability [10] and the rheology [9,11] of foams but systematic investigation is missing in the literature.

Adsorbed protein layers at liquid/gas interfaces show viscoelastic behavior, when the surface concentration is sufficiently high due to an evolving contact network. The classical, most often used explanation is attractive interactions resulting from covalent cross-linking [12,13]. The underlying mechanisms are analogous to the gelling caused by heat or chemical denaturation [14]. However, several studies executed on protein films at the air/water interface have not been able to confirm that covalent cross-linking is the dominating source of interfacial elasticity [14–18]. Instead they propose a colloidal view of the protein layers [19,20] where the interfacial elasticity is a result of densely packed loose proteins. Cicuta et al. [19] showed that an adsorbed layer of β-lactoglobulin behaves similarly to an adsorbed layer of colloidal polystyrene particles. Elastic behavior sets in when a maximum packing fraction at the interface is exceeded and the protein molecules start to act like soft disks.

The surface dilational modulus is often referred to as the crucial surface layer property determining the foam stability. Unfortunately, the studies of interfacial viscoelasticity are mainly focused on small protein concentrations that are substantially lower than the concentrations needed to create stable foams [21–24].

In the present work, we discuss the parameters influencing the rheological foam properties yield stress τ_y and storage modulus G_0. In order to cover a broad variety of interfacial features we worked with different protein and surfactant systems that are known to create different interfacial layers. We suggest a phenomenological expansion of Masons equations [4,5] for τ_y and G_0 including the liquid viscosity η_L. Moreover, we present a way to predict the critical gas volume fraction ϕ_c from the bubble size distribution in the foam based on a model equation developed for the calculation of the maximum packing fraction of solid spheres with arbitrary particle size distribution. Additionally, we characterize the surface elasticity in dilation and shear and discuss the relationship between interfacial viscoelastic properties and bulk foam rheology. All measurements on the solutions and foams were carried out at equal protein or surfactant concentrations enabling a direct comparison of interfacial and macroscopic foam properties.

Since the yield stress τ_y is a key feature regarding foam rheology we also include an elaborate discussion on the determination of this quantity and the deformation and flow of the foams investigated here at stresses below and above τ_y.

2. Experimental details

2.1. Solution preparation and measurements

Surfactant foams were made from a mixture of 2% (w/w) of the nonionic surfactant Triton X-100 ($C_{14}H_{22}O(C_2H_4O)_n$, n = 9–10, BASF) and 0.2% (w/w) of the anionic surfactant sodium dodecyl sulfate ($C_{12}H_{25}NaO_4S$, Roth) dissolved in different mixtures of distilled water and glycerol (≥99.5%, Carl Roth). For the protein foams we used 0.1% and 1% (w/w) whey protein isolate (WPI, Fonterra) as well as 3% (w/w) micellar casein that was kindly provided by the group of Hinrichs (University of Hohenheim, Germany) and used as received. For the determination of the gas volume fraction the conductivity of the solution must be sufficiently high. The natural pH of all solutions was pH 7 ± 0.2.

The surface tension of all solutions was measured with the pendant drop method (Krüss, DSA 100) at 21 °C. For the protein solutions the surface tension is time dependent. After 20 min measurement time a quasi-equilibrium value was reached that was used to calculate the Laplace pressure of the foam bubbles. As the protein foams were made at higher temperatures a systematic error arises in our calculations. Niño et al. [25] found that the temperature dependence of the surface tension of the protein solutions is mainly attributed to the temperature dependent surface tension of water. Including this assumption we can estimate the error to be less than 5%.

The liquid viscosities were measured with the ARES controlled strain rheometer from TA Instruments using a double wall Couette geometry (32/34 mm). All solutions showed Newtonian behavior in the range of imposed shear rates $\dot{\gamma} = 1$–$250\ s^{-1}$.

Interfacial dilational viscoelastic properties were determined at 21 °C using the oscillating bubble method (Krüss, DSA 100). The oscillations are generated by a piezo pump that pulsed with a frequency of 0.1 Hz and amplitude of 0.3. As the generation of the drop was carried out manually it was not possible to keep the drop volume for each measurement exactly the same. Hence, the amplitude resulted in a surface deformation between 2% and 3%, depending on the drop volume. The viscoelastic properties were measured at a drop age of 30 min. Therefore, oscillatory deformation was applied for a time period of 100 s and 1200 pictures were analyzed to calculate $E^* = E' + iE''$.

Interfacial shear viscoelastic properties were determined at 25 °C with the stress controlled rotational rheometer DHR3 from TA Instruments using the double wall ring geometry (D_{ring} = 70 mm). Details about this measuring geometry can be found in [26]. After 30 min aging of the surface the viscoelastic properties were recorded at a frequency of 0.7 Hz and a deformation amplitude of 1%. For every sample solution we confirmed that the amplitude did not exceed the linear viscoelastic regime and therefore we assume that it did not affect the network formation of the proteins.

2.2. Foam preparation and measurements

The protein solutions were preheated to 50 °C in a water bath to obtain foams that are stable enough for reproducible rheological measurements. At this temperature adsorption kinetics is supposed to be fast enough for quick stabilization of the gas bubbles but the temperature is still low enough to exclude protein denaturation [27]. This assumption finds confirmation in experiments (results not shown) with higher whey protein concentrations (3 wt%) where we were able to produce foams between 20 and 50 °C. Independent of process temperature, all foams showed identical yield stresses and storage moduli normalized by the Laplace pressure, thus taking into account the variation in bubble size. Furthermore, the protein solutions preheated to 50 °C and subsequently cooled down to 21 °C did exhibit the same surface tension as the untreated protein solutions. This further supports the assumption that an increase in temperature up to 50 °C does not affect the protein structure. Surfactant solutions were used at room temperature (21 °C).

For foam preparation solutions were poured on a glass filter (pore size 9–16 μm) fused in a glass pipe (diameter = 60 mm, height = 53 mm). From the bottom side nitrogen was purged

through the pores ($\dot{V}$ = 60–80 ml/min). As soon as the foam reached the column height the nitrogen flow was stopped and recording of the foam age was started.

The time dependent gas volume fraction was determined from conductivity measurements using an electrode with integrated temperature sensor (WTW, Cond 340i). The ratio of foam to solution conductivity κ ($\kappa = \kappa_{foam}/\kappa_{solution}$) was used to calculate the gas volume fraction (Eq. (1)) [28]

$$\phi = 1 - \frac{3\kappa(1+11\kappa)}{1+25\kappa+10\kappa^2} \quad (1)$$

As the protein foams cool down over time the temperature dependent conductivity of the protein solutions was determined in advance. In this way the κ-values referring to the foam temperature could be calculated.

The bubble size distribution was determined from images taken with an endoscopic CCD camera (Lumenera LU 160, resolution 1392 × 1040) that was placed inside the foam. The Sauter mean radius r_{32} was extracted from image analysis with the software iPS (Visiometrics, Germany).

Foam rheological measurements were carried out with the controlled stress rotational rheometer Rheoscope 1 (Thermofisher, Germany) using a parallel plate geometry with a diameter of 60 mm. The surfaces were covered with sandpaper and the gap was set to 6 mm to minimize wall slip effects. The measurement time was 60 s in order to limit time dependent changes in foam structure. Each foaming system was measured at different foam ages and hence, different gas volume fractions ϕ between 80% and 94%.

The apparent yield stress was determined from steady shear measurements. The stress was continuously increased. Depending on foam composition the initial stress was between 3 and 10 Pa and the final stress between 25 and 115 Pa. On the experimental timescales employed here the apparent yield stress was independent of start and end point of the selected stress ramp as well as on the number of data points taken. Preliminary experiments with continuous and stepwise increasing stresses (up to 6 s per data point) did not lead to significant differences in the resulting yield stress value.

The moduli G' and G'' of the foams were determined from oscillatory shear measurements with varying stress amplitude at a frequency f = 1 Hz. The linear viscoelastic moduli did not show frequency dependence between 0.01 and 10 Hz. Hence, the measured G'-value in the linear viscoelastic regime is called plateau modulus G_0.

3. Results and discussion

3.1. Foam and solution properties

In Table 1 the values of the liquid viscosity η_L, the Sauter mean radius r_{32} and the surface tension σ measured for the different foam systems are summarized. Note that the mean bubble radius increases with time due to degradation processes and the liquid phase viscosity of the protein foams increases due to cooling of the foams.

3.2. Bubble size distribution

The bubble size distribution determines the maximum packing fraction that can be reached before the spherical bubbles start to deform. This critical value increases with broadening of the size distribution. From a physical point of view, it is the transition point where a gas dispersion turns into a jammed system with a yield stress and elastic properties [5,6]. In previous studies the critical gas volume fraction was treated as a fit parameter or an estimated value between 0.63 and 0.71 for random close packing and hexagonal close packing was used, respectively.

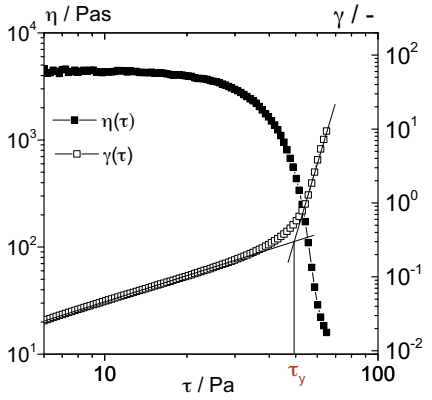

Fig. 1. viscosity and deformation versus shear stress for a WPI foam (ϕ = 83%) made from a protein solution dissolved in a water/glycerol (60/40) mixture.

Based on a large number of data sets Sudduth et al. [29] have proposed an empirical model to calculate the maximum packing fraction ϕ_c of suspensions from the size distribution of the suspended particles. Assuming a n-modal discrete distribution results in Eq. (2), where $\phi_{c,mono}$ is the maximum packing fraction of a monodisperse suspension ($\phi_{c,mono}$ = 0.63) and r_x is the xth moment of the particle size distribution

$$\phi_c = \phi_n - (\phi_n - \phi_{c,mono}) \exp\left(0.271 - \left(1 - \frac{r_5}{r_1}\right)\right) \quad (2)$$

with

$$\phi_n = 1 - (1 - \phi_{c,mono})^n$$

and

$$r_x = \frac{\sum_{i=1}^{n} N_i r_i^x}{\sum_{i=1}^{n} N_i r_i^{x-1}}$$

This equation is supposed to be valid for foams as well as they can be considered as highly concentrated suspensions as long as $\phi \leq \phi_c$. Hence, the critical gas volume fraction ϕ_c was calculated for each foam from the measured bubble size distribution.

Depending on the foam age the calculated ϕ_c values varied between 0.65 and 0.69 for the surfactant foams, between 0.71 and 0.75 for the 1% WPI, 0.74–0.78 for the 0.1% WPI foams and between 0.67 and 0.69 for the casein foams, i.e. in all cases the corresponding bubble size distribution broadens with time. The initial maximum packing fractions reflect very well the different adsorption behavior of the foaming agents. Time dependent surface tension measurements reveal that the surfactants used here adsorb very fast at the interface and are able to instantly stabilize the rising gas bubbles before coalescence can occur. This leads to very homogeneous bubble size distributions. Casein adsorbs slower than the SDS/Triton X100 surfactant mixture and whey protein even slower than casein. Accordingly, the width of the bubble size distribution increases in the order surfactant, casein, whey protein and this is directly reflected in the corresponding ϕ_c values.

3.3. Steady shear measurements

Steady shear measurements with increasing applied stress provide flow curves that are usually used to determine the viscosity in dependence of the shear stress or strain rate and if applicable the yield stress is deduced. For the foams used in this study the measured viscosity vs. shear stress curves usually split up into two sections as exemplary shown in Fig. 1 exemplary for a WPI foam. In

Table 1
Measured liquid viscosities η_L, Sauter mean radius r_{32} and surface tension σ for the different foaming systems. The given ranges are according to initial and final foam ages where the rheological measurements took place. The maximum deviations of the measured values from the average data listed above are given in the last line.

Glycerol/%	Surfactants			WPI 1%	*WPI 0.1%*		Casein		
	η_L/ mPa s	r_{32}/μm	σ/mN/m	η_L/ mPa s	r_{32}/μm	σ/mN/m	η_L/ mPa s	r_{32}/μm	σ/mN/m
0	1.2	72–177	31.9	0.8–1.1 *0.9–1.0*	96–212 *242–328*	49.8*52.9*	1.3–1.8	124–166	48.4
20	2.1	67–197	31.3	1.4–1.7 *1.6–1.7*	89–202 *195–258*	49.8*53.1*	3.0–3.6	136–151	48.1
30	–	–	–	–	–	–	3.8–4.8	177–186	47.5
40	4.6	72–164	30.7	2.9–3.8 *3.0–3.3*	96–193 *180–204*	50.3*53.2*	–	–	–
60	12.3	77–192	30.7	7.5–10.5 *7.8–10.0*	131–165 *191–209*	51.2*52.8*	–	–	–
Max. deviation/%	1.1	5.1	0.3	1.3 *1.4*	10.6 *26.0*	1.5 *1.5*	2.0	10.4	0.2

the first section we find an almost constant apparent zero shear viscosity that changes over to a shear thinning region within a narrow range of shear stresses. Theoretically there may also exist a third section at higher stresses, the high shear plateau. This regime is not found in our measurements because the foam structure changes with time and applied stress. In contrast to the value for the apparent zero shear viscosity the stress where the viscosity starts to decrease drastically does not depend on the measuring parameters at constant measurement times as already found by Møller et al. [30] for other densely packed foam and emulsion systems with an apparent yield stress. This characteristic stress is defined as the apparent yield stress. Here we determine this value by plotting the deformation versus the shear stress. Two regions with different slopes can be identified as also depicted in Fig. 1. In the first region the slope is close to 1 and hence, only small deformations occur (caused by coarsening induced bubble rearrangements). In the second region the rate of deformation drastically increases indicating foam flow. The stress at which the tangents to each regime intersect is defined as the apparent yield stress τ_y here.

We found the apparent viscosity level in the first region to strongly depend on measuring parameters like initial and final stress as well as measuring time per data point (see Fig. 2b). Similar results have already been reported by Møller et al. [30] who argue that the apparent zero shear viscosity would rise up to infinity if the measurement time would do so. From creep tests (see Fig. 2a) we are able to confirm that the apparent viscosity below the yield stress ($\tau \ll \tau_y$) monotonically increases with time. At stresses close to the yield stress the viscosity stays constant for a certain time period before it drastically decreases. Stresses higher than τ_y lead to a monotonic decrease in viscosity during the period of observation. Based on the results of Cohen-Addad et al. [31] and Vincent-Bonnieu et al. [32] we propose the following explanation. Foams are thermodynamically unstable systems and change their structure over time. Liquid films between the bubbles become thinner due to drainage and eventually burst leading to coalescence of the bubbles. At stresses far below the yield stress these local relaxations induce an apparent highly viscous flow [31]. Hence, the measured apparent viscosity is a result of the displacement of the upper plate due to bubble rearrangements induced by coalescence. The coalescence rate is correlated to the number of separating lamellae, it decreases with time and hence, the apparent viscosity increases with time. The absolute value of the yield stress of a foam decreases with foam age because the average bubbles size increases and the distribution broadens with time. This is the reason why at stresses close to, but still below the yield stress ($\tau < \tau_y$) the foam starts to flow after a certain time period, for the example shown in Fig. 2a after 160 s. Stresses far beyond the yield stress ($\tau > \tau_y$) instantly induce flow. The monotonic decrease of the viscosity is caused by the degrading processes mentioned before.

The viscosities in the shear-thinning region have to be considered as apparent values because they were not measured at steady state. From Fig. 2a it can be extracted that reaching a steady state viscosity at a given shear stress if accessible at all takes far longer than the total measurement time of 60 s employed for the stress ramp in the experiments discussed here. Such long timescales are not appropriate for the characterization of foams because of the time dependent structure evolution.

Here, we restrict ourselves to the determination of τ_y which is reproducible and robust with respect to the choice of experimental parameters. It should be noted that the determination of steady shear viscosity data is prone to systematic errors not only because the foam structure changes with time and applied stress or strain. An additional error arises because the flow profile in the shear gap is not necessarily homogeneous. Shear banding phenomena have been observed in several studies [33,34] and need to be considered when measuring foam viscosity. In Fig. 3 this is illustrated for surfactant foam but similar results were also found for the protein foams investigated here. The positions of 17 bubbles were tracked over a time period of 5 s at a constant shear rate of $\gamma = 0.2\,s^{-1}$. Obviously, the velocity does not change linearly as it is required for a correct viscosity calculation. Instead, two flow regimes with different shear rates are observed.

3.4. Yield stress

Even if a true viscosity is hard to define and depends on measuring parameters, the yield stress of our foaming systems does not seem to be markedly affected by that. Varying gap sizes between 3 and 8 mm, different initial and final stresses in stress ramp experiments as well as different measuring times per data point (0.2–6 s) at a constant total measurement time of 60 s did not lead to significant differences in the yield stress. In Fig. 4, the yield stress values for all created foams are shown in dependence of ϕ–ϕ_c where ϕ_c has been determined from the bubble size distribution as described in Section 3.2. The experimental data are normalized by the Laplace pressure (σ/r_{32}) in order to account for the different average bubble sizes and multiplied with the empirically determined factor $(\eta_L/\eta_W)^{-0.3}$. Here, η_L is the continuous phase viscosity and η_W is the viscosity of water. As already reported previously [9] this leads to a collapse of all data points for each particular foaming system onto a master curve. Based on the equation proposed by Mason [4,5], the yield stress can be described by the following empirical equation:

$$\tau_y = k \cdot \left(\frac{\sigma}{r_{32}}\right) \cdot \left(\frac{\eta_L}{\eta_W}\right)^{0.3} \cdot (\phi - \phi_c)^2 \quad (3)$$

The pre-factor k is the only fit parameter in this equation, all other quantities are determined independently. Comparing the

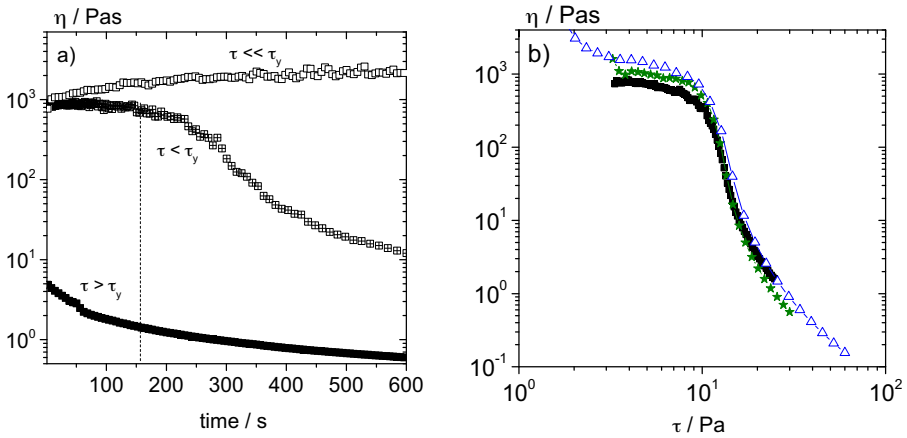

Fig. 2. (a) Creep tests for a foam made from the surfactant mixture dissolved in water with $\tau \ll \tau_y$ at 1 Pa (open symbols), $\tau < \tau_y$ at 8 Pa (crossed symbols) and $\tau > \tau_y$ at 20 Pa (closed symbols), (b) apparent viscosity versus shear stress for the same surfactant foam under different measurement conditions at a constant measurement time of 60 s: ■ shear stress continuously increasing from 3 to 25 Pa, ★ stepwise increase of shear stress from 3 to 30 Pa (2 s per data point), △ stepwise increase of shear stress from 1 to 60 Pa (2 s per data point).

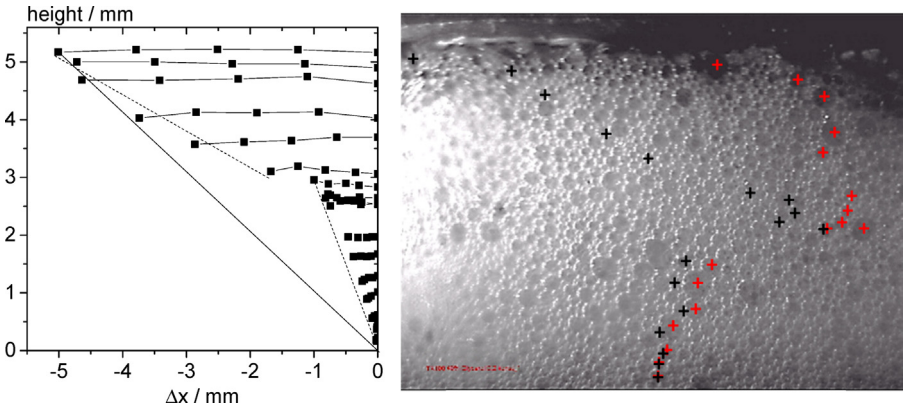

Fig. 3. Left side: velocity profile of a surfactant foam containing 40% glycerol at constant shear rate ($\dot{\gamma} = 0.2\,s^{-1}$). Right side: Foam image with initial bubble positions marked by red crosses and final positions reached after 5 s marked by black crosses. (For interpretation of the references to color in this figure legend, the reader is referred to the web version of this article.)

results for the different foaming systems leads to the general conclusion that the surfactant foams possess lower yield stresses than the protein foams at a given value of $\phi - \phi_c$ which in turn lie close together. The *k*-factor is 4–5 times higher for the protein foams than for the surfactant foams. The different *k*-factors presumably arise from different interfacial layer properties as will be discussed in more detail in Section 3.6.

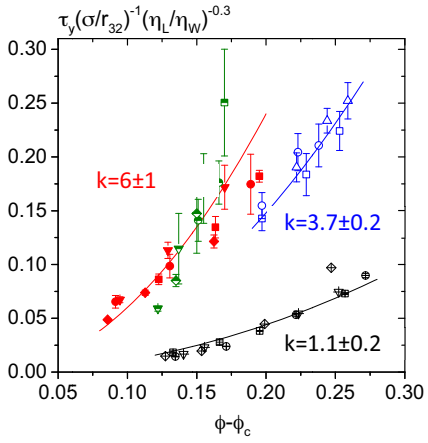

Fig. 4. Apparent yield stress τ_y normalized by Laplace pressure (σ/r_{32}) and solution viscosity ratio (η_L/η_W) vs. $\phi - \phi_c$ for foams made from different proteins and a surfactant mixture (closed symbols 1% WPI, semi-closed symbols 0.1% WPI, open symbols casein and crossed symbols surfactant mixture) dissolved in various water/glycerol mixtures (glycerol content ■, 0%; ●, 20%; ▼, 30%; ▲, 40%; ♦, 60%).

3.5. Oscillatory shear measurements

In Fig. 5a and b exemplary amplitude sweep curves are shown for the different foaming system but similar physical foam properties ϕ, σ/r_{32} and η_L. The curves keep their characteristic shape independent of glycerol content or gas volume fraction. All systems show $G' > G''$ at low stress amplitudes in the linear viscoelastic regime ($\tau_0 < \tau_{LVE}$) and $G'' > G'$ in the flow regime ($\tau_0 > \tau_c$). For the 0.1% WPI and especially for the casein system there is a sharp transition between both regimes and $\tau_c \approx \tau_{LVE}$. But for the 1% WPI and the surfactant foams a third regime can be distinguished between linear viscoelastic and flow regime. For the former the moduli decrease simultaneously and for the latter G' decreases while G'' increases before crossing.

The 1% WPI foams exhibit high storage modulus values at very low stress amplitudes. Presumably the whey proteins build a network across the lamella that causes such high moduli. Dimitrova et al. [35] investigated the disjoining pressure in dependence of the film thickness for a 0.2 wt% β-lactoglobulin (BLG) solutions. Their results can be described by DLVO theory only for film thicknesses between 22 and 40 nm. Below these values the interaction

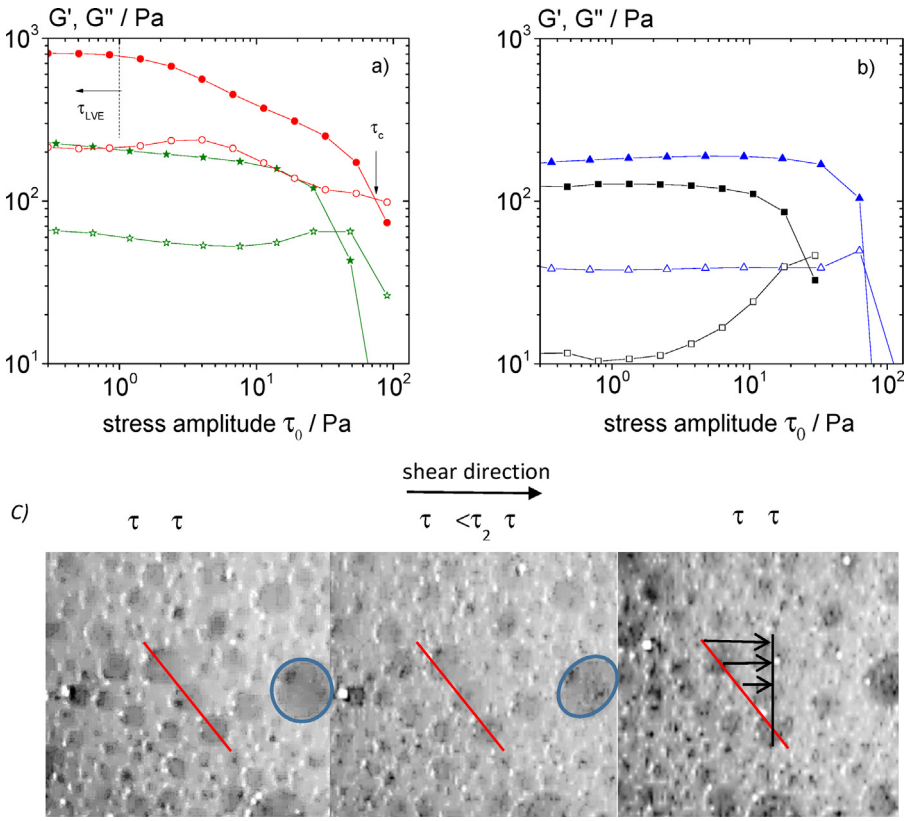

Fig. 5. Oscillatory stress amplitude sweep measurements of G' (closed symbols) and G'' (open symbols) for (a) ● 1% WPI foam ($\phi = 0.90$, $\sigma/r_{32} = 261$ Pa, $\eta_L = 3.8$ mPa s), ★ 0.1% WPI foam ($\phi = 0.92$, $\sigma/r_{32} = 369$ Pa, $\eta_L = 3.0$ mPa s), (b) ▲ casein foam ($\phi = 0.91$, $\sigma/r_{32} = 269$ Pa, $\eta_L = 3.8$ mPa s) and ■ surfactant foam ($\phi = 0.89$, $\sigma/r_{32} = 241$ Pa, $\eta_L = 4.6$ mPa s), (c) foam images taken from video recordings during oscillatory deformation of a 1% WPI foam at different stress amplitudes. Pictures are side views of the shear gap taken at the maximum displacement during an oscillation cycle with $\tau_1 = 0.3$ Pa, $\tau_2 = 7$ Pa (bubbles deform but stay at their position), $\tau_3 = 100$ Pa (bubbles have moved).

between opposing protein layers is dominated by a steric repulsion even though the thickness of the adsorption layer, as measured for a 0.1 wt% BLG solution, is only about 3–4 nm [36]. Therefore, the authors conclude that the proteins form a network across the lamella. As BLG is the main component of the whey proteins, this might also be the case here. Intermediate stress amplitudes probably destroy this network without moving the bubbles past each other. Video recordings of the foam in the shear gap (Fig. 5c) confirm that the bubbles deform but stay at their position during the decrease of both moduli and start moving just before the moduli ross over.

The increase in G'' for the surfactant foams can be explained as follows. As the stress amplitude is applied some of the foam films get stretched while others are being compressed leading to regions with lower and regions with higher surfactant concentrations. In order to equilibrate this imbalance, a Marangoni flow from the compressed regions to the stretched ones is induced [37]. This is a dissipative process that becomes stronger with higher stress amplitudes and therefore should lead to an increases G''.

In Fig. 6 the plateau moduli normalized by Laplace pressure are plotted versus $\phi - \phi_c$. Each measurement series can be described by the equation proposed by Mason et al. (Eq. (4)) with the fit parameter a depending on the foam system

$$G_0 = a \cdot \left(\frac{\sigma}{r_{32}}\right) \cdot \phi(\phi - \phi_c) \tag{4}$$

For the surfactant foams and the 0.1% WPI foams all data points collapse onto a master curve but for the other two protein foams $G_0(\sigma/r_{32})^{-1}$ increases with increasing glycerol content. This increase is most likely not directly attributed to the increase

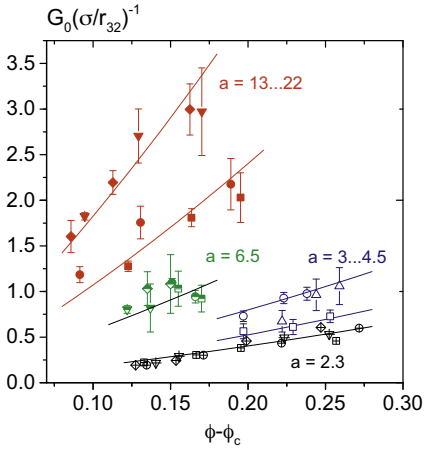

Fig. 6. Plateau moduli normalized by Laplace pressure vs. $\phi - \phi_c$ for foams made from 1% WPI (closed symbols), 0.1% WPI (semi-closed symbols), casein (open symbols) and surfactant mixture (crossed symbols) dissolved in various water/glycerol mixtures (glycerol content ■, 0%; ●, 20%; ▼, 30%; ▲, 40%; ♦, 60%).

in liquid viscosity since G_0 is an elastic modulus which is by definition not related to viscous dissipative processes. Instead this variation in the pre-factor a is due to changes in the interfacial layer properties caused by modified intermolecular interactions. The dielectric constant decreases with increasing glycerol content in the solvent mixtures [38] and hence, the range of electrostatic interactions decreases, too. This should result in a denser packing of proteins at the interface. Moreover, glycerol increases the chemical potential of the protein which decreases its solubility

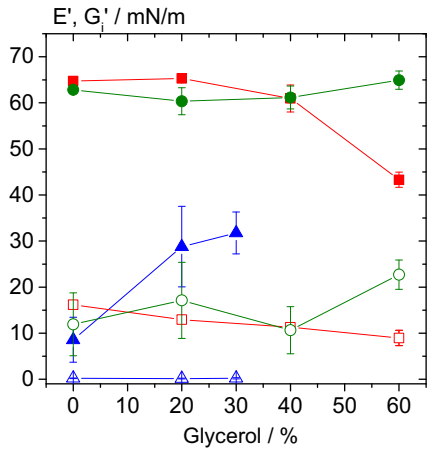

Fig. 7. Surface elastic moduli of WPI and casein dissolved in various water/glycerol mixtures with different glycerol content in dilation (closed symbols) and shear (open symbols) for 3% casein (triangles), 1% WPI (rectangles) and 0.1% WPI (circles). Measurements were performed after 30 min aging of the surface at a frequency of 0.1 Hz (dilation) and 0.7 Hz (shear).

[39,40]. This hypothesis is supported by the observation that dissolution of WPI is significantly slower in glycerol/water mixtures and dissolution time increases with glycerol content. Furthermore, it was not possible to dissolve the proteins in pure glycerol solution. This glycerol-induced salting-out effect occurring due to preferential hydrating of the proteins dissolved in water/glycerol mixtures was shown to apply for various proteins including β-lactoglobulin. However, it is well known that glycerol prevents denaturation of proteins and in that sense increases its stability [39,40]. Nevertheless, this change in solubility due to added glycerol may depend on the weight fraction of glycerol in the solvent, the type of protein as well as on pH and ionic strength of the solution. Various studies report an increased solubility of protein due to added glycerol, e.g. for Bovine Pancreatic Trypsin Inhibitor or T7 RNAP [49,50] but this seems not to apply for the WPI solutions investigated here. Hence, we assume that at a critical glycerol content protein aggregates should be formed and their number should increase with increasing glycerol content. Especially in the case of foams made from 1% WPI solutions these aggregates could promote the network formation across the lamellae and therefore increase foam elasticity. Foams made from 0.1% WPI solutions do not show this dramatic increase in elasticity with increasing glycerol content presumably because the solubility limit has not been reached yet and protein aggregation does not occur.

3.6. Interfacial rheology

The surfactants investigated here build mobile interfacial layers that do not show elastic behavior at the concentration used. The interfacial storage moduli in dilation (E') and shear (G_i') for the WPI and casein solutions are shown in Fig. 7. Interfacial loss moduli of all solutions were low compared to the storage moduli and are therefore not shown. For the casein solutions the elastic modulus in dilation E' increases with glycerol content. Dilational deformation is sensitive to the intrinsic deformation of the molecules [41]. The decreasing range of electrostatic repulsion should result in a more compact conformation and a denser packing of proteins at the interface, thus resulting in a higher elasticity. Moreover, using glycerol for stabilizing the native structure of proteins is well known in the field of biochemistry. Gekko et al. [39,40] investigated the mechanisms behind this phenomenon and came to the following conclusion. The chemical potential of glycerol increases by contact with the protein. Since this is thermodynamically unfavorable the system is supposed to reduce the protein–solvent interface. As a result the proteins preferably keep the compact, folded state. The most surface active component of the complex casein micelle and therefore presumably the main part of the adsorption layer is β-casein [42]. The latter is a flexible protein and the glycerol induced structure change could possibly result in a lower deformability which in turn could lead to the higher elastic dilational moduli. The shear elastic modulus G_i' is very low and does not change with addition of glycerol. Cicuta et al. [43] investigated β-casein surface layers in shear and did not find elastic behavior as well. They propose that the surface mobility arises due to the loop-tail formation of these flexible molecules at the interface, i.e. at high surface concentrations the hydrophilic tails are extended into the solution [44]. When a deformation is applied this conformation possibly enables the proteins to move over or under each other in order to relax stress.

The results for 1% WPI show a different trend. The dilational modulus decreases when a glycerol content of 40% is exceeded and in shear we observe a weak monotonic decay with increasing glycerol content. Rullier et al. [45,46] investigated the structure of native and aggregated BLG with respect to the stability of foams made from these proteins. They found the aggregates to be less surface active than native proteins. However, the foam stability could be increased by adding aggregates to the native proteins. Davis and Foegeding [47] investigated the dilational elasticity of native WPI mixed with different amounts of polymerized WPI. Adding up to 50% aggregated proteins increased the dilational elasticity whereas higher amounts led to a sharp decrease in E′. Transferring these results to our experiments it is likely that the addition of glycerol to 1% WPI solutions leads to partial aggregation of the proteins as already suggested in Section 3.5. This in turn results in less surface activity and elasticity. The elasticity of the 0.1% WPI solutions is practically independent of glycerol content indicating that glycerol does not markedly affect the protein structure and that no significant aggregation occurs at this concentration. The surface shear experiments of the 0.1% WPI solutions show strong variations for unknown reasons and within experimental error no trend can be observed regarding the dependence on glycerol content.

3.7. Correlation of foam and interfacial properties

The correlation between interfacial elasticity and foam properties has been addressed in many studies. In most cases high foam stability and yield stress correspond to high interfacial elasticity [11,48].

Among the systems investigated here, the 0.1% and 1% WPI solutions show similar and highest interfacial elastic moduli and the corresponding foams exhibit the highest normalized yield stresses (see Fig. 4). Casein solutions possess lower interfacial dilational and almost no interfacial shear elasticity corresponding to lower foam yield stress. The surfactant solutions, that do not show any measurable interfacial elasticity, exhibit the lowest foam yield stresses.

According to Fig. 4 the effect of glycerol on foam yield stress is mainly due to the corresponding change in solution viscosity and captured by the scaling factor $(\eta_L/\eta_w)^{0.3}$. In contrast a complex behavior of glycerol on the surface elasticity of the protein solution is found. The decrease in E′ at high glycerol content which is attributed to the formation of aggregates resulting in a network formation across the lamellae does not show up in the reduced yield stress. Presumably this network already breaks at $\tau < \tau_y$ and therefore does not contribute to the yield stress.

The relationship between protein interfacial elasticity and bulk foam elasticity is more complex. Comparing the different foaming agents investigated here we generally found highest foam elasticity for the corresponding solutions with highest interfacial elasticity. For the 0.1% WPI and the casein samples there is a direct

correlation between surface elasticity of the solution and the interfacial and bulk elasticity of the corresponding foam. Both, rheological properties of 0.1% WPI solutions and corresponding foams do not vary with glycerol content. But casein foams and solutions both become more elastic upon addition of 20% glycerol. Note, for the solution this behavior is observable only in dilation as casein solutions exhibit only very weak surface shear elasticity. In contrast, for 1% WPI solutions, the effect of glycerol on the interfacial elasticity differs from its effect on the bulk rheological properties of the foams. Adding glycerol leads to a decrease in interfacial elasticity, especially if the glycerol content of the solvent exceeds 40% whereas at the same time the foam elastic modulus drastically increases. This phenomenon is presumably due to protein aggregation. Aggregates are less surface active and decrease interfacial elasticity but probably enhance network formation across the foam lamellae and therefore increase foam elasticity.

4. Conclusion

We have investigated the effect of solution viscosity and surface elasticity on the apparent yield stress and bulk elasticity of foams made from protein and surfactant solutions. Whey protein solutions with different concentration, micellar casein and mixture of a non-ionic and an ionic surfactant have been employed for this study. The surface active ingredients have been used in various water/glycerol mixtures in order to study the effect of solvent viscosity on foam rheology.

Based on the equations proposed by Mason we can describe the effect of gas volume fraction and Laplace pressure on τ_y and G_0 (Eqs. (3) and (4)). Here we calculate the critical volume fraction ϕ_c from the bubble size distribution of the foams. This distribution is determined from the analysis of foam images taken with an endoscopic CCD camera. The ϕ_c values found for the different foaming systems are discussed in terms of foam formation and gas bubble stabilization properties of the employed proteins and surfactants. Distinct features of the transition from the linear viscoelastic region ($G' \gg G''$) to the non-linear deformation regime ($G'' > G'$) are observed for the different foam systems and can be attributed to structural features of the foam lamellae.

As expected the storage modulus G_0 is independent of the solution viscosity for the foams made from surfactant, casein and 0.1% WPI solutions. The increase of G_0 with increasing glycerol content found for the foams made from 1% WPI solutions is attributed to the formation of protein aggregates finally inducing the formation of a network structure across the lamellae.

The apparent yield stress τ_y is found to be the critical stress at which the gas bubbles start to slide past each other. This quantity directly depends on solution viscosity and this relationship is captured by an empirical factor $\left(\frac{\eta_L}{\eta_W}\right)^{0.3}$ valid for all investigated foams irrespective of gas volume fraction and type of foaming agent.

In general, protein-stabilized foams exhibit higher reduced τ_y and G_0 values at given $(\phi - \phi_c)$ than surfactant foams. We attribute this to the surface elasticity of the corresponding solutions which is highest for both WPI solutions, significantly lower for the casein solutions and negligibly small for the surfactant solutions.

For casein a weak increase of reduced G_0 with increasing glycerol content is observed for the foams which corresponds to an increase in surface elasticity of the respective solutions. We attribute this to a more compact conformation of the casein molecules resulting from a decrease of solvent quality with increasing glycerol content. The 0.1% WPI system exhibits a higher foam elastic modulus G_0 than the casein or surfactant systems and this directly correlates to the high surface elasticity of the solution, both in shear and dilation. The scenario is more complex for the 1% WPI system. In this case the added glycerol is supposed to induce protein aggregation. This results in a decrease of the dilation modulus E' at glycerol contents beyond 20% but at the same time G_0 increases and we assume this is due to the formation of a network bridging the opposing protein layers across the lamellae. This network formation obviously does not affect the reduced yield stress τ_y which does not reveal a specific variation with glycerol content for the foams made from different protein solutions. Therefore we conclude that the protein network is destroyed at stresses $\tau < \tau_y$.

Acknowledgments

The authors would like to thank the group of Kulozik (Technische Universität München, Germany) for the supply of high quality β-lactoglobulin and the group of Peukert (Universität Erlangen-Nürnberg, Germany) for providing the measurement device DSA 100 for the drop shape analysis.

We acknowledge the funding by the DFG-AiF cluster project on "Protein Foams" Wi 3138/10-1.

References

[1] G.M. Campbell, E. Mougeot, Creation and characterisation of aerated food products, Trends Food Sci. Technol. 10 (1999) 283–296.
[2] H.M. Princen, Rheology of foams and highly concentrated emulsions, J. Colloid Interface Sci. 112 (1986) 427–437.
[3] H.M. Princen, A.D. Kiss, Rheology of foams and highly concentrated emulsions, J. Colloid Interface Sci. 128 (1989) 176–187.
[4] T.G. Mason, J. Bibette, D.A. Weitz, Elasticity of compressed emulsions, Phys. Rev. Lett. 75 (1995) 2051–2054.
[5] T.G. Mason, J. Bibette, D.A. Weitz, Yielding and flow of monodisperse emulsions, J. Colloid Interface Sci. 179 (1996) 439–448.
[6] A. Saint-Jalmes, D.J. Durian, Vanishing elasticity for wet foams: equivalence with emulsion and role of polydispersity, J. Rheol. 43 (1999) 1411–1422.
[7] S. Marze, A. Saint-Jalmes, D. Langevin, Protein and surfactant foams: linear rheology and dilatancy effect, Colloids Surf. A 263 (2005) 121–128.
[8] S. Marze, R.M. Guillermic, A. Saint-Jalmes, Oscillatory rheology of aqueous foams: surfactant, liquid fraction, experimental protocol and aging effects, Soft Matter 5 (2009) 1937.
[9] M. Lexis, N. Willenbacher, Einfluss der Flüssigkeitsviskosität auf das rheologische Verhalten von Schäumen, Chem. Ing. Tech. 85 (2013) 1317–1323.
[10] P. Wierenga, H. Gruppen, New views on foams from protein solutions, Curr. Opin. Colloid Interface Sci. 15 (2010) 365–373.
[11] J. Davis, E. Foegeding, F. Hansen, Electrostatic effects on the yield stress of whey protein isolate foams, Colloids Surf. B 34 (2004) 13–23.
[12] G.B. Bantchev, D.K. Schwartz, Surface shear rheology of β-casein layers at the air/solution interface: formation of a two-dimensional physical gel, Langmuir 19 (2003) 2673–2682.
[13] A. Williams, A. Prins, Comparison of the dilational behaviour of adsorbed milk proteins at the air–water and oil–water interfaces, Colloids Surf. A 114 (1996) 267–275.
[14] P.A. Wierenga, H. Kosters, M.R. Egmond, A.G. Voragen, H.H. de Jongh, Importance of physical vs. chemical interactions in surface shear rheology, Adv. Colloid Interface Sci. 119 (2006) 131–139.
[15] S. Roth, B.S. Murray, E. Dickinson, Interfacial shear rheology of aged and heat-treated β-lactoglobulin films: displacement by nonionic surfactant, J. Agric. Food Chem. 48 (2000) 1491–1497.
[16] A.W. Perriman, M.J. Henderson, S.A. Holt, J.W. White, Effect of the air–water interface on the stability of β-lactoglobulin, J. Phys. Chem. B 111 (2007) 13527–13537.
[17] J.T. Petkov, T.D. Gurkov, B.E. Campbell, R.P. Borwankar, Dilatational and shear elasticity of gel-like protein layers on air/water interface, Langmuir 16 (2000) 3703–3711.
[18] P. Cicuta, E.M. Terentjev, Viscoelasticity of a protein monolayer from anisotropic surface pressure measurements, Eur. Phys. J. E 16 (2005) 147–158.
[19] P. Cicuta, E. Stancik, G. Fuller, Shearing or compressing a soft glass in 2D: time-concentration superposition, Phys. Rev. Lett. 90 (2003).
[20] E. Santini, J. Krägel, F. Ravera, L. Liggieri, R. Miller, Study of the monolayer structure and wettability properties of silica nanoparticles and CTAB using the Langmuir trough technique, Colloids Surf. A 382 (2011) 186–191.
[21] R. Miller, J.K. Ferri, A. Javadi, J. Krägel, N. Mucic, R. Wüstneck, Rheology of interfacial layers, Colloid. Polym. Sci. 288 (2010) 937–950.
[22] K. Engelhardt, M. Lexis, G. Gochev, C. Konnerth, R. Miller, N. Willenbacher, W. Peukert, B. Braunschweig, pH effects on the molecular structure of β-lactoglobulin modified air–water interfaces and its impact on foam rheology, Langmuir 29 (2013) 11646–11655.
[23] J. Krägel, S. Derkatch, R. Miller, Interfacial shear rheology of protein–surfactant layers, Adv. Colloid Interface Sci. 144 (2008) 38–53.

[24] R. Wüstneck, J. Krägel, R. Miller, V.B. Fainerman, P.J. Wilde, D.K. Sarker, D.C. Clark, Dynamic surface tension and adsorption properties of β-casein and β-lactoglobulin, Food Hydrocoll. 10 (1996) 395–405.
[25] M. Rosario Rodríguez Niño, C.C. Sánchez, M.C. Fernández, J.M. Patino, Rodríguez, Protein and lipid films at equilibrium at air–water interface, J. Am. Oil Chem. Soc. 78 (2001) 873–879.
[26] S. Vandebril, A. Franck, G.G. Fuller, P. Moldenaers, J. Vermant, A double wall-ring geometry for interfacial shear rheometry, Rheol. Acta 49 (2010) 131–144.
[27] J. de Wit, Thermal behaviour of bovine β-lactoglobulin at temperatures up to 150 °C: a review, Trends Food Sci. Technol. 20 (2009) 27–34.
[28] K. Feitosa, S. Marze, A. Saint-Jalmes, D.J. Durian, Electrical conductivity of dispersions: from dry foams to dilute suspensions, J. Phys.: Condens. Matter 17 (2005) 6301–6305.
[29] R.D. Sudduth, A new method to predict the maximum packing fraction and the viscosity of solutions with a size distribution of suspended particles. II, J. Appl. Polym. Sci. 48 (1993) 37–55.
[30] P.C.F. Møller, A. Fall, D. Bonn, Origin of apparent viscosity in yield stress fluids below yielding, Europhys. Lett. 87 (2009) 38004.
[31] S. Cohen-Addad, R. Höhler, Y. Khidas, Origin of the slow linear viscoelastic response of aqueous foams, Phys. Rev. Lett. 93 (2004).
[32] S. Vincent-Bonnieu, R. Höhler, S. Cohen-Addad, Slow viscoelastic relaxation and aging in aqueous foam, Europhys. Lett. 74 (2006) 533–539.
[33] P. Coussot, J. Raynaud, F. Bertrand, P. Moucheront, J. Guilbaud, H. Huynh, S. Jarny, D. Lesueur, Coexistence of liquid and solid phases in flowing soft-glassy materials, Phys. Rev. Lett. 88 (2002).
[34] G. Ovarlez, S. Rodts, X. Chateau, P. Coussot, Phenomenology and physical origin of shear localization and shear banding in complex fluids, Rheol. Acta 48 (2009) 831–844.
[35] T.D. Dimitrova, F. Leal-Calderon, T.D. Gurkov, B. Campbell, Disjoining pressure vs thickness isotherms of thin emulsion films stabilized by proteins, Langmuir 17 (2001) 8069–8077.
[36] P.J. Atkinson, E. Dickinson, D.S. Horne, R.M. Richardson, Neutron reflectivity of adsorbed β-casein and β-lactoglobulin at the air/water interface, J. Chem. Soc. Faraday Trans. 91 (1995) 2847–2854.
[37] D.M.A. Buzza, C.-Y.D. Lu, M.E. Cates, Linear shear rheology of incompressible foams, J. Phys. II France 5 (1995) 37–52.
[38] L. Bergmann, C. Schaefer (Eds.), Lehrbuch der Experimentalphysik: Bd. 2 Elektromagnetismus, 8th ed., de Gruyter, Berlin, New York, 1999.
[39] K. Gekko, S.N. Timasheff, Mechanism of protein stabilization by glycerol: preferential hydration in glycerol–water mixtures, Biochemistry 20 (1981) 4667–4676.
[40] K. Gekko, S.N. Timasheff, Thermodynamic and kinetic examination of protein stabilization by glycerol, Biochemistry 20 (1981) 4677–4686.
[41] J. Maldonado-Valderrama, J.M. Rodríguez Patino, Interfacial rheology of protein–surfactant mixtures, Curr. Opin. Colloid Interface Sci. 15 (2010) 271–282.
[42] A. Saint-Jalmes, M.-L. Peugeot, H. Ferraz, D. Langevin, Differences between protein and surfactant foams: microscopic properties, stability and coarsening, Colloids Surf. A 263 (2005) 219–225.
[43] P. Cicuta, Compression and shear surface rheology in spread layers of β-casein and β-lactoglobulin, J. Colloid Interface Sci. 308 (2007) 93–99.
[44] P. Cicuta, I. Hopkinson, Studies of a weak polyampholyte at the air–buffer interface: the effect of varying pH and ionic strength, J. Chem. Phys. 114 (2001) 8659.
[45] B. Rullier, B. Novales, M.A. Axelos, Effect of protein aggregates on foaming properties of β-lactoglobulin, Colloids Surf. A 330 (2008) 96–102.
[46] B. Rullier, M.A. Axelos, D. Langevin, B. Novales, β-Lactoglobulin aggregates in foam films: correlation between foam films and foaming properties, J. Colloid Interface Sci. 336 (2009) 750–755.
[47] J. Davis, E. Foegeding, Foaming and interfacial properties of polymerized whey protein isolate, J. Food Sci. 69 (2004).
[48] P.A. Wierenga, L. van Norél, E.S. Basheva, Reconsidering the importance of interfacial properties in foam stability, Colloids Surf. A 344 (2009) 72–78.
[49] M. Farnum, C. Zukoski, Effect of glycerol on the interactions and solubility of bovine pancreatic trypsin inhibitor, Biophys. J. 76 (1999) 2716–2726.
[50] R. Sousa, Use of glycerol, polyols and other protein structure stabilizing agents in protein crystallization, Acta Crystallogr. D 51 (1995) 271–277.

4 Relating foam and interfacial rheological properties of β-lactoglobulin solutions

Soft Matter

PAPER

View Article Online
View Journal | View Issue

Cite this: *Soft Matter*, 2014, **10**, 9626

Relating foam and interfacial rheological properties of β-lactoglobulin solutions

M. Lexis and N. Willenbacher*

Received 3rd September 2014
Accepted 6th October 2014

DOI: 10.1039/c4sm01972e

www.rsc.org/softmatter

We have determined bulk rheology of β-lactoglobulin (BLG) foams and surface viscoelasticity of corresponding protein solutions by varying pH as well as type, valency and concentration of the added salt in a wide range. Foam rheology was characterized by the storage modulus G_0, the apparent yield stress τ_y, and the critical strain $\gamma_{c,foam}$ defining the cessation of the linear viscoelastic response. These quantities were determined at gas volume fractions ϕ between 82% and 96%. Surface viscoelasticity was characterized in shear and dilation, corresponding shear and dilational moduli G_i', E' as well as the critical stress $\tau_{c,surface}$ and strain $\gamma_{c,surface}$ marking the onset of non-linear response in oscillatory surface shear experiments were determined at fixed frequency. Beyond the widely accepted assumption that G_0 and τ_y are solely determined by the Laplace pressure within the droplets and the gas volume fraction we have found that both quantities strongly depend on corresponding interfacial properties. G_0 increases linearly with G_i' and even stronger with E', τ_y varies proportional to $\tau_{c,surface}$ and $\gamma_{c,foam}$ scales linearly with $\gamma_{c,surface}$. Furthermore, deviations from these simple scaling laws with significantly higher reduced G_0 and τ_y values are observed only for foams at pH 5 and when a trivalent salt was added. Then also the dependence of these quantities on ϕ is unusually weak and we attribute these findings to protein aggregation and structure formation across the lamellae than the dominating bulk rheology.

1. Introduction

Foams that are stabilized by proteins play an important role in the food industry. The aerated structure gives a special look, mouthfeel and taste to the product which is well accepted by the customers. The foam structure consisting of jammed gas bubbles is responsible for the peculiar rheological behavior. Under low stresses the bubble network is able to store energy. The bubbles get deformed but do not move past each other. Hence, in this regime the elastic properties dominate. When a certain stress, called yield stress, is exceeded, the bubbles start sliding past each other and the foam as a whole flows easily like a liquid. Foam properties like stability and rheology are important issues not only for the end product but also during processing, where transport, heating and mixing take place. Understanding and controlling the parameters influencing foam properties are of great interest in food technology and many studies in this regard have been established. It is well known that the gas volume fraction, bubble size distribution and surface tension are the most important parameters that influence elastic properties and yield stress of so-called liquid foams including low viscosity of the continuous phase (eqn (1) and (2)).[1–5] The latter was found to be additionally affected by the liquid viscosity.[6,7] In eqn (1) and (2), the predictions of the storage modulus and yield stress initially proposed by Mason *et al.* and extended in our previous study are shown.

$$G_0 = a\left(\frac{\sigma}{r_{32}}\right)\phi(\phi - \phi_c) \quad (1)$$

$$\tau_y = k\left(\frac{\sigma}{r_{32}}\right)\left(\frac{\eta_L}{\eta_W}\right)^{0.3}(\phi - \phi_c)^2 \quad (2)$$

where σ is the surface tension, r_{32} the Sauter mean radius, ϕ the gas volume fraction, and ϕ_c represents the maximum packing fraction of the bubbles before they start to deform into non-spherical shapes. The latter has usually been an estimated value but can also be calculated from the measured bubble size distribution, as we have proposed recently.[7] The prediction of the yield stress includes an empirically determined factor for the (weak) contribution of the liquid viscosity, where η_L is the continuous phase viscosity and η_w the water viscosity under the same conditions. This phenomenological extension of the model equation proposed by Mason *et al.*[1,2] has been derived from measurements on foams made from casein, whey protein isolate and a mixture of synthetic surfactants. The solvent viscosity was varied using different water–glycerol mixtures and sugar solutions.[8] Each equation includes a numerical pre-factor, k and a, respectively. Values between 0.5 and 1 have been used for these constants so far in the literature without further discussion.[1,2,5] In a recent study we found k values between 1 and 7 and a values varying between 2 and 22.

Department of Chemical Engineering, Karlsruhe Institute of Technology, 76131 Karlsruhe, Germany. E-mail: norbert.willenbacher@kit.edu

The film dilational modulus is defined by $E = -A\mathrm{d}\pi/\mathrm{dln}\,A$ where π is the surface pressure, and A is the area of the film. The modulus E is thus a measure of the resistance of a film to change in its area. The surface shear rheology gives information about the resistance of an adsorbed layer at the interface against shear. Hence, it is sensitive to the structural state of the adsorbed molecules. From a colloidal view a surface elastic modulus arises either from attractive interactions between neighboring particles or particles caged at high packing density.[9] From interfacial oscillatory shear measurements another quantity can be extracted, the critical shear stress $\tau_{c,surface}$ which denotes the end of the linear viscoelastic regime. For $\tau > \tau_{c,surface}$ the deformation response becomes non-linear indicating a structural change in the surface layer.[10] Surface shear rotational experiments also show yielding behavior for several protein solutions which was investigated by Martin *et al.*[11] They came to the conclusion that the critical shear stress indeed induces a fracture within the protein film and can therefore be regarded as an intrinsic property of the protein layers. A higher critical stress represents a higher strength of the protein layer.

Surface rheology has been mainly discussed in terms of foam formation and stability.[12–16] Little is known so far about the correlation between foam rheology and the surface viscoelasticity of corresponding protein solutions although these features must be coupled since shearing a foam induces stretching and compression of the lamellae and hence the surfactant layer at the air liquid interface. The group of Cohen-Addad has thoroughly investigated the linear viscoelastic response G^* of surfactant foams in a broad frequency range. Based on the model of Princen[17] they have proposed a relationship between $G^*(\omega)$ and the complex angular modulus $A^*(\omega)$ determined from dynamic compression tests of two adjacent bubbles connected by a single lamella. The quantity $A^*(\omega)$ is further assumed to be proportional to the dilational modulus $E^* = E' + iE''$. In particular, they could show that the fast relaxation processes observed in foams are determined by the surfactant transport within the liquid films.[18] The frequency ω_c characterizing the onset of this scaling regime is assumed to be proportional to the ratio of the dilational modulus E' and the effective interfacial viscosity including the surface viscosity E''/ω_c, the solution viscosity and the lamellar thickness as well as the bubble diameter. Different scaling laws relating ω_c to the foam modulus G are proposed for rigid and mobile interfaces and these scaling laws are confirmed experimentally for two different types of surfactant foams.[19] Deviations from the simple $G^* \sim \omega^{1/2}$ scaling are observed for foams made from surfactants providing very rigid interfaces ($E^* \approx 102$ Pa).[20] So far, a systematic comparison between foam plateau modulus and interfacial shear or dilational moduli for protein foams is missing.

The viscous stress in continuously sheared foams scales with the capillary number Ca as $\tau_v \sim \mathrm{Ca}^n$ and the exponent n depends on surface mobility and viscoelasticity. For rigid interfaces $n = 1/4$ and for mobile interfaces $n = 1/2$ have been predicted theoretically and confirmed experimentally.[21–23]

A direct empirical correlation between the yield stress and the interfacial dilation modulus E' of whey protein foams made at different pH, concentration and valency of added salt has been proposed by Davis *et al.*[24] However, they did not take into account the effect of bubble size (distribution) and gas volume fraction on τ_y, although pH and ionic strength are known to affect the absolute value of this quantity substantially. Dimitrova and Leal-Calderon[25] reported a correlation between shear modulus of concentrated emulsions stabilized by different proteins and dilational moduli of the corresponding protein solutions. But it should be noted that their E' values were taken from the literature probably determined at protein concentration, pH and ionic strength conditions different from those relevant for the probed emulsions. Finally, it should be mentioned that also for particle stabilized so-called Pickering emulsions the modulus G_0 is not only determined by the interfacial tension between the liquid phases but also by an elastic contribution resulting from the attractive interaction among the stabilizing particles.[26]

In this study we attempt to directly correlate the surface and foam rheological properties of β-lactoglobulin (BLG) solutions. Therefore, the interfacial layer properties were systematically changed by varying the ionic strength, the type of salt and the solution pH. We propose a unique relationship between foam modulus G_0 and interfacial moduli G_i' or E', between the foam yield stress τ_y and the critical stress or strain at which an interfacial layer structure breaks down. We demonstrate the validity of this correlation in a wide range of gas volume fractions irrespective of bubble size distribution and Laplace pressure. Finally we discuss the limitation of this approach in terms of structure formation across lamellae induced under certain conditions of ionic strength, ion valency and pH.

2. Experimental details

2.1 Solution preparation and measurements

Solutions of 1 wt% β-lactoglobulin (BLG, used as received) were prepared by dissolving the protein powder kindly provided by the group of Ulrich Kulozik (University of Munich, Germany) in ultrapure water (Millipore, 18 MΩ). Variation of pH was achieved by adding appropriate amounts of NaOH or HCl (Carl Roth 1 N standard solutions), respectively. Ionic strength was varied by adding NaCl (99.5%, Roth Chemicals) between 10 and 100 mM. The influence of ion type and valency was investigated by the addition of 50 mM KCl, LiCl, NH_4Cl (99%, Roth Chemicals), $CaCl_2$ (98%, Roth Chemicals) or $NdCl_3$ (99.9%, Alfa Aesar).

The surface tension of all solutions was measured by the pendant drop method (Krüss, DSA 100) at 21 °C and a drop age of 30 min as described elsewhere.[7]

The liquid viscosities were measured with an Ares rotational rheometer (TA Instruments) using Couette geometry (17/16.5 mm). All solutions showed Newtonian behavior in the range of imposed shear rates $\dot{\gamma} = 10$–$1000\ s^{-1}$ with viscosities between 0.94 and 1.1 mPas.

Interfacial dilational elasticities were determined at 21 °C and a drop age of 30 min using the oscillating bubble method

(Krüss, DSA 100). The oscillations were generated by using a piezo pump that pulsed with a frequency of 0.1 Hz and amplitude of 0.3. The amplitude resulted in drop deformation between 2 and 3%, depending on the drop volume. As the drop was generated manually it was not possible to keep the volume for every measurement exactly the same. Oscillatory deformation was applied for a time period of 100 s and 1200 pictures were analyzed to calculate $E^* = E' + iE''$.

Interfacial shear viscoelastic properties were determined at 25 °C and a surface age of 30 min with a stress controlled rotational rheometer (TA Instruments, DHR3) using the double wall ring geometry (D_{ring} = 70 mm). Details about this measuring geometry can be found in.[27] The viscoelastic properties were recorded at a frequency of 0.7 Hz and a deformation amplitude of 1%, which did not exceed the linear viscoelastic regime of any sample solution. From these measurements we have determined the surface elastic modulus G_i'. Measurements with increasing deformation amplitude allowed for the determination of the width of linear viscoelastic regime (LVE). When the non-linear deformation response sets in, G_i' starts to decrease and the end of the LVE was determined to reach when $G_i' = 0.9^* G_{iLVE}'$. At this point the critical deformation $\gamma_{c,surface}$ and shear stress $\tau_{c,surface}$ were extracted.

It should be noted that we have characterized the interfacial rheology of protein solutions at the same concentration at which foam preparation and foam rheology was done. This is in contrast to many other studies on interfacial rheology where experiments were done at much lower concentration of amphiphiles in order to ensure a monolayer of the surface active ingredient at the air/water interface. But one has to be aware that the structure of an interfacial layer, especially in the case of proteins, can substantially change with concentration and a correlation of foam and interfacial rheology can only be expected if the interfacial layer is the same in both sets of experiments. However, multiple layers of proteins may be present at the surface, *i.e.* the thickness of the layer may not be negligible. Therefore, the measured quantities E', G_i' have to be treated as apparent values.

2.2 Foam preparation and measurements

The protein solutions were preheated to 50 °C in a water bath to obtain foams that are stable enough for reproducible rheological measurements. The increase in temperature speeds up adsorption kinetics but does not affect the protein structure. Foams were produced using a glass filter fused in a glass pipe as described elsewhere[7] and nitrogen was purged through the pores at $\dot{V}$ = 60 ml min^{-1}. As soon as the foam reached the column height the nitrogen flow was stopped and recording of the foam age was started.

The time-dependent gas volume fraction was determined using a conductivity electrode with an integrated temperature sensor (WTW, Cond 340i) as described in a previous study.[7] The measuring gap of the electrode had a length of 2 cm. The foam volume within the gap is similar to that we have used for rheological characterization. Hence, the measured conductivity is an appropriate average value. Conductivity measurements were performed in a region of the foam column close to that from where the samples for rheological measurements were taken.

Fig. 1 shows the drainage velocity for the protein foams with different ionic strengths and different pH. Increasing the amount of NaCl leads to slower liquid drainage. This can be attributed to the reduced electrostatic repulsion between the proteins leading to closer protein packing and increased probability of aggregation. Such protein aggregates are able to plug the junctions of the Plateau borders so that the drainage of the liquid is slowed down. Moreover, the surface mobility can have an influence on foam drainage.[28,29] As the interface is supposed to become more rigid with increasing ionic strength (at least upon addition of 20 mM as discussed in Section 3.1.4) this might be an additional reason for the slower drainage. The pH dependent drainage velocity shows a minimum at pH 5. This is very close to the isoelectric point (IEP) where the protein net charge is close to zero and therefore, aggregates plugging the liquid channels occur more frequently. Higher distance to the IEP increases the protein solubility and at the same time the drainage velocity.

The bubble size distribution was determined by taking pictures with an endoscopic CCD camera (Lumenera LU 160, resolution 1392 × 1040) that was placed inside the foam. The Sauter mean radius r_{32} was extracted from image analysis using the software iPS (Visiometrics, Germany).

Foam rheological measurements were carried out with Rheoscope 1 (Thermofisher, Germany) using parallel plate geometry with a diameter of 60 mm. The surfaces were covered with sandpaper to minimize wall slip effects and the gap was set to 6 mm. The measurement time was 60 s in order to limit time dependent changes in the foam structure. Each foaming system was measured at different foam ages and hence, different gas volume fractions ϕ between 82 and 94%.

The apparent yield stress was determined from steady shear measurements where increasing stresses were applied. Depending on the foam composition the initial stresses were set between 3 and 5 Pa and the final stresses between 50 and 125 Pa. As already extensively discussed in ref. 7 the apparent yield stress is independent of the start and end point of the stress ramp experiment as well as on the number of data points taken. In particular, it was shown that the sample deformation within

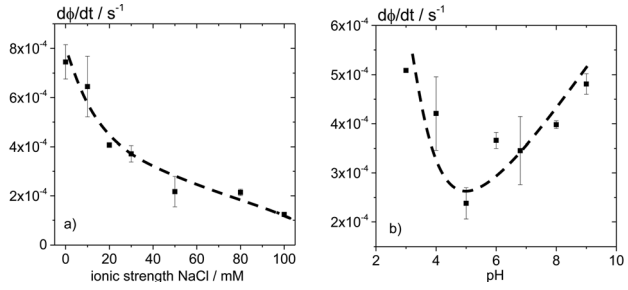

Fig. 1 Drainage velocity of the protein foams with different ionic strengths (a) or pH (b). Data were calculated from the time period in which each foam drained from 85% to 86% gas volume fraction.

the gap is non-uniform when the yield point is exceeded. We have assumed that this effect is weak just around the yield point, and experiments that determined τ_y and γ_c were highly reproducible but the parameters should be treated as apparent values.

The moduli G' and G'' of the foam were determined from oscillatory shear measurements by varying the stress amplitude at a frequency $f = 1$ Hz. The moduli did not show frequency dependence between 0.01 and 10 Hz. Hence, the measured G'-value in the linear viscoelastic regime is called plateau modulus G_0. The deformation amplitude that decreased G' down to $0.9*G_0$ was taken as critical deformation $\gamma_{c,foam}$. It is worth noting that this critical deformation at which non-linear deformation sets in is well below the yield point γ_y at which bubbles start to flow past each other. This yielding occurs at the stress or deformation amplitude at which $G' = G''$.[7]

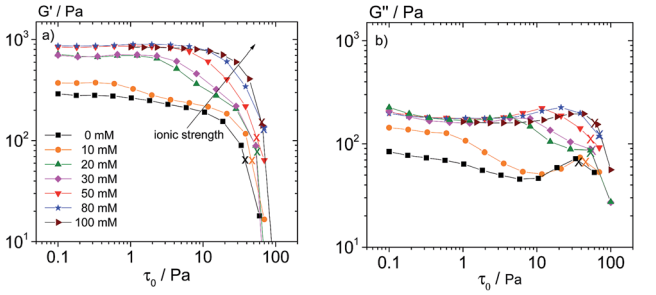

Fig. 2 Oscillatory shear experiments at a fixed frequency $f = 1$ Hz but varying stress amplitude for BLG foams ($\phi = 89\%$) at different ionic strengths of NaCl.

3. Results and discussion

3.1 Variation of ionic strength

3.1.1 Foam and solution properties. In Table 1 the values of the surface tension measured after 30 minutes surface aging, the mean Sauter radii of the foam bubbles and the range of gas volume fractions where foam rheology measurements took place are shown. The surface tension does not significantly change with the addition of NaCl to the protein solutions. The initial mean bubble size decreases when adding 50 mM salt but does not change upon further addition of NaCl.

3.1.2 Oscillatory shear measurements. In Fig. 2 oscillatory shear stress amplitude sweeps are shown for the BLG foams with different ionic strengths at similar gas volume fraction $\phi = 89\%$. For all foams G' and G'' stay nearly constant at low stresses in the linear viscoelastic regime. G' is always much higher than G'' and when G' increases, G'' also increases. All G' curves (Fig. 2a) show a decrease before they cross the G'' curve (intersections marked with crosses) with a negative slope increasing with increasing ionic strength. In the same stress amplitude range the G'' values (Fig. 2b) also show interesting behavior. For the foams without salt and with 10 mM NaCl the curves go through a local minimum and a subsequent local maximum just before crossing the G' curve. For higher ionic strengths the minimum in G'' essentially vanishes and the curves just exhibit a pronounced maximum which is shifted to higher stress amplitude values with increasing ionic strength. Such peaks have already been found for surfactant foams with gas volume fractions higher than 74%.[30] The foams with lower gas volume fractions did not show this maximum which was explained by the occurrence of plastic deformation prior to yielding. Other studies[31,32] consider the point, where dissipation is maximal, as the transition point from elastic to viscous behavior, hence as the yield point. The simultaneous decrease of G' and G'' for salt concentrations up to 30 mM indicates a gradual structure break down. Video recordings of sheared foams reveal that the bubbles start to slide past each other, *i.e.* the foam yields, when the maximum in G'' or the crossover of G' and G'' is reached as also reported in earlier studies.[31,32] Similar behavior has been reported for whey protein isolate foams[7] and was explained as follows: in several studies BLG has been found to form aggregates in thin liquid films that are able to "glue" the surfaces together.[33,34] The simultaneous decrease of both moduli was interpreted as a gradual destruction of the intralamellar protein networks before the bubbles start to move past each other. But there is no direct experimental proof for this intralamellar network and a structural break down might also occur within the interface where the proteins form aggregated networks due to dominant attractive interactions. This network structure seems to be fully developed at high ionic strengths (80 mM, 100 mM) and then provides a uniform rigid surface layer stabilizing the foam and leading to a sharp decay of G' and G'' and a well defined yield point. At lower ionic strength the moduli decay simultaneously in a broad range of stress amplitude values between the onset of non-linear deformation and final yielding. The extended range between the LVE regime and the yield point is attributed to a gradual breakdown of the non-uniform, imperfect network structure within the interface (and/or across the lamellae) supposed to be present at lower ionic strength when attractive interactions are partly balanced by electrostatic repulsion.

Table 1 Surface tension of the protein solutions after 30 minutes surface aging, bubble radii and gas volume fractions in the range of foam ages where the rheological measurements took place. The maximum error is the standard deviation of three measurements at a given ionic strength

Ionic strength/mM	0	10	20	30	50	80	100	Max. error/%
σ/mN m^{-1}	51.5	50	49.5	49.6	50.1	49.5	49.9	1
r_{32}/μm	110–154	114	121	124	78–175	80–140	77–145	14
ϕ/%	87–96	89	89	89	86–93	85–93	84–91	1

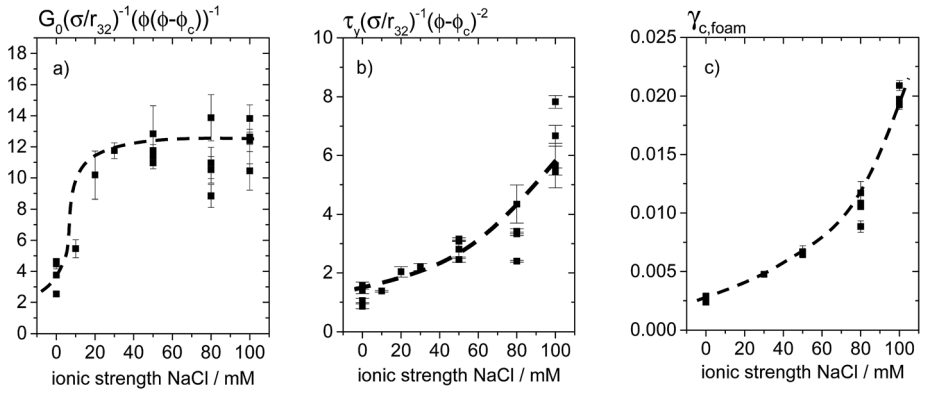

Fig. 3 (a) Storage moduli normalized by Laplace pressure (σ/r_{32}) and $\phi(\phi - \phi_c)$, (b) yield stresses normalized by Laplace pressure and $(\phi - \phi_c)^2$, and (c) critical deformation of BLG foams. All rheological quantities are measured at various gas volume fractions (see Table 1) and different ionic strengths.

3.1.3 Yield stress and storage modulus of the foams. Fig. 3 shows the yield stress values and the storage moduli normalized by Laplace pressure σ/r_{32} and $(\phi - \phi_c)^2$ or $\phi(\phi - \phi_c)$, respectively and the critical deformation of the BLG foams for different NaCl concentrations. The normalization is derived from eqn (1) and (2) and results in a collapse of data taken at different gas volume fractions ϕ to a single master curve. The normalized storage moduli increase sharply and then levels off to a constant value of about 12 at an ionic strength of 30 mM. At such high salt concentrations adsorption of the proteins at the interface is enhanced due to a reduced electrostatic repulsion. Also a change to a compact folded shape that allows closer packing at the interface and increased lateral attraction due to counterion screening may occur.[35] Accordingly, these closer packing of proteins increases the stress needed to deform the bubbles which corresponds to the measured storage modulus. Additionally, the protein aggregates that might occur more frequently at higher ionic strength could improve network formation thus further adding a mechanical strength. These effects are only observed up to 20 mM NaCl, higher ionic strength does not lead to further increase of the normalized G_0 values. In contrast, the normalized yield stress and critical deformation increase monotonically with increasing ionic strength.

3.1.4 Surface rheology. Fig. 4a shows the elastic moduli of the surfaces in dilation (E') and in shear (G_i'). Both quantities show the same trend when increasing the ionic strength. Adding 10 mM NaCl leads to the increase of E' and G_i' but further addition of salt does not have any effect. The increase of attractive interactions probably causes the higher E' and G_i' values after addition of the salt. In Fig. 4b and c the critical shear stress $\tau_{c,surface}$ and deformation $\gamma_{c,surface}$ of the surface layer are plotted *versus* the ionic strength. In contrast to the surface elastic moduli, $\tau_{c,surface}$ increases monotonically, indicating that a higher stress is required to destroy the interfacial layer structure formed at higher ionic strength. Finally, $\gamma_{c,surface} \approx \tau_{c,surface}/G_i'$ increases monotonically with increasing ionic strength. Hence, the stress needed to deform the protein structure at the interface is not affected by ionic strength higher than 10 mM but the stress and deformation that are needed to break the structure increase continuously with ionic strength in the range investigated here.

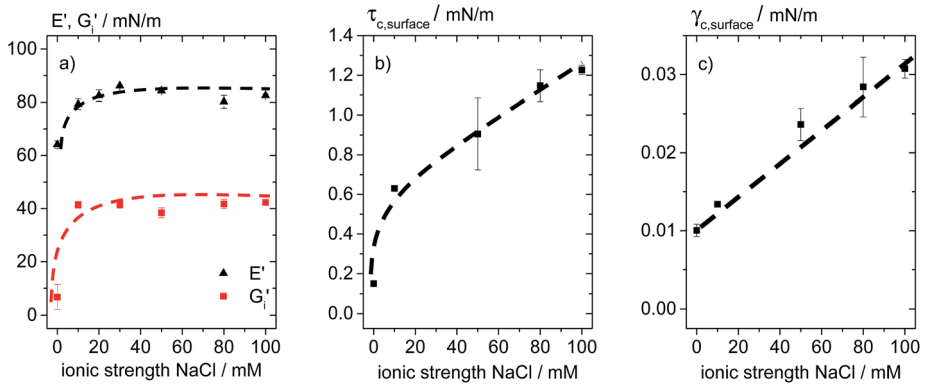

Fig. 4 (a) Surface elastic modulus in dilation (E') and shear (G_i'), (b) critical shear stress $\tau_{c,surface}$, and (c) critical deformation $\gamma_{c,surface}$ of the surface layer depending on the ionic strength for 1% BLG solutions.

Table 2 Surface tension of the protein solutions with different kinds of salt after 30 minutes surface aging. Bubble radii and gas volume fractions were determined at various times in the range of foam ages where the rheological measurements took place. In all cases the salt concentration was chosen as 50 mM. The standard deviation of three measurements performed at a constant foam age and for a given kind of salt was calculated. The maximum standard deviation obtained from data for different foam ages and kinds of salt is listed here as maximum error

	NH_4Cl	KCl	LiCl	$CaCl_2$	$NdCl_3$	Max. error/%
σ/mN m^{-1}	46.6	48.7	47.5	47.1	48.7	2
r_{32}/μm	93–183	84–175	93–145	105–278	220–270	10
ϕ/%	86–92	82–90	84–90	84–91	92–95	1
ϕ_c	71.5	71.3	70.7	73.0	84.9	4

3.2 Variation of the kind and the valency of the cation

3.2.1 Foam and solution properties. Table 2 shows the characteristic properties of the solutions and foams prepared with 50 mM salt of different types and valencies. The surface tension is not significantly affected by the kind of added salt, whereas the initial bubble radii and the bubble size distribution increase with the valency of the cation. Especially when 50 mM $NdCl_3$ were added, the foams possess comparably big bubbles with a broad size distribution as reflected by the high ϕ_c value.[7] This is most likely due to the occurrence of aggregated proteins as a consequence of the strongly suppressed electrostatic repulsion in the presence of trivalent ions. More and/or bigger protein clusters result in lower affinity of the proteins to adsorb at the interface. Hence, not all arising bubbles can be immediately stabilized what leads to an overall increase of the bubble size and a broader distribution.

3.2.2 Yield stress and storage modulus of the foams. Fig. 5a–c show the reduced storage moduli, reduced yield stresses and $\gamma_{c,foam}$ data, respectively for the different salts added. No difference is observed for the foams made from solutions including different monovalent salts. The addition of the divalent salt $CaCl_2$ leads to lower values in reduced G_0 but to higher values in reduced τ_y and $\gamma_{c,foam}$ compared to the monovalent salts. In particular, for the latter the difference is very pronounced. Each ion behaves differently when coming into contact with the protein. It is a balance between binding to the protein and preferential hydration (exclusion of the salt from the protein surface) of the protein.[36,37] Ca^{2+} is known to bind very strongly to BLG which could lead to conformational changes of the protein resulting in an increase of the hydrophobic surface area leading to stronger protein–protein interactions. Also, the formation of ionic bridges cross-linking the protein molecules is likely to occur.[38,39] The results for the foams made from BLG solutions with 50 mM $NdCl_3$ also differ strongly from those obtained for foams including monovalent ions. For both, the reduced G_0 and τ_y, we have found very high values, whereas $\gamma_{c,surface}$ is not significantly higher than for the monovalent ions. The reason for the high τ_y and G_0 values is again attributed to aggregation of proteins resulting from their low solubility at this high ionic strength. This is supported by the turbidity of the solutions observed after adding the salt. The mechanism that causes these high values of the rheological parameters is presumably again the formation of a structure across the lamellae. The reduced τ_y values additionally vary with gas volume fraction ϕ. In fact, the ϕ-dependent τ_y for these foams is lower than that predicted by eqn (2). We assume that the network structure is not destroyed as long as $\tau < \tau_y$ as it was the case for the foams investigated in ref. 7, but additionally contributes to the high yield stress. At lower ϕ and therefore thicker lamellae the protein network spanning the lamellae is expected to have more influence and hence causes high yield stress values leading to the unexpected weak variation of τ_y with ϕ. This phenomenon does not show up in the critical deformation of the foams. Finally, the different effects of divalent Ca^{2+} and trivalent Nd^{3+} on foam rheology clearly demonstrate that the corresponding protein structure and packing is strongly affected by the type and valency of the added ions.

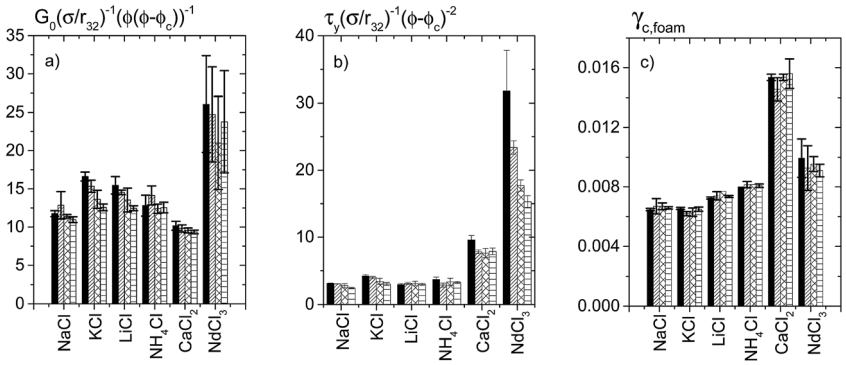

Fig. 5 (a) Reduced storage moduli, (b) reduced yield stresses and (c) critical deformation for foams made from 1% BLG dissolved in an aqueous 50 mM salt solution measured at different gas volume fractions ϕ (see Table 2). For each salt ϕ increases from left to right.

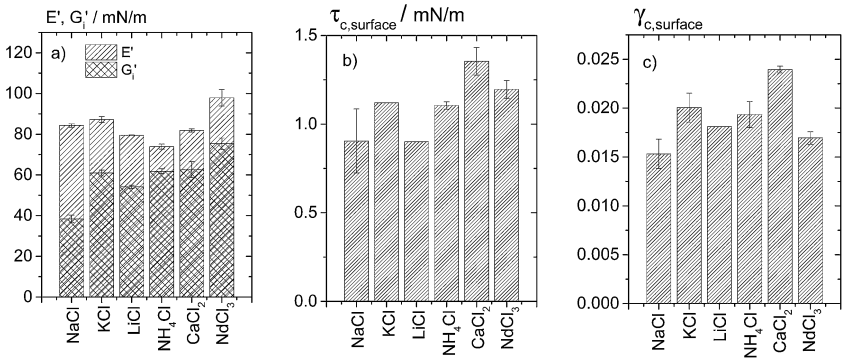

Fig. 6 (a) Surface elastic modulus in dilation (E') and shear (G_i'), (b) critical shear stress $\tau_{c,surface}$ and (c) critical deformation $\gamma_{c,surface}$ of the surface layer for 1% BLG solutions containing 50 mM salt of different types and valency.

3.2.3 Surface rheology. In Fig. 6a–c the surface moduli E' and G_i', the critical deformation of the surface layer $\gamma_{c,surface}$ and the critical stress of the surface layer $\tau_{c,surface}$ are shown for the protein solutions containing different salts. The results show similarities to those found for the foams (Section 3.2.2). Monovalent ions affect E', G_i', $\gamma_{c,surface}$ and $\tau_{c,surface}$ in a similar way. $CaCl_2$ increases $\gamma_{c,surface}$ and $\tau_{c,surface}$ but not the surface elastic moduli. The stronger binding of Ca^{2+}, as described in Section 3.2.2 may also explain why the critical stress and deformation needed to break the protein structure is higher with Ca^{2+} than for other ions. The solutions containing $NdCl_3$ show the highest E' and G_i' values but low $\gamma_{c,surface}$ values similar to the monovalent case and $\tau_{c,surface}$ is in between the values for the monovalent ions and Ca^{2+}. In general, the effect of di- and trivalent ions on interfacial rheology is much less pronounced than on foam rheology. This strongly suggests that foam rheology in these cases is strongly determined by the structure formation across the lamellae.

3.3 Variation of pH

3.3.1 Foam and solution properties. Table 3 shows the characteristic properties of the BLG foams and solutions at different pH. The initial average bubble sizes and bubble size distributions ($\phi_c = 71.5 \pm 1.9$ for all foams) are practically independent of pH. The surface tension varies with a minimum at pH 5 as already found in ref. 24 and 39.

3.3.2 Oscillatory shear stress amplitude sweeps. In Fig. 7 oscillatory shear stress amplitude sweeps for foams at pH values between 3 and 8 are shown. Interestingly, the curves possess different shapes at different pH. At and below the IEP ($\approx$pH 5) G' and G'' are almost constant before crossing (at pH 3 the foams are very unstable and therefore the moduli slightly decrease). The curves obtained at pH above the IEP can be divided into four regimes. After a short linear viscoelastic regime, both moduli decrease simultaneously, then G'' increases again before the moduli cross over and finally both decrease again. The simultaneous decrease of G' and G'' indicates a gradual structural break down as described in Section 3.1.2.

3.3.3 Yield stress and storage modulus of the foams. In Fig. 8 the plateau moduli and yield stresses of BLG foams at various gas volume fractions normalized by the Laplace pressure as well as the critical deformation are shown depending on the pH. Around the isoelectric point the foams exhibit the maximum yield stress, elastic modulus and critical deformation. Low pH, especially pH 3, leads to very unstable foams that possess very low elasticity and yield stress whereas foams at high pH are fairly stable. This behavior has already been reported in ref. 39 and was explained by conformational changes of the protein structure at different pH. Also, different electrostatic interactions between the proteins due to the change in their net charge across the IEP occur. At pH 5 the net charge vanishes which was shown to lead to thick disordered protein layers at the surface. The proteins also tend to aggregate at the isoelectric point. Once trapped in a foam lamella these protein clusters presumably support the network formation across two adjacent surfaces and give additional mechanical strength to the foam structure resulting in such high values for storage modulus and yield stress. In ref. 7 the proposed network formation in whey protein isolate foam lamellae was found to

Table 3 Surface tension of the protein solutions at various pH after 30 minutes surface aging, bubble radii and gas volume fractions in the range of foam ages where the rheological measurements took place. The maximum error is the maximum standard deviation of three measurements at a given pH

pH	3	4	5	6	6.8	8	9	Max. error/%
σ/mN m^{-1}	47.6	48.3	45.5	48.9	51.5	52.2	52.0	1
r_{32}/μm	104–109	118	93.8–145	102	110–154	103	106–175	7
Φ/%	86–88	88	84–91	89	87–96	88	87–94	0.4

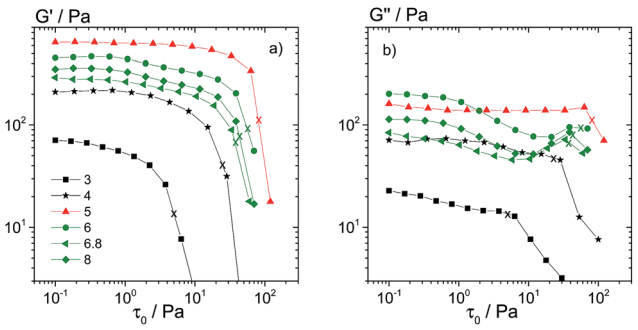

Fig. 7 Oscillatory shear measurements with varying stress amplitude of BLG foams at different pH: (a) storage modulus G' and (b) loss modulus G'' *versus* the stress amplitude at a fixed frequency $f = 1$ Hz. The intersection of G' and G'' is marked with crosses.

increase G_0 but did not affect the yield stress. From oscillatory amplitude sweeps it could be concluded that the whey protein network is destroyed at $\tau < \tau_y$, as it is the case for every pH $\neq$ 5. This suggests the existence of weak, non-uniform networks gradually destroyed as the stress amplitude increases. At pH 5 the destruction of the protein network seems to go along with yielding of the foam indicating a strong uniformly collapsing structure. Above pH 6.8 all three foam rheological parameters do not significantly depend on pH.

3.3.4 Surface rheology. Fig. 9a shows the pH dependence of the surface elastic moduli in shear and dilation for the 1% BLG solutions. Both moduli increase up to pH 6 followed by a local minimum around pH 7. The minimum probably arises because this is the natural pH of the solution and no ions are added to adjust the pH. The maximum change in the ionic strength due to adjusting pH is approximately 10 mM and according to Fig. 4a this corresponds to a drastic increase in G_i' as well as E'. Against expectation, the surface moduli do not show a maximum around the IEP as it has been reported for various proteins including BLG in several studies of interfacial shear[41–44] and dilational properties.[24,40,45] But it should be noted that the protein concentration used in those studies is much lower (at least 5–10 times) than the concentration used here which was chosen to be that high to meet the conditions used for foam preparation and foam rheology measurement. Burgess *et al.*[35] have also worked with high protein concentrations of BSA and HI_gG similar to the concentrations used in this study and measured surface shear elasticities as a function of pH. Surprisingly, they found a minimum in G_i' at the IEP and explained this phenomenon by low protein–protein interactions due to a compact shape of the proteins. This explanation is in disagreement with the other studies mentioned above which conclude a strong attraction among proteins at the IEP. They attributed the attractive interactions to close and effective contacts among proteins because of the low net charge.[24,35] We assume that the difference in the reported results arises mainly from different protein concentrations. Exceeding a critical protein concentration results in the formation of multilayers at the surface. Wüstneck[46] measured surface elastic properties of gelatin layers and found the elastic modulus to decrease at a certain concentration that he attributed to the onset of multilayer formation. Also, the formation of protein aggregates, which becomes more significant as the protein concentration increases, can lead to a decrease in the surface elasticity as we discussed extensively in a previous study.[7] The reason for the lower values at pH 3 compared to the values at pH 6.8 despite the same distance to the isoelectric point is differences in the protein structure and hydrophobicity as already discussed in ref. 24 and 40.

3.4 Correlation between interfacial and foam rheology

In Fig. 10 the normalized storage moduli of all foams investigated in this study are plotted *versus* the surface elastic moduli G_i' and E'. Additionally, data points for whey protein isolate foams (0.1% and 1%) and 3% casein foams (data taken from ref. 7) are included. A clear correlation is observed between the normalized foam moduli and surface moduli of the corresponding protein solutions except for the 1% BLG solutions at pH 5 and with $NdCl_3$ as well as the 1% WPI solution. The relationship between G_0 and G_i' is obviously linear whereas our data suggest a stronger quadratic or cubed dependence of G_0 on E'. These findings directly demonstrate that surface elasticity is

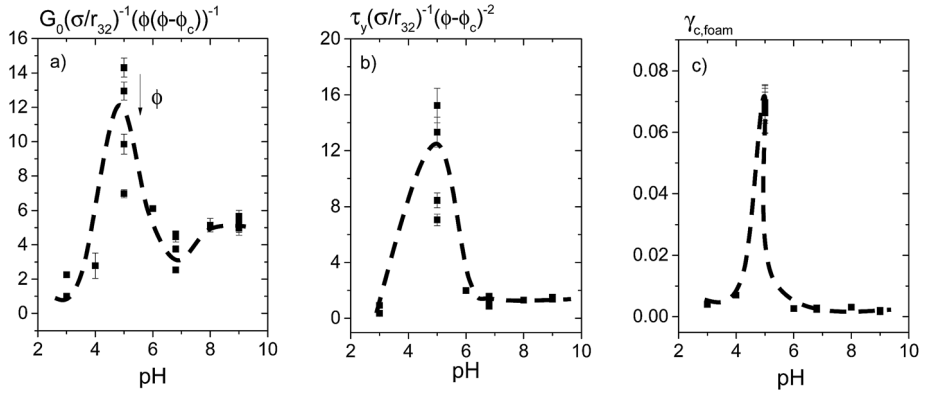

Fig. 8 (a) Storage moduli normalized by Laplace pressure (σ/r_{32}) and $\phi(\phi - \phi_c)$, (b) yield stresses normalized by Laplace pressure and $(\phi - \phi_c)$,[2] and (c) critical deformation of BLG foams. All rheological quantities are measured at various gas volume fractions (see Table 3) and different pH.

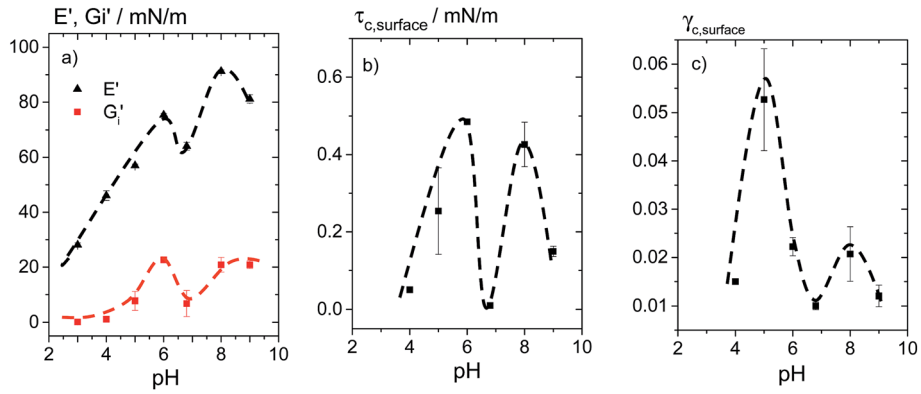

Fig. 9 (a) Surface elastic modulus in dilation (E') and shear (G_i'), (b) critical shear stress $\tau_{c,surface}$ and (c) critical deformation $\gamma_{c,surface}$ of the surface layer for 1% BLG solutions at different pH.

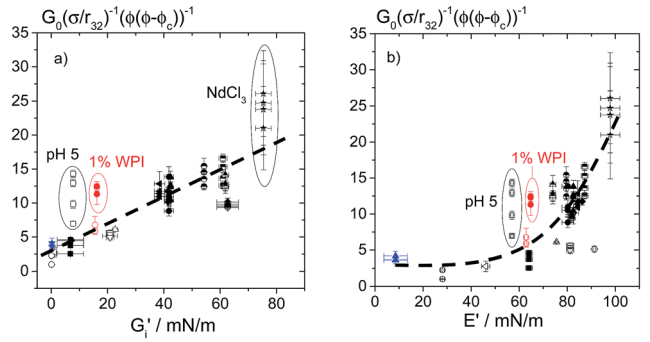

Fig. 10 Storage moduli normalized by Laplace pressure (σ/r_{32}) and $\phi(\phi - \phi_c)$ *versus* (a) surface shear elastic modulus G_i' and (b) surface dilational elastic modulus E' ○ pH 3, △ pH 4, □ pH 5, △ pH 6, ◇ pH 8, ▽ pH 9, pH 6.8 and NaCl: ■ 0 mM, ◆ 10 mM, ▲50 mM, ● 80 mM, ▲100 mM, 50 mM ▬KCl, ▲ NH_4Cl, ◓LiCl, ◆$CaCl_2$, ★$NdCl_3$ ○ 0.1% WPI, ● 1% WPI, ▲3% casein.

another important parameter controlling foam elasticity besides the Laplace pressure inside the bubbles, gas volume fraction and bubble size distribution. Accordingly, the prefactor a in eqn (1) is solely determined by the surface elastic moduli G_i' or E'. For the three cases where deviations from the simple correlations between foam and surface elasticity are observed, protein aggregation and structure or network formation across foam lamellae are supposed to be decisive for foam elasticity as already discussed in detail in Section 3.2 and 3.3, as well as ref. 7.

Fig. 11 a and b display the reduced yield stresses of all investigated BLG foams as a function of critical stress $\tau_{c,surface}$ or $\gamma_{c,surface}$ characterizing the onset of non-linear response of the corresponding protein solutions in interfacial shear rheology experiments. The relationship between the normalized foam yield stress and these characteristic surface rheological parameters can be approximated by a linear correlation as the simplest approach. This demonstrates that the parameter k in eqn (2) is determined by surface rheological features of the corresponding BLG solutions. But again the foams made at pH 5 and those made from the BLG solutions including 50 mM $NdCl_3$ clearly deviate from this simple correlation and again we conclude that this is due to a structure or network formation across foam lamellae as discussed above which also dominates the yielding of the foam. Finally, Fig. 11c shows the correlation between the critical deformation $\gamma_{c,foam}$ characterizing the

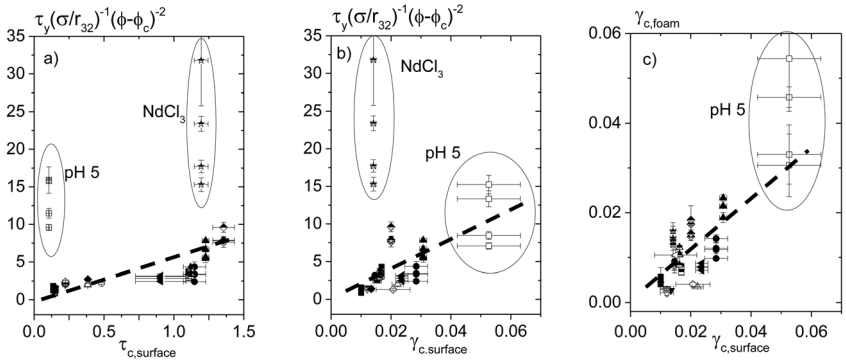

Fig. 11 Yield stresses normalized by Laplace pressure and $(\phi - \phi_c)^2$ *versus* (a) critical shear deformation of the surface $\tau_{c,surface}$, (b) critical shear deformation of the surface $\gamma_{c,surface}$, and (c) critical deformation of the foams $\gamma_{c,foam}$ *versus* critical deformation of the surface $\gamma_{c,surface}$. ○ pH 3, △ pH 4, □ pH 5, △ pH 6, ◇ pH 8, ▽ pH 9, pH 6.8 and NaCl: ■ 0 mM, ◆ 10 mM, ▲ 50 mM, ● 80 mM, ▲100 mM, 50 mM ▬KCl, ▲NH_4Cl, ◓LiCl, ◆$CaCl_2$, ★$NdCl_3$.

onset of non-linear response during oscillatory shear of the foams and the critical deformation $\gamma_{c,surface}$ obtained in oscillatory surface shear experiments. Again, a clear correlation between characteristic foam and surface rheological properties is found including all investigated BLG systems except those at pH 5. This once more confirms that foam rheology is tightly related to surface rheological properties of the corresponding protein solutions. Moreover, the deviation of the data for the BLG systems at pH 5 from this correlation and the strong dependence of $\gamma_{c,surface}$ on gas volume fraction further supports the conclusion that in this case foam rheology is dominated by the structure across the foam lamellae instead of the opposing protein surface layers alone.

4. Conclusions

We have investigated the correlation between the rheological behavior of BLG foams and the surface shear and dilational viscoelastic properties of corresponding protein solutions. Foam rheology is characterized here in terms of the frequency independent storage modulus G_0 reflecting the elasticity of the foam "at rest" and the apparent yield stress τ_y determining the onset of flow, *i.e.* the stress at which bubbles start to slide past each other. Moreover, the transition from linear to non-linear response was characterized using stress amplitude sweep oscillatory shear experiments. From these experiments the critical strain γ_c defining the cessation of linear viscoelastic response was extracted. These foam rheological quantities were determined at gas volume fractions between 82% and 96%. The surface viscoelasticity was characterized in shear and dilation. The corresponding shear G_i' and dilational E' moduli as well as the critical strain γ_c and stress τ_c marking the onset of non-linear response in oscillatory surface shear experiments were determined at a fixed frequency. Solution pH as well as concentration, type and valency of the added salt has been varied systematically thus varying foam rheology and surface viscoelasticity in a wide range.

Since protein conformation, solubility and aggregation in the bulk and at the surface may strongly change with protein concentration surface viscoelastic properties were determined at the same protein concentration as used for foam preparation.

Foam as well as interfacial moduli G_0, G_i' and E', respectively, strongly increases upon addition of salt to the protein solution but levels off at an ionic strength of about 20–30 mM NaCl. The quantities τ_y, $\gamma_{c,foam}$, $\tau_{c,surface}$, and $\gamma_{c,surface}$ characterizing the transition from linear to non-linear response increase monotonically with increasing ionic strength. A characteristic change from a gradual decrease of G' with increasing stress amplitude in oscillatory shear experiments to a sharp decrease at a higher critical stress is found when more and more salt is added. This indicates the formation of a stronger and more uniform structure of the foam and the interfacial protein layers as the attractive interactions among proteins become dominant.

The type and valency of the added salt has little effect on the surface viscoelastic properties of the protein solutions. But foam rheology drastically changes when divalent (Ca^{2+}) or trivalent ions (Nd^{3+}) are added. Adding Nd^{3+} results in a drastic increase in G_0 and τ_y but also in an anomalously weak variation of τ_y with gas volume fraction not captured by eqn (2). In contrast, addition of Ca^{2+} mainly shows up in a strong increase of $\gamma_{c,foam}$. These findings indicate the formation of an aggregated protein network structure across foam lamellae, which then determines the foam properties but does not show up in interfacial viscoelasticity. The different effects of Nd^{3+} and Ca^{2+} suggest that different structures are formed within the lamellae.

Variation of pH has little effect on foam rheological parameters G_0, τ_y and $\gamma_{c,foam}$ except at pH 5 which is the isoelectric point. At this point all these quantities exhibit distinct maxima and again τ_y and G_0 show an unusually weak dependence on the volume fraction not captured by the scaling laws (eqn (1) and (2)) confirmed by various previous studies. This again indicates the formation of a network structure of aggregated protein molecules across the lamellae and this is further supported by the non-monotonic variation of surface viscoelastic parameters not showing similar strong and distinct maxima at pH 5.

Finally, a unique correlation between foam rheological properties and surface viscoelasticity of corresponding BLG solutions could be established using all the collected data mentioned above. The reduced foam storage modulus increases monotonically with G_i' and E' except for the foams made at pH 5 and in the presence of the trivalent salt. Moreover, the correlation between the reduced apparent yield stress and $\tau_{c,surface}$ or $\gamma_{c,surface}$ is well approximated by a linear relationship and $\gamma_{c,foam}$ is proportional to $\gamma_{c,surface}$ within experimental uncertainty. Once more, the foam rheological parameters obtained at pH 5 and when Nd^{3+} is added are significantly higher than expected from these simple correlations.

In summary, we conclude that the widely accepted physical models predicting foam modulus and yield stress from the Laplace pressure within the gas bubbles and the gas volume fraction do not fully capture the physics of these phenomena. The pre-factors a and k in eqn (1) and (2) are not just numerical constants on the order of one but are found to vary between $1 < a$ and $k < 30$. A unique correlation between foam rheological properties and surface viscoelastic parameters is found except in cases where attractive interactions among proteins are dominant and are supposed to be strong enough to form a network structure across foam lamellae.

Acknowledgements

The authors would like to thank the group of U. Kulozik (Technische Universität München, Germany) for the supply of high quality β-lactoglobulin and the groups of W. Peukert (Universität Erlangen-Nürnberg, Germany) and M. Wilhelm (Karlsruhe Institute of Technology, Germany) for access to measuring equipments. We acknowledge funding by the DFG-AiF cluster project "Mesoscale modeling of the rheology of foamed food products" Wi 3138/10-1.

References

1 T. G. Mason, J. Bibette and D. A. Weitz, *Phys. Rev. Lett.*, 1995, **75**, 2051–2054.

2 T. G. Mason, J. Bibette and D. A. Weitz, *J. Colloid Interface Sci.*, 1996, **179**, 439–448.
3 H. M. Princen, *J. Colloid Interface Sci.*, 1986, **112**, 427–437.
4 H. M. Princen and A. D. Kiss, *J. Colloid Interface Sci.*, 1989, **128**, 176–187.
5 S. Marze, A. Saint-Jalmes and D. Langevin, *Colloids Surf., A*, 2005, **263**, 121–128.
6 M. Lexis and N. Willenbacher, *Chem. Ing. Tech.*, 2013, **85**, 1317–1323.
7 M. Lexis and N. Willenbacher, *Colloids Surf., A*, 2014, **459**, 177–185.
8 N. Willenbacher and M. Lexis, in *Foam Films and Foams: Fundamentals and Application*, ed. R. Miller and L. Liggieri, Tayler and Francis, 2014, in preparation.
9 P. Cicuta and E. M. Terentjev, *Eur. Phys. J. E*, 2005, **16**, 147–158.
10 J. Krägel, S. Derkatch and R. Miller, *Adv. Colloid Interface Sci.*, 2008, **144**, 38–53.
11 A. Martin, M. Bos, M. Cohen Stuart and T. van Vliet, *Langmuir*, 2002, **18**, 1238–1243.
12 S. Rouimi, C. Schorsch, C. Valentini and S. Vaslin, *Food Hydrocolloids*, 2005, **19**, 467–478.
13 M. A. Bos, B. Dunnewind and T. van Vliet, *Colloids Surf., B*, 2003, **31**, 95–105.
14 A. Martin, K. Grolle, M. Bos, M. Stuart and T. van Vliet, *J. Colloid Interface Sci.*, 2002, **254**, 175–183.
15 J. Maldonado-Valderrama, A. Martín-Rodriguez, M. J. Gálvez-Ruiz, R. Miller, D. Langevin and M. A. Cabrerizo-Vílchez, *Colloids Surf., A*, 2008, **323**, 116–122.
16 P. Wilde, *Curr. Opin. Colloid Interface Sci.*, 2000, **5**, 176–181.
17 H. M. Princen, *J. Colloid Interface Sci.*, 1983, **91**, 160–175.
18 S. Besson, G. Debrégeas, S. Cohen-Addad and R. Höhler, *Phys. Rev. Lett.*, 2008, **101**, 214504.
19 K. Krishan, A. Helal, R. Höhler and S. Cohen-Addad, *Phys. Rev. E: Stat., Nonlinear, Soft Matter Phys.*, 2010, **82**, 011405.
20 S. Costa, R. Höhler and S. Cohen-Addad, *Soft Matter*, 2012, **9**, 1100.
21 N. Denkov, S. Tcholakova, K. Golemanov, K. Ananthapadmanabhan and A. Lips, *Phys. Rev. Lett.*, 2008, **100**, 138301.
22 N. D. Denkov, S. Tcholakova, K. Golemanov, K. P. Ananthpadmanabhan and A. Lips, *Soft Matter*, 2009, **5**, 3389.
23 N. D. Denkov, V. Subramanian, D. Gurovich and A. Lips, *Colloids Surf., A*, 2005, **263**, 129–145.
24 J. Davis, E. Foegeding and F. Hansen, *Colloids Surf., B*, 2004, **34**, 13–23.
25 T. D. Dimitrova and F. Leal-Calderon, *Adv. Colloid Interface Sci.*, 2004, **108–109**, 49–61.
26 S. Arditty, V. Schmitt, F. Lequeux and F. Leal-Calderon, *Eur. Phys. J. B*, 2005, **44**, 381–393.
27 S. Vandebril, A. Franck, G. G. Fuller, P. Moldenaers and J. Vermant, *Rheol. Acta*, 2010, **49**, 131–144.
28 A. Saint-Jalmes, Y. Zhang and D. Langevin, *Eur. Phys. J. E*, 2004, **15**, 53–60.
29 M. Durand and D. Langevin, *Eur. Phys. J. E*, 2002, 35–44.
30 A. Saint-Jalmes and D. J. Durian, *J. Rheol.*, 1999, **43**, 1411–1422.
31 S. Marze, R. M. Guillermic and A. Saint-Jalmes, *Soft Matter*, 2009, **5**, 1937.
32 N. Jager-Lézer, J.-F. Tranchant, V. Alard, C. Vu, J.-L. Grossiord and P. C. Tchoreloff, *Rheol. Acta*, 1998, **37**, 129–138.
33 B. Rullier, M. A. Axelos, D. Langevin and B. Novales, *J. Colloid Interface Sci.*, 2009, **336**, 750–755.
34 B. Rullier, B. Novales and M. A. Axelos, *Colloids Surf., A*, 2008, **330**, 96–102.
35 D. J. Burgess and N. O. Sahin, *J. Colloid Interface Sci.*, 1997, **189**, 74–92.
36 R. A. Curtis, J. M. Prausnitz and H. Blanch, *Biotechnol. Bioeng.*, 1998, **57**, 11–21.
37 S. N. Timasheff and T. Arakawa, *J. Cryst. Growth*, 1988, **90**, 39–46.
38 H. Zhu and S. Damodaran, *J. Agric. Food Chem.*, 1994, **42**, 856–862.
39 C. A. Zittle, E. S. DellaMonica, R. K. Rudd and J. H. Custer, *J. Am. Chem. Soc.*, 1957, **79**, 4661–4666.
40 K. Engelhardt, M. Lexis, G. Gochev, C. Konnerth, R. Miller, N. Willenbacher, W. Peukert and B. Braunschweig, *Langmuir*, 2013, **29**, 11646–11655.
41 D. Graham and M. Phillips, *J. Colloid Interface Sci.*, 1980, **76**, 240–250.
42 S. Pezennec, F. Gauthier, C. Alonso, F. Graner, T. Croguennec, G. Brulé and A. Renault, *Food Hydrocolloids*, 2000, **14**, 463–472.
43 S. H. Kim and J. E. Kinsella, *J. Food Sci.*, 1985, **50**, 1526–1530.
44 S. A. Roberts, I. W. Kellaway, K. M. G. Taylor, B. Warburton and K. Peters, *Langmuir*, 2005, **21**, 7342–7348.
45 D. Graham and M. Phillips, *J. Colloid Interface Sci.*, 1980, **76**, 227–239.
46 R. Wüstneck, *Colloid Polym. Sci.*, 1984, **262**, 821–826.

5 Outlook

5.1 Other measurement techniques

The structure formation of adsorbed proteins at liquid/air interfaces is still a frequently discussed phenomenon und not completely understood so far. Also, it is not clear how and to which extent protein aggregates adsorb at interfaces. Deeper insight into these interfacial phenomena might be gained by executing x-ray scattering experiments. Stubenrauch et al.[1] already showed for polymer/surfactant complexes at the water/air interface the applicability of this measurement technique for the determination of the roughness and thickness of the adsorbed layer. Furthermore, the electron density variation perpendicular to the surface can be obtained which might deliver useful information about structural changes and intermolecular interactions during adsorption in the case of protein layers[2].

Another method for the investigation of structure formation at interfaces is multiple particle tracking (MPT) where the formation and mechanical properties of adsorbed protein layers at the air/liquid interface can be studied. Tracking the Brownian motion of tracer particles (diameter approximately 0.1-1 µm) allows for the quantification of local mechanical properties as well as the microscopic heterogeneity of the protein layers. MPT measurements of BLG surface layers to air and dodecane interfaces have been executed by Lee et al.[3,4]. Fig. 7.1 shows the mean-squared displacements of 1 µm colloids confined to the air interface of a solution of 50 µg/mL β-lactoglobulin. Until t_a = 40 min a relatively uniform diffusive probe motion is observed. Between t_a = 40 min and t_a = 60 min a bimodal distribution of particle motions and for t_a > 110 min a highly localized motion with constant $\langle \Delta r^2(\tau) \rangle$ occurs. Thus, passive microrheology indicates the formation of a uniform elastic film in approximately one and a half hours for the experimental solution conditions. With the help of such experiments differences in the interfacial layer formation of protein solutions at different conditions (pH, salt content) could be identified.

[1] *C. Stubenrauch, P.-A. Albouy, R. v. Klitzing, D. Langevin, Langmuir **2000**, 16, 3206-3213.*
[2] *D. Gidalevitz, Z. Huang, S. A. Rice, Proc. Natl. Acad. Sci., **1999**, 96, 2608-2611.*
[3] *M. H. Lee, D. H. Reich, K. J. Stebe, R. L. Leheny, Langmuir **2009**, 26, 2650–2658.*
[4] *M. H. Lee, S. P. Cardinali, D. H. Reich, K. J. Stebe, R. L. Leheny, Soft Matter **2011**, 7, 7635–7642.*

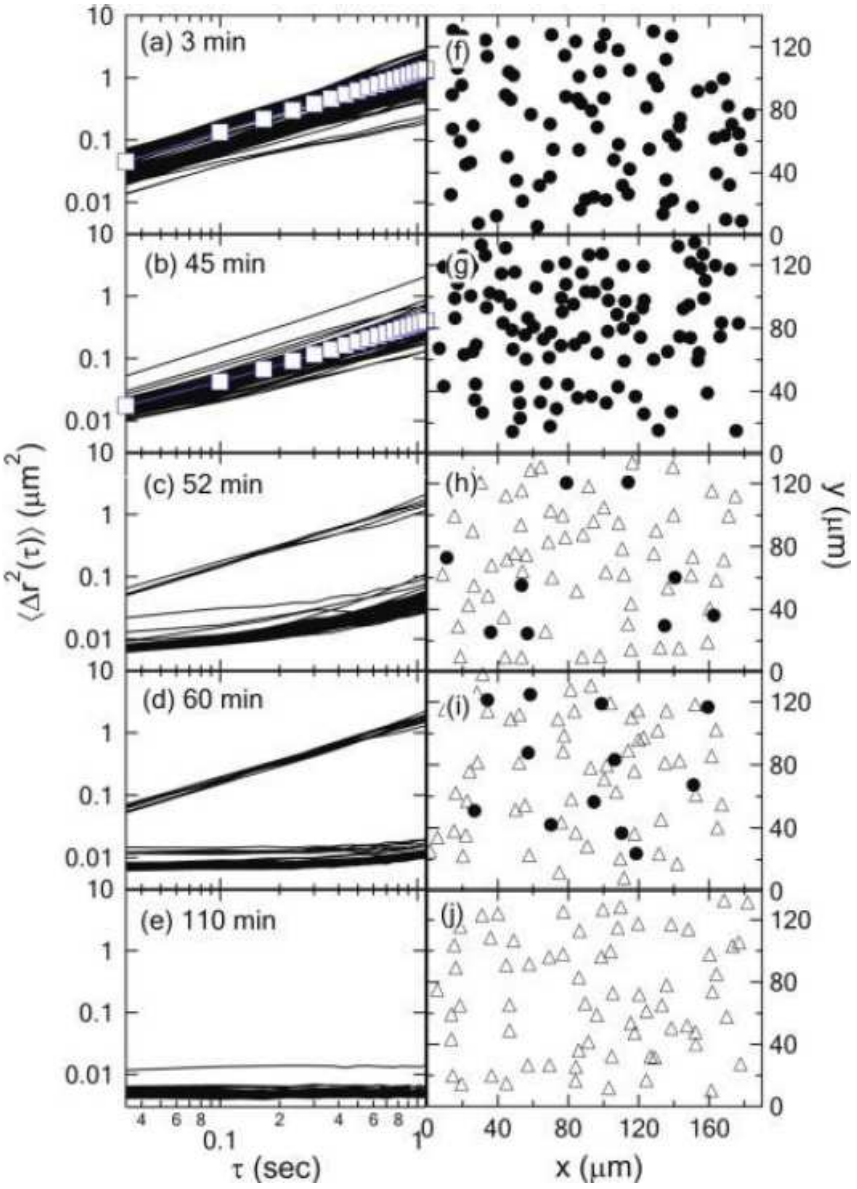

Figure 5.1: *(a-e) Mean-squared displacements of individual 1 μm colloids confined to the air interface of a solution of 50 μg/mL β-lactoglobulin with pH=5.2 during formation on an interfacial protein layer at various age t_a since the introduction of the protein into solution a) t_a=3 min, b) t_a=45min, c) t_a=52min, d) t_a =60min, and e) t_a=110 min. The open squares in a) and b) are the ensemble-averaged mean-squared displacements. The blue lines are the results of fits of the ensemble averages to a diffusive form, $\Delta r^2(\tau) = 4D\tau$. (f-j) Maps of the interface at these ages showing the positions of the colloids exhibiting diffusion (●) and*

localized motion (Δ).Data taken from[3]

5.2 Other materials

The direct correlation between interfacial and bulk foam rheological properties has been investigated only for foams made from BLG solutions so far. Whether these correlations apply as well for other protein or surfactant systems exhibiting interfacial elasticity is a fundamental question in colloid and interface science. Very well investigated proteins with good foaming properties are for example bovine serum albumin or egg white protein. Also, a broader range of surface elastic moduli should be studied to point out possible limitations of the correlations found in this dissertation. Mixtures of surfactants with co-surfactants as used in[5] consisting of sodium lauryl-dioxyethylene sulfate, cocoamidopropyl betaine and lauryl alcohol.or myristic acid for example provide high surface elastic moduli.

Commonly used surfactants in the food industry are polyglycerol esters (PGE) obtained from edible oils[6]. Foams made from PGE show remarkable stability against Ostwald ripening[7]. The interfacial layers possess peculiar properties as PGE builds aggregates at the interface. Relating foam and interfacial properties of such a system would therefore be another interesting study.

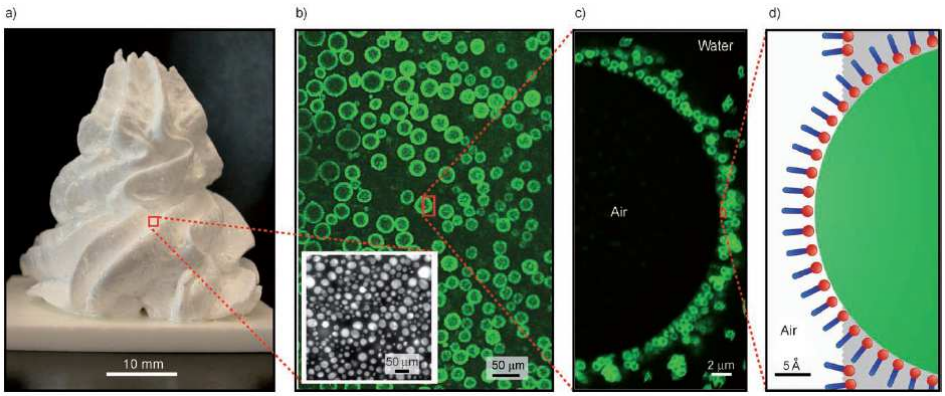

Figure 5.2. *Hierarchical features of the particle-stabilized foams containing short amphiphilic molecules. High-volume macroscopic foams a) with bubble sizes within the range 10–50 mm,*

b) are formed through the adsorption of submicrometer-sized colloidal particles at the air–liquid interface

c) particles attach at the air–water interface as a result of the surface hydrophobicity imparted by the adsorbed amphiphilic molecules, as indicated schematically in

[5] *S. Costa, R. Höhler, S. Cohen-Addad, Soft Matter* ***2012****, 9, 1100-1112.*
[6] *C. Curschellas, K. Nagy, E. Windhab, H. J. Limbach, Journal of Colloid and Interface Science* ***2013****, 393, 182-191.*
[7] *C. Curschellas, D. Z. Gunes, H. Deyber, B. Watzke, E. Windhab, H. J. Limbach, Soft Matter* ***2012****, 8, 11620-11631.*

d) the confocal images shown in b) and c) were obtained after dilution of concentrated foams (insert in b) containing fluorescently labeled silica particles and hexylamine as amphiphile[8].

Another mechanism for stabilizing foams is to use nanoparticles. By adjusting the surface hydrophobicity of these particles very stable foams can be created as depicted in Fig. 7.2. The surface rheological properties of these systems are not well investigated so far and would therefore give rise to future work and relating them to the rheological properties of corresponding foams is a particular challenge.

5.3 Technical improvements

Technical improvements should be made concerning the optical detection of the bubbles. The lens of the endoscope used in this work is surrounded by a ring shaped lighting. Dependent on the bubble size distribution this leads to an inhomogeneous illumination (Fig. 7.3a) which complicates the automated analysis of the pictures with Matlab. Using a local threshold function for the binarisation of the image the inhomogeneous illumination can be mostly balanced (Fig. 7.3b) but it could be further improved by using multiple light sources, e.g. small LEDs surrounding the lens of the endoscope, which can be controlled separately. Another complication for the automatic analysis of the bubble sizes is the punctual reflection of the lamellae (Fig. 7.3c). Normally the liquid phase appears darker than the gas phase which helps differing the both. At some points the liquid phase inside the lamellae reflects the light leading to white spots which in turn lead to interruptions in the bubble contour as well as to disturbing spots inside the gas phase (Fig. 7.3d). The Matlab program detects circles defining the bubble surface whereas little gaps in the profile can be bridged. If there are too many gaps in the profile the algorithm is not able to identify a circle anymore and if there are too many spots inside the gas phase this can lead to incorrect detection of bubbles. Hence, the reflections need to be reduced, either by enhancing the illumination and / or by using a polarizing filter in front of the endoscope.

The bubble size distribution of most of the foams produced in this work had to be analyzed manually (IPS, Visiometrics) which is a time-consuming process. Therefore, the image quality necessarily needs to be improved in future works for automatized bubble detection.

[8] *U. T. Gonzenbach, A. R. Studart, E. Tervoort, L. J. Gauckler, Angew. Chem. Int. Ed.* ***2006****, 45, 3526–3530.*

a)

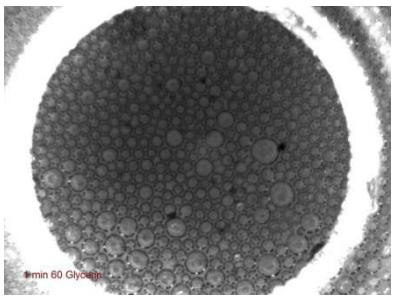

b)

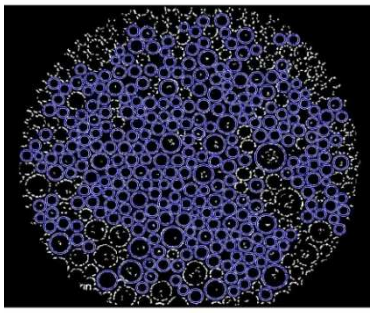

c)

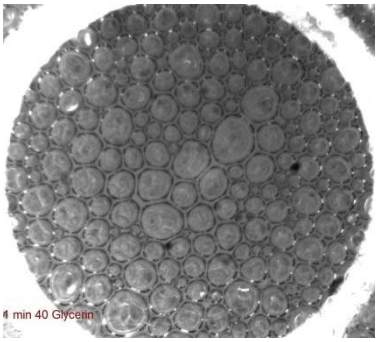

d)

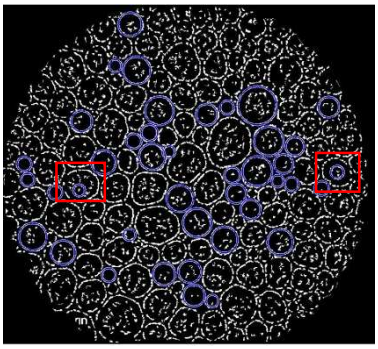

Figure 5.3: *a) Image of a surfactant foam,*
b) image from a) after image processing
c) image of a surfactant foam with many light reflections disturbing the analysis shown in
d) only few correct bubbles and some wrong bubbles are detected (framed by red rectangles)